BEHAVIOURAL ANALYSIS OF ZEBRAFISH

RELAXIN-3A MUTANT

CHIA SHU MING JOANNE

NATIONAL UNIVERSITY OF SINGAPORE

2017

BEHAVIOURAL ANALYSIS OF ZEBRAFISH

RELAXIN-3A MUTANT

CHIA SHU MING JOANNE

(B.Sc. (Hons.), NUS)

A THESIS SUBMITTED FOR THE DEGREE OF

DOCTOR OF PHILOSOPHY

NUS GRADUATE SCHOOL FOR INTEGRATIVE

SCIENCES AND ENGINEERING

NATIONAL UNIVERSITY OF SINGAPORE

2017

Supervisor:
Associate Professor Suresh Jesuthasan

Examiners:
Assistant Professor Eyleen Goh
Associate Professor Ajai Vyas, Nanyang Technology University
Professor Andrew Gundlach, The University of Melbourne

Declaration

I hereby declare that this thesis is my original work and it has been written by me in its entirety. I have duly acknowledged all sources of information which have been used in the thesis.

This thesis also has not been submitted for any degree in any university previously.

Chia Shu Ming Joanne

19 January 2017

Acknowledgements

I would like to thank my supervisor, Assoc. Prof. Suresh Jesuthasan, for his mentorship and guidance throughout the course of this project, and for all the ideas that helped it take shape.

I would also like to thank my thesis advisory committee, Assoc. Prof. Tang Bor Luen, Assoc. Prof. Gavin Dawe, and Dr. Judy Sng, for the critical and insightful advice that has enriched this thesis.

Many thanks to the lab members for enhancing the work environment in the lab, I have thoroughly enjoyed working with you: Dr. Ruey-Kuang Cheng, for assisting with the setting up of the behavioural experiments in this thesis, patiently helping me with the analysis and showing me how amazing Microsoft Excel can be; Asst. Prof. Ajay Mathuru, for teaching me how to stress and how not to stress my fish at the same time, advice on statistics, and for the many wonderful discussions over coffee time, scientific and otherwise; Dr. Michelle Kee for the technical help during the initial days of RNA work, and keeping us healthy with 4pm apple and chocolate time; Dr. Charlotte Lupton for setting up the high resolution melt analysis (HRMA), teaching me how to use R, and editing my presentations and this thesis; Dr. Lin Qian for teaching me about light-evoked zebrafish behaviours, and how to handle my behaviour setups and experiments with care; Caroline Kibat for challenging me to be more efficient, leading the CRISPR team, and always helping with troubleshooting the molecular biology; Mahathi Ramaswamy for always being the first to listen to my experimental woes, and providing critical advice on how to improve them; Seetha Krishnan for advice on statistics, and teaching me about calcium imaging and data analysis; Gadisti Aisha for the help

Table of contents

Summary

The neuropeptide relaxin-3 (RLN3) is produced in response to stress, and has been implicated in a variety of behaviours, including arousal, locomotion, feeding and anxiety in mouse and rats. The mature peptide, consisting of A- and B-chains, is evolutionarily conserved, with high sequence similarity in all vertebrates. In the zebrafish, expression patterns of the Rln3/Rxfp3 system overlap with rodents. Hence, this thesis uses zebrafish to ask whether any of the proposed roles of RLN3 based on mammalian anatomy and behaviour are evolutionarily conserved.

CRISPR/Cas9 was used to mutate the zebrafish relaxin-3a gene (*rln3a*). Genetic characterisation of CRISPR-injected fish identified a 7 base pair (bp) deletion mutation in the *rln3a* locus, which caused a reduction in *rln3a* transcripts. The novel tank diving assay, analogous to the large open field test in rodents, uses natural behaviours such as initial bottom-dwelling and locomotion to evaluate anxiety and stress responses in adult fish. When tested with this paradigm, *rln3a* mutants spent less time at the bottom half of the tank in the first minute than WT siblings, reflecting a slightly anxiolytic phenotype. The application of additional stress prior to the onset of the assay resulted in reduced locomotion in mutants. Another stress-related response is dark-induced hyperactivity in larval zebrafish. Two-photon imaging revealed that dark stimuli caused depolarisation in the lateral PAG neurons, where *rln3a* expression has been observed in larval zebrafish, implicating the involvement of Rln3 in such behaviours. However, using the visual motor response assay, a test in which larvae were exposed to repeated cycles of light and dark stimuli, no difference in locomotor activity between

mutants and WT siblings was observed. Moreover, although food intake is related to stress and associated with Rln3 signalling, the *rln3a* disruption did not cause long-term changes in body weight of mutants in comparison to their WT siblings. Mutants displayed increased expression of the paralogue, *rln3b*, which could partially compensate for the loss of *rln3a*, resulting in a lack of phenotypic difference.

Unexpectedly, a single nucleotide polymorphism (SNP) of C/T in the 158th position of *rln3a* coding DNA (c.158C>T) was found in the WT siblings, which resulted in a non-synonymous mutation in the C-peptide. To test the effects of this polymorphism on behaviour, the visual motor response of WT fish possessing the T variant ($rln3a^{c.158T}$) was tested against siblings possessing the C variant ($rln3a^{c.158C}$). In WT siblings of mutants, $rln3a^{c.158T}$ showed increased locomotor activity in the first 10 minutes of the dark periods compared to $rln3a^{c.158C}$. However, in non-sibling WT, no difference in activity was detected between SNP variants, indicating that genetic background influences such behavioural effects.

In conclusion, these studies suggest that the loss of *rln3a* in zebrafish only mildly affects stress responses, locomotor responses to dark stimuli and feeding behaviours. Unexpectedly, the c.158C>T polymorphism in the C-peptide was associated with hyperactivity in the visual motor response in fish from a specific genetic background, suggesting a possible biological role to this undefined peptide.

List of tables

List of figures

List of symbols

5-HT	5-hydroxytryptamine (serotonin)
actb1	*Danio rerio* beta actin 1
BEP	Binge-eating prone
BLAST	Basic Local Alignment Search Tool
cAMP	Cyclic adenosine monophosphate
Cas9	CRISPR-associated protein 9
CRF	Corticotrophin-releasing factor
CRISPR	Clustered regularly interspaced short palindromic repeats
crRNA	CRISPR RNA
Ct	Cycle threshold
dHbL	Dorsal lateral habenula
dpf	Days post fertilisation
DIO	Diet-induced obesity
DSBs	Double-stranded breaks
ERK	Extracellular signal-regulated kinase
H3	Human relaxin-3
HRMA	High resolution melt analysis
hsp	Heat shock promoter
i.c.v.	Intracerebroventricular
IGL	Intergeniculate leaflet
indels	INsertions/DELetions
INSL	Insulin-like peptide
ISH	*In situ* hybridisation
GABA	gamma-aminobutyric acid

GPCR	G-protein coupled receptor
LGR	Leucine-rich repeat-containing GPCR
NHEJ	Non-homologous end joining
NI	Nucleus incertus
PAG	Periaqueductal gray
PAM	Protospacer adjacent motif
PCR	Polymerase chain reaction
qRT-PCR	Quantitative reverse transcriptase PCR
RFLP	Restriction fragment length polymorphism
RLN3	Relaxin-3
RXFP	Relaxin family peptide receptors
SALPR	Somatostatin- and angiotensin-like peptide receptor
SAT	Spontaneous alternation task
SNP	Single nucleotide polymorphism
TALENs	Transcription activator-like effector nucleases
$T_a Opt$	Optimal annealing temperature
tracrRNA	Trans-activating RNA
vmDTg	Ventromedial dorsal tegmental nucleus
ZFNs	Zinc finger nucleases

1. INTRODUCTION

1.1 Neuropeptides and behavioural responses to stress

In response to a threat, adaptive behavioural responses are produced by emotional states such as fear and anxiety to counteract stressors. Fear can lead to fight or flight responses when a threat is imminent, whereas anxiety involves increased arousal, attention and risk assessment to a potential threat (Gray & McNaughton 2003, McNaughton & Corr 2004). Multiple brain circuits are implicated in fear and anxiety, such as the amygdala, hypothalamus, hippocampus and periaqueductal gray (Steimer 2002, Tovote et al. 2015). These brain regions act by controlling signalling molecules such as neuromodulators and neuropeptides.

Neuropeptides are defined as relatively small protein molecules which modulate brain activity (Burbach 2011). In contrast to small molecule transmitters, which are stored in small clear core vesicles, neuropeptides are located in dense core vesicles and generally require higher levels of stimulation to be released (Purves et al. 2004). Neuropeptides tend to have longer lasting effects as they do not get reabsorbed by the presynaptic terminal, and are able to act at a distant target (van den Pol 2012). Upon binding to their receptors, which are typically G-protein coupled receptors (GPCRs), signalling cascades are triggered, modifying intracellular ionic concentrations to affect the excitability of the target neuron, influencing synaptic output (Marder 2012, van den Pol 2012).

Such properties of neuropeptides on a cellular level modulate the functional connectivity of the brain within the restrictions of a fixed anatomical network

(Getting 1989, Nadim & Bucher 2014). Neuropeptide signalling is complex, whereby single neuropeptides are able to control multiple types of behaviours, with simple behaviours often being controlled by numerous neurotransmitters (Marder & Bucher 2007). Furthermore, is has been established that co-transmission of small-molecule transmitters with neuropeptides are common, providing additional flexibility to neuronal circuits according to spatial and temporal profiles of the neurotransmitters (Nusbaum et al. 2017, Vaaga et al. 2014). This enables the control of adaptive behavioural responses such as arousal, feeding, and defensive mechanisms to threat (Herbert 1993, Taghert & Nitabach 2012). Indeed, multiple neuropeptides have been implicated in stress-related behaviours, such as neuropeptide Y, corticotrophin-releasing factor (CRF), arginine vasopressin and oxytocin (Reichmann & Holzer 2016, Rotzinger et al. 2010). A relatively new neuropeptide that is thought to be involved in stress responses is relaxin-3 (RLN3) (Kumar et al. 2016, Smith et al. 2014b), which will be investigated in this thesis.

1.2   Relaxin-3

1.2.1   Background – the relaxin family peptides

Seven members of the relaxin (RLN) family exist in humans: RLN H1, H2, and H3; and insulin-like peptides (INSL) 3, 4, 5, and 6. All members of this family possess similar primary and tertiary structural characteristics. RLNs are translated as a preprohormone with a signal peptide and three peptide chains (B-C-A). The signal peptide and C-peptide (connecting peptide) are proteolytically cleaved, resulting in the mature form consisting of B- and A- chains held together by disulphide bonds. The motif (RXXXRXXI/V) is the defining feature of the RLN

family, which is important for receptor binding (Bathgate et al. 2006, Gundlach et al. 2013, Ma & Gundlach 2007). The four known RLN family peptide receptors (RXFP) were found to be leucine-rich repeat containing GPCR (LGR) 7, LGR8, GPCR135 (or previously named somatostatin- and angiotensin-like peptide receptor, SALPR) and GPCR142, which are more recently called RXFP1-4 respectively (Halls et al. 2007, Wilkinson & Bathgate 2007).

The RLN family peptides act mostly as hormones in peripheral systems. The main functional, circulatory form of RLN in humans is H2 (denoted as RLN1 in the rodent orthologue and collectively known as RLN) and was initially discovered to have roles for development of the reproductive tract and mammary apparatus for mammalian parturition and lactation in pregnant females. Later, RLN was discovered to have diverse effects on non-reproductive tissues, such as vasodilatory actions which are cardioprotective, reducing fibrosis and promoting wound healing, and neutralising allergies (Sherwood 2004). RLN has also been discovered to act centrally by regulating osmolarity, blood pressure and neurosecretion during pregnancy (Ma & Gundlach 2007). INSL3 has survival and anti-apoptotic functions related to its expression and secretion in the Leydig cells of the testis (Minagawa et al. 2012, Sagata et al. 2015), whereas INSL5 is an orexigenic hormone in the gastrointestinal tract (Grosse et al. 2014). The other INSLs are less well known, with putative roles in placental growth for INSL4 (Millar et al. 2005), and Sertoli cells in the testies for INSL6 (Lu et al. 2006). The endogenous receptor for RLN and RLN1 is RXFP1, while RXFP2 is the receptor for INSL3, and RXFP4 for INSL5, but the other ligand-receptor pairings are undetermined (Hsu 2003, Liu et al. 2003a, Sudo et al. 2003, Wilkinson & Bathgate 2007).

The *RLN3* gene in human and mouse was originally identified through genomic database searches of related peptides from the RLN/INSL family (Bathgate et al. 2002). Unlike RLN, RLN3 is not found in the circulation, but is predominantly localised in the brain, produced within the secretory pathway in neurons, and present in dense core vesicles (Ma et al. 2007, Tanaka et al. 2005), consistent with its description as a neuropeptide. The endogenous receptor for RLN3 has been identified as RXFP3/GPCR135 (Liu et al. 2003b), as RLN3 is the only member of the RLN family peptide that binds to RXFP3, and the receptor mostly restricted to the brain. Cell-based assays indicate that RLN3 activation of RXFP3 causes a decrease in cyclic adenosine monophosohate (cAMP) levels (Liu et al. 2003b), and interactions with $G_{i/o}$ (inhibitory/olfactory) proteins lead to increase of ERK1/2 (extracellular signal-regulated kinase 1/2) levels (van der Westhuizen et al. 2007), although how this relates to effects *in vivo* is unclear (Smith et al. 2011). Although there is some degree of cross-reactivity between RLN3 and RXFP1 and RXFP4, with RLN3 able to activate them both *in vitro* and *in vivo* (Wilkinson & Bathgate 2007), RXFP3 is widely considered to be the cognate receptor for RLN3. In rats, *Rxfp1* is widely expressed in the brain, in a pattern which corresponds to Rln binding sites, but does not correspond to areas with *Rln3* expression (Ma et al. 2006). *Rxfp4* mRNA or binding sites are not detectable in mouse brain (Sutton et al. 2005), and RXFP4 is a psuedogene in rats (Chen et al. 2005).

1.2.2   Brain expression of RLN3 and RXFP3

Within the brain, RLN3 is found in a localised region of the brainstem – the

ventromedial area of the dorsal tegmental nucleus (vmDTg) in the rat (Burazin et al. 2002) and in the mouse (Bathgate et al. 2002, Smith et al. 2010), and this locus is more commonly known as the NI. Smaller populations of RLN3 neurons present in the medial, ventral and lateral PAG, pontine raphe nucleus and the area dorsal to the substantia nigra in rats (Ma et al. 2007, Tanaka et al. 2005) and mice (Smith et al. 2010). *RLN3* mRNA has been detected in macaque (Ma et al. 2009b), while the teleost paralogues *rln3a* and *rln3b* have also been found in zebrafish NI and PAG (Donizetti et al. 2008). In both species, the NI was identified and defined by *RLN3* expression. There is also a report of RLN3 immunoreactivity in the dorsal raphe nucleus, pontine reticular nucleus and the dorsal and ventral tegmental areas in human brain tissue (Silvertown et al. 2010), although expression of RLN3 mRNA was not reported as an important control in this study.

In contrast to the confined expression of RLN3, RLN3-containing nerve axons send projections to widespread areas in the brain, which correspond to RXFP3 receptor localisation (Figure 1.1). In summary, in the rodent brain, RLN3 projections and receptors are found in: areas regulating the stress response, such as the periventricular nucleus of the hypothalamus, the bed nucleus of stria terminalis, the amygdala, the PAG and the periventricular thalamic area; areas involved in arousal, sleep and vision such as the dorsal and median raphe nuclei, the lateral preoptic area, the superior and inferior colliculus and the intergeniculate leaflet (IGL); regions of the hypothalamus that mediate feeding and metabolism, such as the lateral hypothalamus, dorsal medial nucleus of the hypothalamus, and the arcuate nucleus; the septohippocampal pathway and cortical regions involved in RLN3 and higher cognition (Ma et al. 2016, Smith et

al. 2014b). These data on RXFP3 expression patterns were amassed from studies detecting RLN3-like immunoreactivity, *RXFP3* mRNA, and radioactive labelling of binding sites using the RLN3 analogue, R3/I5 (Liu et al. 2005) by Ma et al. 2007, Sutton et al. 2004, and Tanaka et al. 2005 (for a comprehensive compiled description, see Smith et al. 2011). Similar expression patterns were seen in mouse brain (Smith et al. 2010).
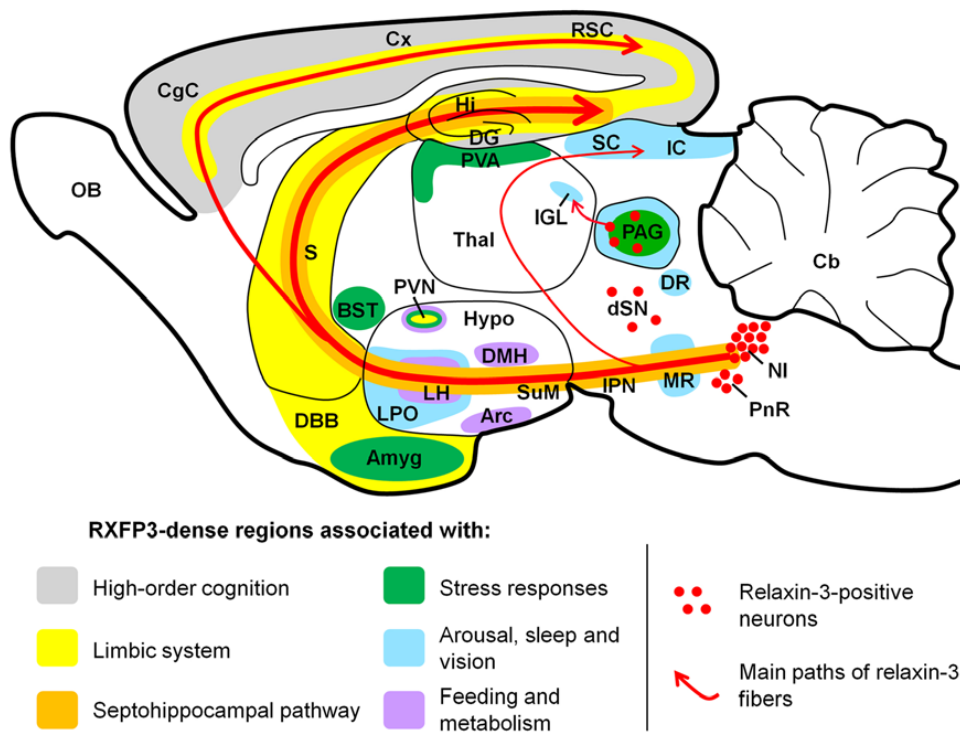
Figure 1.1 RLN3/RXFP3 system in the rodent brain

Schematic parasagittal representation of the rodent brain, illustrating the ascending relaxin-3 system and the distribution of RXFP3 in regions grouped by function. Amyg, amygdala; Arc, arcuate nucleus; BST, bed nucleus of stria terminalis; Cb, cerebellum; CgC, cingulate cortex; Cx, cerebral cortex; DBB, diagonal band of Broca; DG, dentate gyrus; DMH, dorsomedial nucleus of hypothalamus; DR, dorsal raphe nucleus; dSN, region dorsal to the substantia nigra; DTg, dorsal tegmental nucleus; Hi, hippocampus; Hypo, hypothalamus; IC, inferior colliculus; IGL, intergeniculate leaflet; IPN, interpeduncular nucleus; LH, lateral hypothalamus; LPO, lateral preoptic area; MLF, medial longitudinal fasciculus; MR, median raphe; NI, nucleus incertus; OB, olfactory bulb; PAG, periaqueductal gray; PVN, paraventricular hypothalamic nucleus; RSC, retrosplenial cortex; S, septum; SC, super colliculus; SuM, supramammillary nucleus; Thal, thalamus.

Figure and legend adapted from Smith et al. (2014b).

As the largest population of RLN3 neurons is found in the NI, most RLN3/RXFP3 networks are described as connections from this primary source. There are extensive descriptions of efferent and afferent connections of the rat NI (Goto et al. 2001, Olucha-Bordonau et al. 2003), which highly correlate with RLN3/RXFP3 expression (refer to Ryan et al. 2011 for a detailed comparison of NI projections and RLN3/RXFP3 expression). Particularly, neuronal tract tracing studies in conjunction with RLN3 immunoreactivity have characterised RLN3-specific projections from the NI to the septal area (Olucha-Bordonau et al. 2012), and amygdala (Santos et al. 2016) in rats.

Additionally, one RLN3 and RXFP3-rich region in the thalamus, the IGL, was demonstrated not to arise from the NI (Tanaka et al. 2005). Neuronal tract tracing determined that this region was mostly innervated by the PAG population of RLN3-containing cells, but scarcely by NI neurons (Blasiak et al. 2013). In this study, IGL cells were also shown to be responsive to RLN3, as the application of RLN3 analogue R3/I5 hyperpolarised 67% and depolarised 33% of the recorded IGL neurons.

1.2.3 Neurochemistry of RLN3 neurons

The identification of neurochemical features of RLN3 neurons have been important in determining how these cells interact with associated brain networks. The NI is predominantly comprised of gamma-aminobutyric acid (GABA), and it is likely that all RLN3 neurons from the NI are GABAergic neurons based on glutamic acid decarboxylase-65 immunoreactivity, although not all GABAergic neurons in the NI express RLN3 (Ma et al. 2007). However, at present it is

unclear whether other populations of RLN3 neurons are GABAergic.

One main feature of RLN3 neurons is that most, if not all, RLN3 neurons express the CRF type 1 receptor (Tanaka et al. 2005). In this study, RLN3 neurons had increased *c-fos* mRNA levels in response to both intracerebroventricular (i.c.v.) administration of CRF and water immersion-restraint stress, and *RLN3* mRNA was also increased in the latter case (Tanaka et al. 2005). Furthermore, a repeat forced-swim test also produced increased RLN3 levels, an effect that was blocked by the CRF1 antagonist, antalarmin (Banerjee et al. 2010). Also, i.c.v. administration of CRF caused excitation of a majority of the RLN3 neurons recorded in the NI, an effect that was also observed in brain slices. Conversely, NI neurons that were RLN3-negative displayed inhibition by CRF (Ma et al. 2013).

RLN3-positive neurons in the rat NI co-express the 5-hydroxytryptamine (5HT, serotonin) -1A receptor, and 5HT depletion by *p*-chlorophenylalanine lead to an increase in RLN3 expression, implying a regulatory role of 5HT on *RLN3* expression (Miyamoto et al. 2008). Furthermore, administration of the anxiogenic drug, FG-7142, in rats before exposure to the elevated plus maze increased c-Fos activation in both the RLN3 populations in the NI and 5HT-ergic cells in the dorsal raphe, suggesting an interaction between the two populations in anxiety-related behaviours (Lawther et al. 2015).

Dopamine type 2 (D_2) receptors were recently identified in the rat NI by immunostaining, as well as reverse-transcriptase polymerase chain reaction (RT-PCR) and western blotting from RNA/proteins extracted from NI tissue (Kumar et

al. 2015). Infusion of the dopamine agonist quinpirole into the NI resulted in reduced locomotion, as well as during novel-environment induced suppression of feeding, suggesting that dopamine is involved in NI-related locomotor behaviours.

1.2.4   Behaviours associated with RLN3

The behavioural role of RLN3/RXFP3 signalling has been investigated based on the known functions of the brain regions containing RXFP3 and target regions of the NI, which will be reviewed in this section. A summary of the behavioural effects seen in null mutation mouse models (Table 1.1) or effects after administration of RXFP3-activating ligands on stress and anxiety behaviours (Table 1.2), arousal and cognition (Table 1.3), and feeding and motivation/reward (Table 1.4) are also provided.

1.2.4.1   Stress and anxiety

One of the main characteristics of *RLN3* is that it is expressed in response to stress-mediated activation of CRF1 receptors. Also, electrical stimulation of RLN3 neurons leads to the activation of the hypothalamic-pituitary-gonadal axis (McGowan et al. 2014). Hence, it is expected that RLN3 would be involved in stress and anxiety responses. However, only slight alterations were detected in behavioural tests for anxiety such as the large open field or elevated plus maze tests, and there are contradictory reports between different groups conducting the studies. In mixed background (129S5:B6) *Rln3* null mutant mice, strong anxiety phenotypes were not found, but after eight weeks of chronic stress, male *Rln3* null mutant mice were more sensitive to the stress, displaying a reduction in body weight and increased depressive-like behaviour in the forced swim test (Smith et

al. 2009). However, backcrossed *Rln3* null mutant mice did not show differences in anxiety and stress behaviours compared to WT littermates (Smith et al. 2012). Using *Rxfp3* null mutant mice, one group reported only slightly decreased anxiety phenotypes in the elevated plus maze and light/dark paradigms (Hosken et al. 2015). Conversely another group reported decreased anxiety reflected by increased entry into the open arms of the elevated plus maze, although similar effects were not observed in other tests (Watanabe et al. 2011b).

Anxiolytic effects were seen after i.c.v. administration of H3 in rats in both the elevated plus maze and shock probe-burying test, and spontaneous locomotion was decreased when placed in a novel environment compared to a habituated environment, indicating decreased stress levels (Nakazawa et al. 2013). Using a specific RXFP3 agonist, RXFP3-A2 (Shabanpoor et al. 2012), a decrease in anxiety was only seen in the light/dark box and elevated plus maze test, but not the open field test (Ryan et al. 2013a). Interestingly, there was no effect of RXFP3-A2 in reducing depressive-like effects in rats that had not been previously tested in other paradigms, but only in previously tested rats (Ryan et al. 2013a). A similar type of study was conducted using the anxiogenic drug benzodiazepine, FG-7142, to elevate levels of anxiety before testing (Zhang et al. 2015). Under basal conditions, the agonist RXFP3-A2 did not have any effect on anxiety levels, but was anxiolytic after FG-7142 administration in the light/dark box and single-chamber social interaction test in mice. Furthermore, i.c.v. administration of the RXFP3 antagonist R3(B1-22)R (Haugaard-Kedstrom et al. 2011), decreased anxiety only in the elevated plus maze, but not in large open field, light/dark box or social interaction tests (Zhang et al. 2015). This suggests that RLN3/RXFP3 signalling may preferentially reduce elevated levels of anxiety in rodents.

1.2.4.2   Arousal and cognition

The NI is postulated to be part of the ascending arousal network, and projects to the medial septum, which is reported as being the 'pacemaker' of hippocampal theta rhythm (Goto et al. 2001, Olucha-Bordonau et al. 2003). Indeed, evoked field potentials and theta hippocampal rhythm were enhanced by the infusion of agonist R3/I5, and blocked by pretreatment of the antagonist, R3(BΔ23–27)R/I5 (Haugaard-Kedstrom et al. 2011) in anaesthetised rats, although there was greater variability in awake rats (Ma et al. 2009a).   Furthermore, R3(BΔ23–27)R/I5 impaired spatial memory in a hippocampal-theta rhythm dependent spontaneous alternation task (SAT) in rats (Ma et al. 2009a). The SAT also increased NI c-Fos activation in NI RLN3-containing cells, implying the involvement of the RLN3/RXFP3 system in this task.

Rln3 null mutant mice were also shown to have deficiencies in behavioural arousal, being hypoactive during the dark (active) phase of the circadian cycle, as reflected by reducing voluntary wheel running and distance travelled in a home cage, and increasing bouts of immobility (Smith et al. 2012). The decreased wheel running activity in the dark phase was also seen in *Rxfp3* null mutant mice (Hosken et al. 2015). In mixed background (129S5:B6) RLN3 mutant mice, hypoactivity was reported in female mice (Smith et al. 2009). However, studies monitoring locomotion during feeding in rats reported that i.c.v. administration of H3 (Hida et al. 2006) or injection into the periventricular nucleus (McGowan et al., 2006) had no effects on locomotor activity. Additionally, i.c.v. administration of RLN3 agonist R3/I5 administration increased overall locomotor activity in the light (inactive) phase, but antagonist R3(BΔ23–27)R/I5 did not produce a difference in dark (active) phase activity in rats (Sutton et al. 2009).

1.2.4.3 Feeding and motivation/reward

RLN3 neurons project to the hypothalamus, where dense RXFP3 receptors are present and exert neuroendocrine actions (Ganella et al. 2013, McGowan et al. 2009). As such, many studies have been conducted to elucidate the role of the RLN3/RXFP3 system in feeding. Administration of RLN3 in rats was demonstrated to have an orexigenic effect (Hida et al. 2006; McGowan et al. 2005, 2006), and increased food intake and related neuropeptide expression changes were more prominent in females than males (Calvez et al. 2015). When the agonist, R3/I5, was used, prominent increases in food intake were observed, with the antagonist, R3(BΔ23–27)R/I5, blocking these effects (Sutton et al. 2009). It must be noted that RLN3 has cross-reactivity with RXFP1, which may confound results, but further studies conducted with more specific agonist and antagonist peptides did demonstrate the same result (Shabanpoor et al. 2012).

In mice, the antagonist R3(B1-22)R blocked intake of regular and palatable food, as well as reducing intake during mild food deprivation, and reduced food anticipatory behaviour associated with food restriction, but the RXFP3 agonists, H3 and RXFP3-A2, did not increase food intake (Smith et al. 2014a). This study highlights the involvement of RLN3 signalling in motivated feeding, and also the some likely differences in rat and mouse behaviours (Smith et al. 2014a). *Rln3* null mutant mice studies are complex, with Sutton et al. (2009) reporting a decrease in body weight in loss-of-function mutant mice, while other studies reported no change in body weight in fully backcrossed mutant mice relative to littermates (Smith et al. 2009, 2012; Watanabe et al. 2011b).

In relation to the control of feeding behaviour, the RLN3/RXFP3 system has also been implicated in obesity in rats. Rats with diet-induced obesity (DIO) develop obesity after being fed a high-energy diet, in contrast to diet-resistant rats (Lenglos et al. 2014a). *Rln3* expression was increased in the NI of DIO rats, and during re-feeding, *RXFP3* was upregulated, compounding orexigenic effects and reversing the effects of caloric restriction (Lenglos et al. 2014b). Moreover, in binge-eating prone (BEP) rats that increase their sucrose intake in response to stress, *Rln3* mRNA levels are increased in the NI with a corresponding increase in *Rxfp3* mRNA in the PVN and the supraoptic nucleus in the hypothalamus (Calvez et al. 2016a). The effects of stress on sucrose consumption of BEP rats were blocked by i.c.v. administration of the RXFP3 antagonist, R3(B1-22)R (Calvez et al. 2016a).

Based on the effects of RLN3 on the motivational aspect of palatable food intake, studies were conducted to examine salt appetite and sucrose preference. After salt depletion from standard chow, i.c.v. administration of RXFP3 antagonist R3(B1-22)R decreased salt consumption in mice (Smith et al. 2014a). To test motivation, sucrose was self-administered by WT and *Rxfp3* null mutant mice under either fixed or progressive ratios (Walker et al. 2015b). Both WT and *Rxfp3* null mutant mice had similar levels of sucrose self-administration under a low fixed ratio reinforcement schedules; however, *Rxfp3* null mutant mice had reduced sucrose self-administration at a higher fixed ratio, and had a lower breakpoint for the progressive ratio scheme, indicating a decreased level of motivation in *Rxfp3* null mutant mice.

Alcohol-seeking behaviour is linked to reward system signalling, and RLN3 signalling appears to be involved. *Rln3* levels in the rat NI, detected by densitometry of radiolabelled mRNA, were positively correlated with levels of alcohol intake (Ryan et al. 2014). Alcohol preference at baseline levels were similar in *Rxfp3* null mutants and WT mice in a free choice assay (Walker et al. 2015a), or operant conditioning assay (Walker et al. 2015b). Another study reported increased alcohol consumption in male *Rln3* null mutant mice (Shirahase et al. 2016). Notably, male WT control mice did not display dose-dependent increase in alcohol consumption at concentrations used in other studies (9–10%). In a model of alcohol relapse, i.c.v. administration of RXFP3 antagonist reduced both cue- and stress- induced reinstatement of alcohol in alcohol-preferring rats using a two-bottle free choice assay (Ryan et al. 2013b). When the RXFP antagonist was infused into the bed nucleus of stria terminalis, an area postulated to regulate drug and alcohol seeking with dense *Rxfp3* and *Crf1* expression, both self-administration of alcohol and stress-induced alcohol reinstatement was reduced. This was corroborated by a study using *Rxfp3* null mutant mice, where stress-induced reinstatement of alcohol consumption was decreased (Walker et al. 2015a).

Orexin inputs into the NI have been demonstrated, at least in part, to regulate alcohol consumption, presumably via effects on RLN3/RXFP3 signalling (Kastman et al. 2016). Yohimbine-induced reinstatement of alcohol was associated with increased *c-fos* expression in the NI, and this effect was blocked by the administration of an orexin-2 receptor antagonist into the NI (Kastman et al. 2016). Electrophysiological studies have also shown that orexin-A depolarises RLN3-positive NI neurons (Blasiak et al. 2015), specifically via the orexin-2

receptors (Kastman et al. 2016), providing a functional link between orexin-A and

RLN3 signalling in the NI that contributes to alcohol seeking behaviour.

Table 1.1 Behaviours associated with *Rln3/Rxfp3* null mouse mutants

Gene	Species	Effect	Assay	Reference
Rln3	Mouse	↓ locomotion (females)	Automated locomotor cell	(Smith et al. 2009)
		↑ sensitivity to stress (males)	Repeated force swim	
Rln3	Mouse	↓ body weight	High fat diet	(Sutton et al. 2009)
Rln3	Mouse	↓ anxiety (slight)	Elevated plus maze	(Watanabe et al. 2011b)
		↑ acoustic startle	Startle response test	
Rln3	Mouse	↓ locomotion in active phase	Voluntary wheel running	(Smith et al. 2012)
Rxfp3	Mouse	↓ locomotion in active phase	Voluntary wheel running	(Hosken et al. 2015)
		↓ anxiety (slight)	Elevated plus maze	
		↓ anxiety (slight)	Light/dark box	
Rxfp3	Mouse	↓ stress-induced alcohol reinstatement	Two-bottle free choice	(Walker et al. 2015a)
Rxfp3	Mouse	↓ motivational sucrose consumption	Operant self-administration	(Walker et al. 2015b)
Rxfp3	Mouse	↑ alcohol consumption (males)	Two-bottle free choice	(Shirahase et al. 2016)

Table 1.2 Stress and anxiety behaviours associated with RXFP3 activation

Compound	Species	Effect	Assay	Reference
H3	Rat	↓ spontaneous locomotion	Spontaneous locomotion	(Nakazawa et al. 2013)
H3	Rat	↓ anxiety	Shock-burying test	
H3	Rat	↓ anxiety	Elevated plus maze	
RXFP3-A2	Rat	↓ anxiety	Light/dark box	(Ryan et al. 2013a)
RXFP3-A2	Rat	↓ anxiety	Elevated plus maze	
RXFP3-A2	Rat	↓ anxiety (non-naïve mice)	Forced swim test	
RXFP3-A2	Rat	↓ elevated anxiety	Light/dark box	(Zhang et al. 2015)
RXFP3-A2	Rat	↓ elevated anxiety	Social interaction	
R3(B1-22)R*	Rat	↓ anxiety (slight)	Elevated plus maze	

antagonist

Table 1.3 Arousal and cognition behaviours associated with RXFP3 activation

Compound	Species	Effect	Assay	Reference
R3/I5	Rat	↑ locomotion in light (inactive) phase	Locomotion	(Sutton et al. 2009)
R3(BΔ23–27)R/I5*	Rat	↓ spatial memory in SAT	SAT	(Ma et al. 2009a)

Table 1.4 Feeding and motivation/reward behaviours associated with RXFP3 activation

Compound	Species	Effect	Assay	Reference
H3	Rat	↑ food intake	Feeding studies	(McGowan et al. 2005)
H3	Rat	↑ food intake	Feeding studies	(Hida et al. 2006)
R3/I5	Rat	↑ body weight	Feeding studies	(Sutton et al. 2009)
R3(BΔ23–27)R/I5*	Rat	↓ agonist-induced body weight	Feeding studies	
RXFP3-A2	Rat	↑ body weight	Feeding studies	(Shabanpoor et al. 2012)
RXFP3-A3*	Rat	↓ agonist-induced weight gain	Feeding studies	
R3(B1-22)R*	Rat	↓ alcohol self administration	Two bottle free choice	(Ryan et al. 2013b)
R3(BΔ23–27)R/I5*	Rat	↓ stress-induced alcohol reinstatement	Alcohol reinstatement	
R3(B1-22)R*	Mouse	↓ food intake	Feeding studies	(Smith et al. 2014a)
H3	Rat	↑ food intake, females > males	Feeding studies	(Calvez et al. 2015)
R3(B1-22)R*	Mouse	↓ salt intake	Sodium depletion/repletion	(Smith et al. 2015)
R3(B1-22)R*	Rat	↓ stress-induced food intake (BEP)	Stress-induced binge eating	(Calvez et al. 2016a)

antagonist

1.2.5 Role of RLN3/RXFP3 signalling and potential implications in human disease

Based on putative functions of the NI, along with the distribution of RLN3 projections and RXFP3 receptors, it has been postulated that RLN3/RXFP3 systems play a part in the ascending arousal network, being activated in response to stressors, exerting control over locomotor behaviour and modulating theta rhythm via its multiple targets in the hypothalamus. These systems are proposed to be involved in neuroendocrine function, signalling energy balance and connecting nutritional status to reproductive function (Ganella et al. 2013, McGowan et al. 2009). Behavioural studies in rodents have indeed shown that RLN3/RXFP3 networks are involved in behavioural arousal, stress responses and anxiety, cognition, motivation, and feeding and metabolism.

Therefore, RLN3/RXFP3 systems have been suggested to be a putative target for the treatment of neuropsychiatric diseases (Kumar et al. 2016, Smith et al. 2014b), although there is currently little evidence or direct clinical relevance. Polymorphisms in *RLN3* genes have been reported to be associated with various metabolic disorders, in a population that was treated with anti-psychotics (Munro et al. 2012). Also, high serum levels of RLN3, which were detected by enzyme-linked immunosorbent assay of human H3 relaxin, were linked with patients with metabolic syndrome (Ghattas et al. 2013). In Alzheimer's patients, neocortical levels of putative protein RXFP1 and RXFP3 immunoreactivity seemed to correlate with levels of depression, but not Alzheimer's disease symptoms (Lee et al. 2016). While the preclinical studies examining effects of the RLN3/RXFP3 particularly relating to the NI have been suggestive (reviewed in Kumar et al. 2016), the link to human disease is weak, prompting additional clinical studies.

1.2.6   Rln3 system in fish

Teleosts possess six RLN family genes, due to an additional round of whole genome duplication: *rln* as an orthologue of *RLN* (or human *RLN2*); two paralogues of *RLN3*, *rln3a* and *rln3b*; an orthologue of *INSL3*, *insl3*; and two paralogues of *INSL5*, *insl5a* and *insl5b* (Good-Avila et al. 2009). In mammals, *RLN* underwent weak purifying selection, while *RLN3* has the lowest rates of substitution, reflecting strong purifying selection and being the most conserved of the RLN peptides (Wilkinson et al. 2005).   Conversely, evolutionary pressures were different in teleost, where *rln*, *rln3a* and *rln3b* all display strong purifying selection, suggesting that *rln* is closer to *rln3* than the mammalian orthologue *RLN* (Good-Avila et al. 2009). An amino acid alignment shows that the B-chain of zebrafish Rln is indeed 80% similar to Rln3a and Rln3b, 76% similar to human RLN3 and only 44% similar to human RLN1 and RLN2 (Fiengo et al. 2012). The A-chain is less conserved, with 45% similarity to Rln3a and Rln3b, 41% similarity with human RLN3 and RLN2, and 39% similarity with human RLN (Fiengo et al. 2012).

In zebrafish, *rln3a* and *rln3b* mRNA is localised in similar brain regions to mammalian *RLN3*. Slight differences exist between the paralogues, where double *in situ* hybridisation (ISH) revealed that *rln3a* is expressed in the NI and PAG, while *rln3b* is only expressed in the NI (Donizetti et al. 2009). Notably, the PAG population of *rln3*-expressing neurons in zebrafish is larger than the putative NI group, compared to the small mammalian PAG population in mammalian counterpart (Donizetti et al. 2008). Also, there is little or no expression of *rln3a* outside the brain, whereas *rln3b* expression was detected in the testes and ovaries. *rln3b* is expressed diffusely before 48 hours post fertilisation (hpf), after

which expression is restricted to the PAG (Donizetti et al. 2009), whereas *rln3a* expression is detected from 72 hpf, restricted in the PAG and NI (Donizetti et al. 2009). Due to the similarity of the rate of evolution and the slight differences in expression between the two paralogues, it is hypothesised that these duplicates have gone through sub-functionalisation, each retaining a partial role of the ancestral form (Donizetti et al. 2009, Good-Avila et al. 2009). Interestingly, *rln* was found to be expressed in zebrafish brain, and adults expressing *rln* in the telencephalic region around the anterior commissure, the preoptic area, and the NI with *rln3a* (Fiengo et al. 2012). Oustide the brain, *rln* is expressed in the pancreas and thyroid gland. This may indicate a role of rln in zebrafish as a neuropeptide with endocrine functions (Fiengo et al. 2012).

On the other hand, there are 10-11 *rxfp* genes in teleosts, of which three have been paired with central functions of the Rln3, whereby Rxfp3.1 is the receptor for Rln3b, and the duplicated Rxfp3.2a and Rxfp3.2b are receptors for Rln3a (Good et al. 2012). Other Rxfp3 receptors are postulated to have roles in the peripheral nervous system or have endocrine functions, such as Rxfp3.3b, Rxfp3.3a1, Rxfp3.3a2 for Insl5a, or Rxfp3.4 (Rxfp3.3a3 in zebrafish) for Insl5b (Good et al. 2012). Zebrafish expression of the *rxfp3.2b* mRNA can be found throughout embryogenesis, while *rxfp3.2a* mRNA was only found at the larval stage (Fiengo et al. 2013). Rxfp3.2b also shared more common brain localisation compared to mammalian RXFP3, being expressed in the optic tectum, thalamus, preoptic area, habenula, pineal gland and various nerve nuclei (Fiengo et al. 2013). Of the other Rxfp3 paralogues in zebrafish, only *rxfp3.1* and *rxfp3.3b* mRNA were expressed in embryonic and larval stages (Donizetti et al. 2015). Rxfp3.1 is the proposed receptor for Rln3b, and *rxfp3.1* mRNA is expressed in the interrenal

gland at the early pharyngula stage (24 hpf), switching expression to the rhombencephalic region in the larval stage (48 hpf) (Donizetti et al. 2015). The *rxfp3.3b* receptor displays more widespread mRNA expression, such as in the PAG, raphe, and caudal region of the hypothalamus in the brain, and the pancreas (Donizetti et al. 2015). These regions correspond to RXFP3 expression in mammalian brain, and it is hypothesiszed that duplicated Rxfp3 receptors in zebrafish underwent sub-functionalisation (Donizetti et al. 2015). Figure 1.2 depicts a simplified version of the Rln3/Rxfp3 system in larval zebrafish at 5 days post fertilisation (dpf), where receptor expression is illustrated only by rxfp3.2b expression.
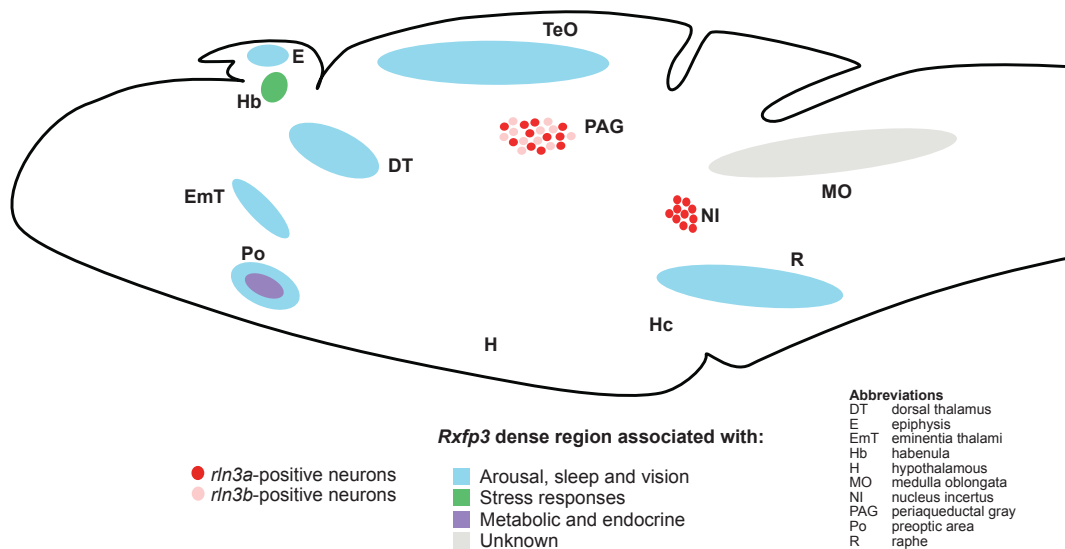
Figure 1.2 Rln3/Rxfp3 system in the zebrafish brain

Schematic of the Rln3/Rxfp3 system in larval zebrafish at 5 dpf. Ligand localisation is based on *rln3a* and *rln3b* mRNA expression as described by Donizetti et al. (2008), whereas receptor localisation is based on *Rxfp3.2b* mRNA expression, as described by Fiengo et al. (2013).

There are only a few studies regarding Rln3 function in teleosts. Transcriptomic analysis of the brains of threespine stickleback identified the activation of the Rln pathway in fish that were exposed to olfactory, tactile and visual cues of a predator, indicating a similar role in stress responses compared to mammalian studies (Sanogo et al. 2011). Despite its highly conserved brain functions, Rln3 in teleosts was also shown to have functions outside the brain. *rln3* and *rxpf3* mRNA expression was observed in zebrafish ovarian tissues, and immunohistochemistry also identified the peptide in killifish (Wilson et al. 2009). H3 was also able to enhance production of 17β-estradiol in maturing follicles of killifish, implying functions in reproductive tissues (Wilson et al. 2009). In euryhaline threespine sticklebacks, the relaxin peptide family had osmoregulatory functions, with *rln*, *rln3a* and *rln3b* transcript levels changing with salinity conditions, particularly *rln3b* (Kusakabe et al. 2014). Transcriptional profiling of zebrafish cardiomyocytes also identified Rln3a as an important player in heart regeneration, acting downstream of Stat3 after injury (Fang et al. 2013). Rln3 administration also increased cardiomyocyte proliferation after Stat3 inhibition (Fang et al. 2013).

1.3 Hypothesis and aims

The research described in this thesis is primarily concerned with elucidating the role of the neuropeptide Rln3 in zebrafish behaviour, which is currently unknown. Previous studies have shown that RLN3 is the most evolutionarily conserved peptide of the RLN family (Wilkinson et al. 2005), where teleost Rln3 evolved similarly to mammalian RLN3 (Good-Avila et al. 2009). There is also evidence for the existence of zebrafish Rln3 homologues (Donizetti et al. 2009, Good-Avila et al. 2009), with similar receptor expression patterns to those in rodent studies

(Donizetti et al. 2009, 2015, Fiengo et al. 2012, 2013), which can be compared in Figure 1.1 and Figure 1.2. Hence, a logical hypothesis would be that this neuropeptide has a conserved function in zebrafish behaviours. Considering that species differences exist between RLN3-mediated behaviours in rats and mice are apparent, one can expect disparities in zebrafish and rodent behaviour as well. However, using a novel model organism can help to identify commonalities between species and consolidate general rules for RLN3 function in behaviour.

The aims of this thesis research are as follows:

1) Establish mutant lines for the Rln3 system in zebrafish using the CRISPR/Cas9 system targeted to both ligand and receptor genes. Genetic characterisation of these mutants is important, as CRISPRs will create mosaic animals with a variety of insertions and deletions (indels). Furthermore, RNA analysis will determine if gene expression is disrupted due to the genetic manipulations.

2) Test the effect of these mutations in Rln3 mediated behaviours. Rodent mutants display phenotypes in feeding, circadian-dependent arousal and anxiety, which can be tested in zebrafish. Zebrafish also display characteristic behaviour to an increase or decrease in illumination, called the visual motor response. In light of the observations that RLN3 is involved in circadian-cycle dependent locomotion in rodents, Rln3 signalling may also be involved in zebrafish responses to light or dark stimuli on a shorter time scale.

Mutate *rln3* locus

Design CRISPR

rln3a
rxfp3.2a
rxfp3.2b

Mutation screening

Sequencing
HRMA
RFLP

Behavioural phenotyping

Feeding

Body length
Body weight

Stress & anxiety

Novel tank diving
- baseline condition
- stressed condition

Visual motor assay

Locomotor activity
- light
- dark
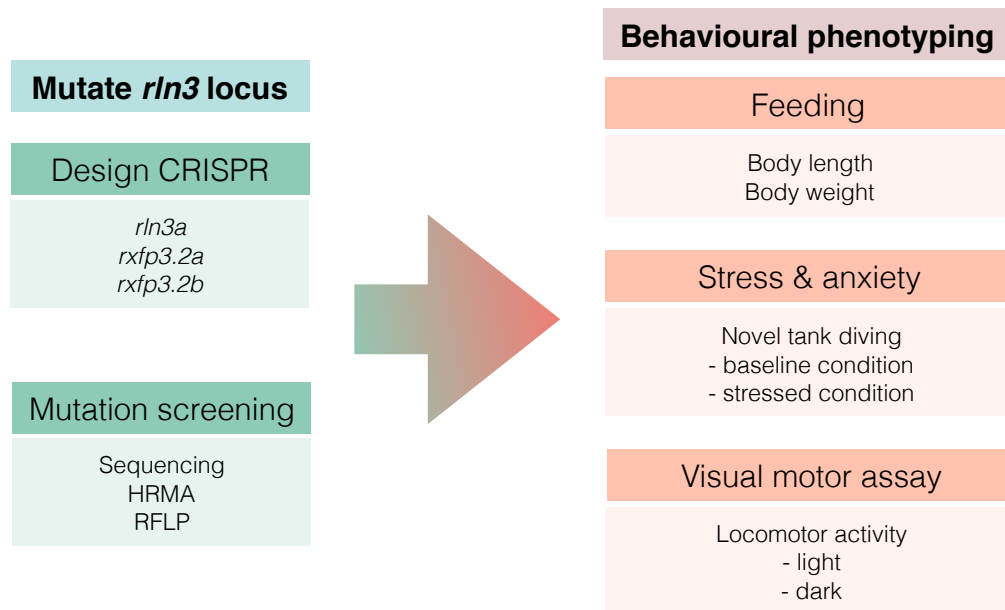
Figure 1.3 Hypothesis and aims

To test the hypothesis that Rln3 has conserved roles in zebrafish behaviour compared to rodents, two aims have been established. Firstly, mutants for the Rln3 system will be created using the CRISPR/Cas9 system, targeting the ligand *rln3a* and the receptors *rxfp3.2a* and *rxfp3.2b*. Multiple mutation screening methods such as sequencing, high resolution melt analysis (HRMA) and restriction enzyme length polymorphism (RFLP) will be employed for mutation detection. Secondly, mutants will be tested in behavioural assays for known Rln3-mediated behaviours in rodents, such as feeding, anxiety, and locomotion.

Overall, these approaches will provide insight into Rln3 functions in zebrafish.

Zebrafish models have several advantages over rodent models, such as ease of

genetic manipulation, possibility for high throughput behavioural assays, relatively

simple behavioural repertoire and transparent larvae for imaging, and this could

reveal novel RLN3-mediated behavioural function and associated network

activity.

2. MUTAGENESIS OF THE RLN3/RXFP3 SYSTEM

2.1 Introduction

To investigate the role of RLN3/RXF3 signalling in behaviour using zebrafish, both ligand and receptor mutants were created. Genome editing techniques recruit engineered DNA-binding nucleases to create double stranded breaks (DSBs) in a targeted locus, which are repaired by non-homologous end-joining (NHEJ) to create insertions or deletions (indels), producing mutations. Techniques such as zinc-finger nucleases (ZFNs) and transcription activator-like effector nucleases (TALENs) (Gaj et al. 2013) have been traditionally used in zebrafish to provide precise, efficient methods for genome engineering, but make use of protein DNA-binding domains for the recognition of target sites, which is costly and hinders the ease of design and usage.

Recently, type II clustered regularly interspaced short palindromic repeats (CRISPRs) found in prokaryotic adaptive immune systems with Cas9 (CRISPR-associated protein 9) nuclease has been developed for genome editing purposes (Cong et al. 2013, Jinek et al. 2012, Mali et al. 2013), making use of an RNA-guided nuclease instead. The system requires the target site to contain a protospacer adjacent motif (PAM) of 'NGG' to be recognised by a CRISPR RNA (crRNA), which, together with a trans-activating RNA (tracrRNA) in the presence of Cas9, creates DSBs. The two RNAs can be combined into a single guide RNA (sgRNA) (Jinek et al. 2012), simplifying the design and implementation of mutating target genes compared to earlier methods (Blackburn et al. 2013, Sander & Joung 2014).

Since the development of CRIPSRs for genome editing, the CRISPR system has been widely validated in zebrafish (Chang et al. 2013, Hwang et al. 2013a, Jao et al. 2013). Zebrafish CRISPR mutants have also been used as models for behaviour such as epilepsy and sleep (Grone et al. 2016, Yelin-Bekerman et al. 2015).

Here, an optimised protocol is described which allows the generation of mutant zebrafish within a week of injection of CRISPR/Cas9 mRNA and sgRNA. The sgRNA template was produced by using polymerase chain reaction (PCR) instead of lengthy cloning methods (Bassett et al. 2013). Additionally, high resolution melt analysis (HRMA) was used as a high throughput method of detecting mutants at high sensitivity (Bassett et al. 2013, Talbot & Amacher 2014). Once mutants have been characterised, restriction enzyme length polymorphism (RFLP) provided and quick and inexpensive way to genotype fish used in experiments. Furthermore, mutants were checked for RNA expression to verify if the mutation resulted in a loss in RNA.

2.2 Methods

2.2.1 Generation of mutants

Zebrafish *rln3* family gene sequences were first obtained from the Ensembl database (http://www.ensembl.org) (Yates et al. 2016). Ensembl transcript identification (ID) are listed in Table 2.1 for the respective genes from the 2014 version (Flicek et al. 2014). CRISPR targets were selected within these sequences using web-based tools such as ZiFit (http://zifit.partners.org/ZiFiT/) (Sander et al. 2007) or CHOPCHOP (http://chopchop.cbu.uib.no) (Montague et al. 2014) (Table 2.1, PAM sequence in bold). CRISPRs were chosen to target exonic regions in the 5' end to disrupt important downstream functional domains, and have minimal off-target effects based on analyses provided by ZiFit or CHOPCHOP.

Table 2.1 List of CRISPR targets

Gene	Ensembl transcript ID	CRISPR targets (5' → 3')
rln3a	ENDSDARG00000070780	GGAGTAAAGGCGCTGGACGC**CGG**
		TTTCCATCGGGATCCTCCGC**AGG**
rxfp3.2b	ENDSDARG00000061846	AGTGGGAGTCTGAAATGGAG**AGG**
rxfp3.1	ENDSDARG00000057410	GGAGATAAACCCGACTTCAT**GGG**

The sgRNAs for these targets were produced using a PCR-based method to create a template for transcription (Bassett et al. 2013). PCR was performed with the primers in Table 2.2 using Phusion High-Fidelity polymerase (ThermoScientific), where the 18-20 bp target sequence (bolded) is incorporated into the forward primer. The product produced was approximately 100 bp long.

The PCR reaction was cycled at (98 °C 30 s, 29 cycles of [98 °C 10 s, 60 °C 30 s, 72 °C 15 s], 72 °C 10 min, 10 °C forever), and the PCR product was purified with the QIAquick PCR purification kit (Qiagen). At least 200 ng purified PCR template was used for transcription of sgRNA with the T7 MEGAscript transcription kit (Life Technologies) for 2–4 h. After 1 h of DNAse treatment, RNA was recovered using ammonium acetate precipitation at –20 °C overnight and then eluted in 20 μL nuclease free water. Neat sgRNA solution (5 μg–10 μg) was stored in 1 μL aliquots at –80 °C for future use. To make the Cas9 mRNA, the expression vector pT3Ts-nCas9n (Addgene plasmid #46757) was linearised using XbaI and transcribed using the mMessage mMachine transcription kit (Life Technologies). Cas9 mRNA was then capped and polyadenylated using the Poly(A) kit (Ambion). After being precipitated in lithium chloride at –20 °C overnight, Cas9 mRNA was eluted in 30 μL nuclease free water and stored similarly to the sgRNA. 1 μg of linearised plasmid template typically yielded about 900 ng–1.3 μg of mRNA. Zebrafish embryos were injected with 1 nL of mixture containing 1 μL neat sgRNA with 1 μL neat Cas9 mRNA at the 1-cell stage.

Table 2.2 List of primers for sgRNA template

Primer (5' → 3')
F   GAAATTAATACGACTCACTATA**(n)**$_{18\text{-}20}$GTTTTAGAGCTAGAAATAGC
R   AAAAGCACCGACTCGGTGCCACTTTTTCAAGTTGATAACGGACTAGC CTTATTTTAACTTGCTATTTCTAGCTCTAAAAC

2.2.2 Detection of mutants

2.2.2.1 DNA extraction and sequencing

To check for mutagenesis, DNA was extracted from either 2–5 dpf embryos or adult fins by digesting in 20 μg/mL Proteinase K solution in TE buffer at 55 °C for 2 h followed by denaturation of Proteinase K at 95 °C for 10 min. Using VectorNTI, primers were designed to flank the CRISPR target site (Table 2.3). PCR was conducted using Taq polymerase (ThermoFisher Scientific) and cycled at 95 °C 2 min, 29 cycles of (95 °C 30 s, T_aOpt 30 s, 72 °C 30 s), 72 °C 10 min, 10 °C forever), where T_aOpt represents the optimal annealing temperature as determined by VectorNTI. The mutated sequence was determined by sequencing the PCR product with BigDye Terminator v3.1 (Life Technologies) and the forward primer. Sequences were aligned to the WT sequence using Geneious version 7.1.5 (www.geneious.com) (Kearse et al. 2012).

Table 2.3 List of primers for genotyping

Gene	Primer (5' → 3')	Size	T_aOpt
rln3a	**F** TCTCAGACTTTATCTCGCAGGGTTATCA	481 bp	56.7 °C
	R TCAAGCAACTTATAGAGCTTAGAGCTGAAA		
rln3a (HRMA)	**F** GCAAAAAGCACAGAACTTCG	214 bp	60.0 °C
	R ATGACAGCACGGATGAACTC		
rxfp3.2b	**F** GCGTCATGCTCAGCCGAGTATAA	569 bp	57.6 °C
	R CTGCAGGTCTGTTAGAGCCAAACC		
rxfp3.1	**F** ATAAAAAACGCAGCGAGCTGTCAG	780 bp	56.8 °C
	R CGACGTCTCTTACTTTTCAACGCC		

2.2.2.2   High resolution melt analysis (HRMA)

High resolution melt analysis (HRMA) is a quantitative reverse transcription PCR (qRT-PCR) based technique that can distinguish PCR amplicon sequences at a resolution of 1 bp, making it a sensitive, high-throughput method of mutation detection. With HRMA, the melt curve of the qRT-PCR reaction is produced using a low ramp rate of 1% during amplicon melting such that slight differences in melting temperature due to single bp changes can be detected, as well as changes in melt curve shape. The HRMA software (Applied Biosystems) would then normalise raw melt curve data and allocate the samples as different variants.

Primers were designed using Primer3web version 4.0.0 (http://primer3.ut.ee) (Untergasser et al., 2012) of about 20 bp in length to a melting temperature of 60 °C, flanking the CRISPR cut site (Table 2.3). Amplicons were designed to be 150–250 bp and checked for a single melt peak using the web-based software uMELT (https://www.dna.utah.edu/umelt/umelt.html) (Dwight et al. 2011). This was found to be a crucial step for HRMA to be accurate as the analysis is based on the melt curve.

Extracted DNA samples were diluted to 20 ng/μL in nuclease-free water and 1 μL was used for each reaction. Injected fish samples were tested along with three WT controls and a no-template control, all in duplicates as technical controls. The reaction mixture was made up following the manufacturer's protocol, using the recommended MeltDoctor (Applied Biosystems) saturating DNA dye. The thermal cycler protocol was set to cycle at (95 °C 10 min, 40 cycles of [95 °C 15 s, 60 °C 1 min], 95 °C 10 s, 60 °C 1 min, 95 °C 15 s, 60 °C 15 s, 10 °C forever). Variant

calls were analysed using the HRM software to determine mutated fish. The mutated sequence was determined by using BigDye (Life Technologies) to sequence the HRM product with the forward primer.

2.2.2.3   Restriction enzyme length polymorphism (RFLP)

WT and mutant alleles were also distinguishable by restriction fragment length polymorphism. After DNA extraction and amplifying the *rln3a* gene (primers used in Table 2.3), 4 μL of PCR product was used in a 10 μL digest reaction using SfoI and CutSmart buffer (NEB) and incubated at 37 °C for 15 min to 1 h. The digested and undigested fragments corresponding to mutant or WT allele could be easily resolved on a 1.5% agarose gel by electrophoresis.

2.2.3   RNA analysis

2.2.3.1   ISH

4 dpf larval zebrafish in a nacre background were treated with 1-phenyl-2-thiourea (PTU) before fixing in 4% paraformaldehyde at 4°C overnight and stored in methanol at –20 °C. A DIG-labelled probe was generated against the entire coding region of the *rln3a* gene using primers adapted from Donizetti et al. (2009) (Table 2.4) with a T3 start site at the 5' end of the reverse primer (in bold). cDNA probes were made and hybridisation was carried out on fixed fish using the protocol described by Thisse and Thisse (2008). Labelled larvae were cleared and mounted in glycerol. They were imaged using differential contrast microscopy, with a 20x 0.5 NA air objective on a Zeiss Imager M2 (Oberkochen, Germany) using an AxioCam Hrc camera. A z-stack was collected and processed using the Extended Focus function to maintain focus throughout the stack.

Table 2.4 Primers for *rln3a* ISH probe

Primer (5' → 3')
F   AAAGCACAGGTAGACCATCAGG
R   **AATTAACCCTCACTAAAGGG**TGCAGCCCCATTTGCAGCAGG

Adapted from Donizetti et al. (2009)

2.2.3.2 RT-PCR

Adult fish were iced and decapitated and brains were dissected in ice-cold Ringer's solution (116 mM NaCl, 2.9 mM KCl, 1.8 mM $CaCl_2$, 5 mM HEPES pH 7.2). RNA was extracted using the PureLink® RNA Mini Kit (ThermoFisher), where freshly dissected whole brains were kept in lysis buffer on ice until all brains were dissected, and then homogenised before proceeding with the manufacturer's protocol. This extraction typically yielded about 100 ng/μL RNA with A260/280 values between 1.80 and 2.10. 70 ng of RNA was then reverse transcribed into cDNA using SuperScript III First Strand Synthesis System for RT-PCR (ThermoFisher), which yielded about 1 μg of cDNA. A control containing no reverse transcriptase (RT–) was conducted with each reverse transcriptase experiment, to check for genomic DNA contamination. PCR using primers to detect the full-length *rln3a* transcript (Table 2.4) was conducted on cDNA samples of WT and mutant fish.

2.2.3.3 qRT-PCR

Primers were designed using the web-based software Primer3web version 4.0.0 (http://primer3.ut.ee) (Untergasser et al. 2012). The primers used are listed Table 2.5, for zebrafish β-actin1 (*actb1*) as an internal control and the gene-specific primer for *rln3a*. Primer pairs were designed to prevent the nonspecific

amplification of genomic DNA where possible. The *actb1* primer spans an exon-exon boundary, while the *rln3a* primers are exonic but spanned a large intron. The primers were first verified by having a single peak on a post-PCR melt curve, which produced single bands after electrophoresis on agarose gel, with no bands with the RT– controls.

qRT-PCR was performed using GoTaq® qPCR Master Mix (Promega) on 10 μL of 100 ng/μL cDNA using the MyiQ™ Real-Time PCR System (Bio-Rad). The PCR reaction was cycled at 95 °C 10 min, 40 cycles of (95 °C 15 s, 60 °C 1 min), 95 °C 10 s, 60 °C 15 s, 10 °C forever. Ten cDNA brain samples per genotype (*rln3a$^{sq4sj-/-}$* mutants and WT sibling) were tested in triplicates, along with both the RT– and no template controls. A standard curve was plotted to indicate that the PCR reaction was close to 100% efficiency. This validated the use of the comparative Ct (threshold cycle) method ($2^{-\Delta\Delta Ct}$ method) (Livak & Schmittgen 2001) which was used to analyse the group differences in expression.

Table 2.5 List of primers for qRT-PCR

Gene	Primer (5' → 3')	Amplicon size
actb1	**F** AGAGCTATGAGCTGCCTGACG	106 bp
	R CCGCAAGATTCCATACCCA	
rln3a	**F** CGTGCTGTCATCTTCACCTG	167 bp
	R GGGAGATTTGAGTCAGTGGC	

2.3 Results

2.3.1 Genetic characterisation of *rln3a* mutants

An understanding of the peptide structure is important in ensuring a loss of function when creating a mutant of the *rln3a* gene. A schematic of the preprocessing of RLN3 based on porcine RLN structure, adapted from Bathgate et al. (2006), is shown in Figure 2.1A. As a member of the RLN family of peptides, which has similar structure to insulin, RLN3 is first translated as preprorelaxin-3 (with signal peptide upstream of the B-chain, not depicted) before proteolytic cleavage into prorelaxin-3 and subsequently RLN3. An alignment between mammalian forms of RLN3 (*Homo sapiens*, *Mus musculus*, *Rattus norvegicus*) and its homologues Rln3a and -3b in zebrafish (*Danio rerio*) revealed that the B-chain and A-chain were highly conserved, but not the C-chain (Figure 2.1B). Important residues in the B-chain and A-chain include the receptor binding residues (red), receptor activating residues (yellow) and disulphide bond forming residues (blue) (Bathgate et al. 2013). These are present in fish, implying similarity in structure and hence function between RLN3 and Rln3a/Rln3b. This similarity has been detected before, as RLN3 is thought to be the ancestral form of RLN family which has been found to exist before teleosts (Wilkinson & Bathgate 2007). Additionally, the B-chain homologue was found in the Japanese lamprey (*Lethenteron japonicum*) by utilising the tblastn function of the Basic Local Alignment Search Tool (BLAST) (https://blast.ncbi.nlm.nih.gov/Blast.cgi), using the zebrafish *rln3a* sequence against the genome database (http://jlampreygenome.imcb.a-star.edu.sg) (Mehta et al. 2013), implying the existence of a more ancestral form of the peptide in a jawless vertebrate.

Of the zebrafish paralogues *rln3a* and *rln3b*, *rln3a* displays the same expression pattern in the brain as the mammalian homologues - being mostly expressed in the NI and PAG (Donizetti et al. 2009) - while *rln3b* is only expressed in the PAG. Hence, sgRNAs were targeted to two sites in the *rln3a* locus related to the binding region for its endogenous receptor (Figure 2.1C). One site was upstream of the receptor-binding region, and the other was within the region.

Sequencing analysis of CRISPR-injected embryos and WT sequences revealed two mutant alleles that were present. The first mutant allele, denoted as variant 1, had a 7 bp deletion, which resulted in a nonsense mutation. This mutant allele has been registered under the name *rln3a*^{sq4sj} in ZFIN, the Zebrafish Model Organism Database (www.zfin.org), and will be referred to by this name in subsequent text. Translating the mutant allele *in silico* indicated that the highly conserved receptor-binding motif was no longer present, and resulted in a premature stop codon (Figure 2.1D). The second mutant allele, denoted as variant 2, had a 9 bp insertion which added the amino acids VKL into the B-chain, but subsequently preserved the reading frame such that there was no disruption in the receptor-binding region, and no stop codon was produced (Figure 2.1E). Presumably, this mutation might not change in the peptide's receptor binding activity, and hence this mutant was not used for future behaviour experiments.
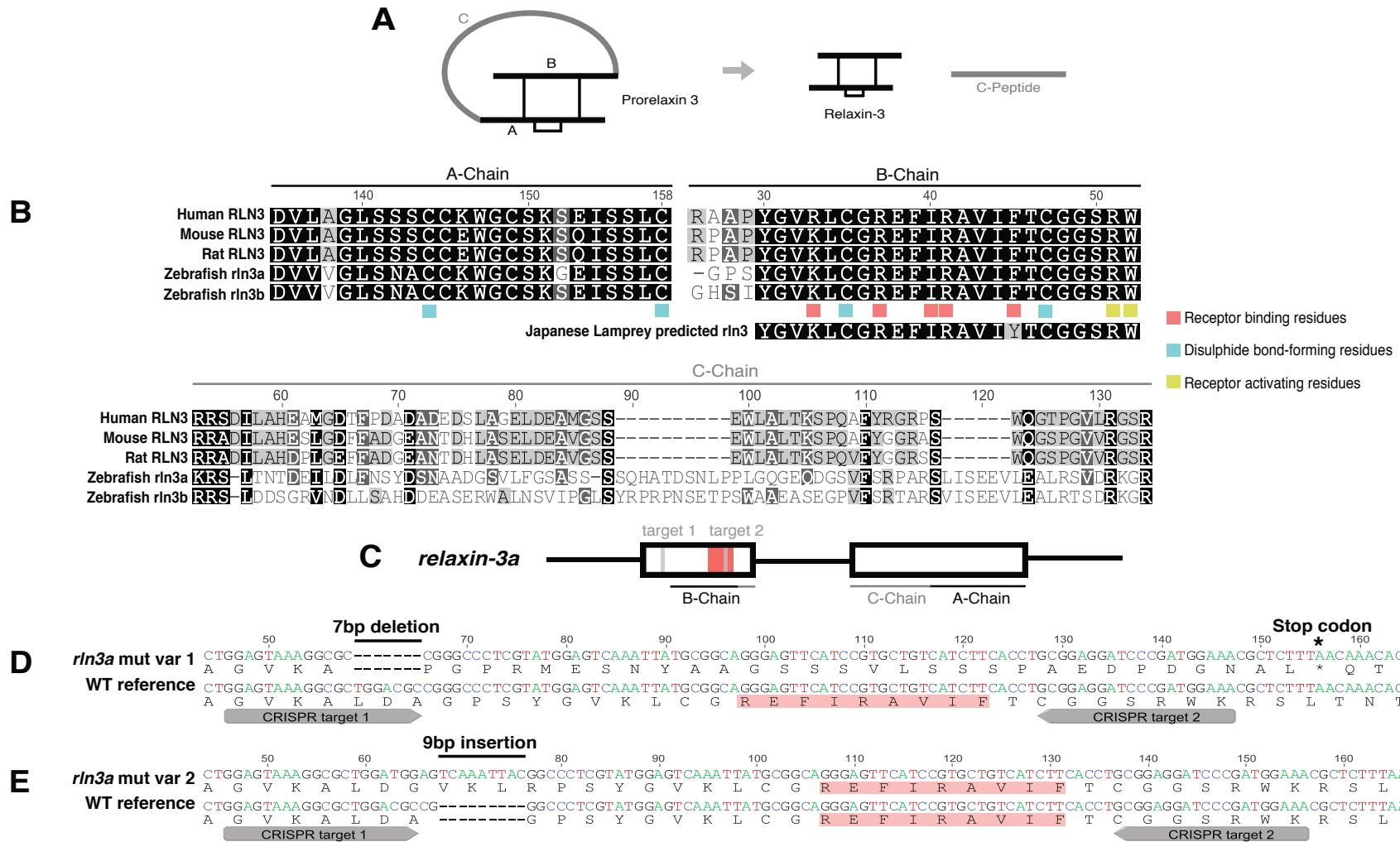
Figure 2.1 Genetic characterisation of *rln3a* mutants

(A) Schematic illustrating the preprocessing of prorelaxin-3 to mature RLN3. (B) Peptide alignment of the A-, B- and C- chains of RLN3 from human, mouse, rat and zebrafish, where A- and B- chains are highly conserved, but not the C-chain. Additionally, the Japanese lamprey was found to have a predicted homologous B-chain peptide. (C) Schematic illustrating the genomic arrangement of zebrafish rln3a, with CRISPR targets designed upstream or within the receptor-binding region in the first exon. (D) Variant 1 (*rln3a^{sq4sj}* allele) which has a 7 bp deletion that leads to a disruption of the receptor binding region and eventually a stop codon. (E) Variant 2 allele possessing a 9 bp insertion, inserting the amino acids VKL into the B-chain but not disrupting the receptor-binding region. No stop codon was produced.

2.3.2   Genetic characterisation of *rxfp3* mutants

RXFP3 is a GPCR containing extracellular domains - the N-terminus and three extracellular loops (exoloop 1, 2 and 3) - which are thought to be involved in ligand binding (Bathgate et al. 2013). Acidic residues found in exoloop 2 and 3 were found to contribute to the binding of the arginine residues in the ligand (Bathgate et al. 2013). A peptide alignment of the mammalian forms of RXFP3 (*Homo sapiens*, *Mus musculus*, *Rattus norvegicus*) and the zebrafish homologues Rxfp3.2a, Rxfp3.2b and Rxfp3.1 revealed that while the N-terminus is not very conserved, the exoloops have a high similarity, with the acidic residues ligand binding residues being present in all zebrafish paralogues (Figure 2.2A).

CRISPR targets were designed near the 5' region of the *rxfp* gene to create a mutation early in the gene. A CRISPR target for *rxfp3.2b* was identified at the start codon of the gene (Figure 2.2B), while for *rxfp3.1* a target was identified the N-terminus (Figure 2.2E). Sequencing analyses revealed multiple mutant alleles, where two variants in each receptor subtype were characterised. The *rxfp3.2b* variant 1 allele consisted of a single bp deletion, leading to an early stop codon in the N-terminus (Figure 2.2C). The second *rxfp3.2b* mutant allele, variant 2,

consisted of a 10 bp insertion, leading to an immediate stop codon after the first

four amino acids (Figure 2.2D). On the other hand, the *rxfp3.1* variant 1 mutant

allele consisted of a 3 bp insertion, after which the reading frame continued and

no stop codon was produced (Figure 2.2F). The *rxfp3.1* variant 2 mutant had a 5

bp deletion in the N-terminus, leading to an early stop codon before the first

exoloop (Figure 2.2G).
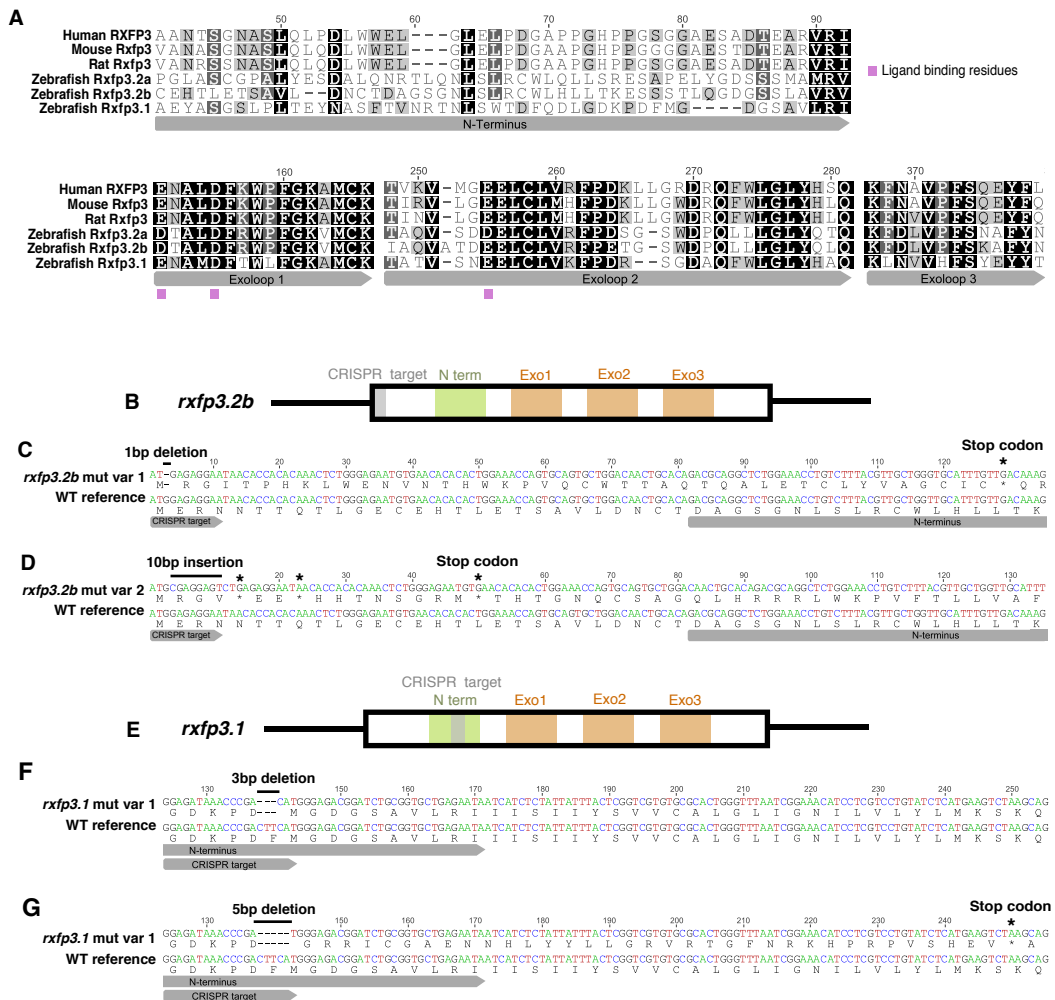
Figure 2.2 Genetic characterisation of *rxfp3* mutants

(A) Peptide alignment for RXFP3 from human, mouse, rat and zebrafish, illustrating the exoloops 2 and 3 contain acidic ligand binding residues which are conserved between all species presented. **(B)** Schematic of the *rfxp3.2b* gene, where the CRISPR target was designed at the start codon. **(C)** *rxfp3.2b* mutant allele variant 1, which consists of a single bp deletion, leading to a stop codon in the N-terminus. **(D)** *rxfp3.2b* mutant allele variant 2, which consists of a 10 bp insertion, leading to a stop codon after the first 4 residues. **(E)** Schematic of the *rxfp3.1* gene, where a CRISPR target was designed in the N-terminus. **(F)** *rxfp3.1* mutant allele variant 1, with a 3 bp deletion and resumed the reading frame after the addition of a single F amino acid. **(G)** *rxfp3.1* mutant allele variant 2, which consists of a 5 bp deletion, leading to a stop codon before the first exoloop in the peptide.

2.3.3 Mutation detection

CRISPR-induced mutations were determined most reliably via Sanger sequencing of PCR products containing the CRISPR target site. However, this method can be tedious and expensive to use on each CRISPR-mutated fish, and hence additional methods of mutation detection were explored. HRMA was used as a sensitive, high-throughput method, where variants from the WT controls could be determined in the F_0, F_1 and F_2 generations and verified by sequencing of representative fish from each group (section 2.3.3.1). Once the mutation type had been determined by sequencing, RLFP analysis (section 2.3.3.2) was used as a simple and inexpensive method to routinely genotype fish.

2.3.3.1   High resolution melt analysis

To determine the mutagenesis level of injected fish, DNA from the fins of 20 injected fish (F_0) was subjected to HRMA using primers designed around CRISPR target 1 (Table 2.3). Of the fish screened, 14 were recognised as a different variant from WT using HRMA, giving a mutation frequency of 70%. Sequencing analysis after HRMA revealed that different types of mutations were present. Multiple peaks in the chromatogram indicated mosaicism due to CRISPR cuts, which occurred around the target sequence (Figure 2.3).

F_1 fish were produced by crossing a single F_0 fish to the AB WT strain. HRMA detected two variants other than the WT variant from 20 F_1 adult fish screened. This demonstrated that the mutations were heritable in the offspring. Seven fish were of one mutant type, denoted as Mutant 1, while 6 fish were of another mutant type, denoted as Mutant 2, giving a total mutation frequency of 65%. Sequencing analysis revealed that the variants had two peaks of equal height

around the CRISPR cut site, representing heterozygosity. The indels produced from the CRISPR cut could then be determined by reading the sequence from the peak that does not correspond to WT sequence. Mutant 1 was found to possess a 7 bp deletion (referred to as variant 1 in Figure 2.4, or $rln3a^{sq4sj}$ in section 2.3.1), whereas Mutant 2 had a 9 bp insertion (referred to as variant 2 in section 2.3.1) (Figure 2.4).

F_1 fish of the same heterozygous phenotype (Mutant 1, $rln3a^{sq4s+/-j}$) were incrossed to produce F_2 fish. Of 8 embryos that were screened, HRMA was able to distinguish the homozygous ($rln3a^{sq4sj-/-}$) mutants (3/8, 37.5%) from the WT (2/8, 25%) and heterozygous ($rln3a^{sq4sj+/-}$) mutants (3/8, 37.5%). Sequencing analysis showed that homozygous mutants had a clean chromatogram peak after the CRISPR cut site, with a distinct 7 bp deletion. Heterozygous fish had chromatograms resembling parent fish (Figure 2.5).
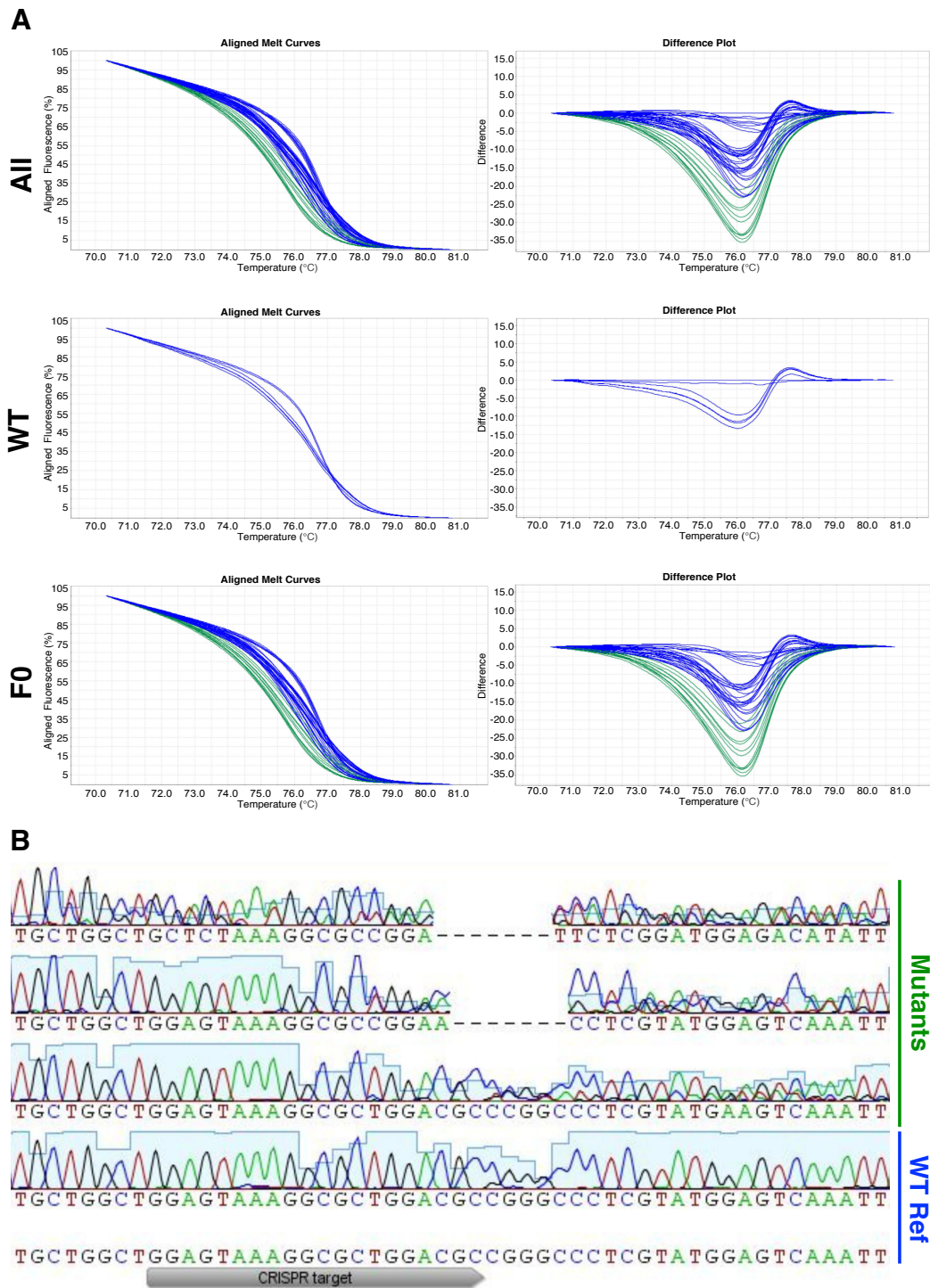
Figure 2.3 HRMA and sequencing of F_0 generation

(A) Aligned melt curves and difference plots of DNA from 20 injected fish and 3 WT controls. Graphs depict all fish, WT control, or F_0 fish only. From the HRMA, green traces represented mutant fish (14/20), while blue traces represent WT (6/20). **(B)** Analysis of 3 sequences. Compared to the WT reference sequences shown in blue, different types of mutations were present in injected fish. Multiple peaks were present around the CRISPR target sequence, indicating mosaicism due to CRISPR cuts.
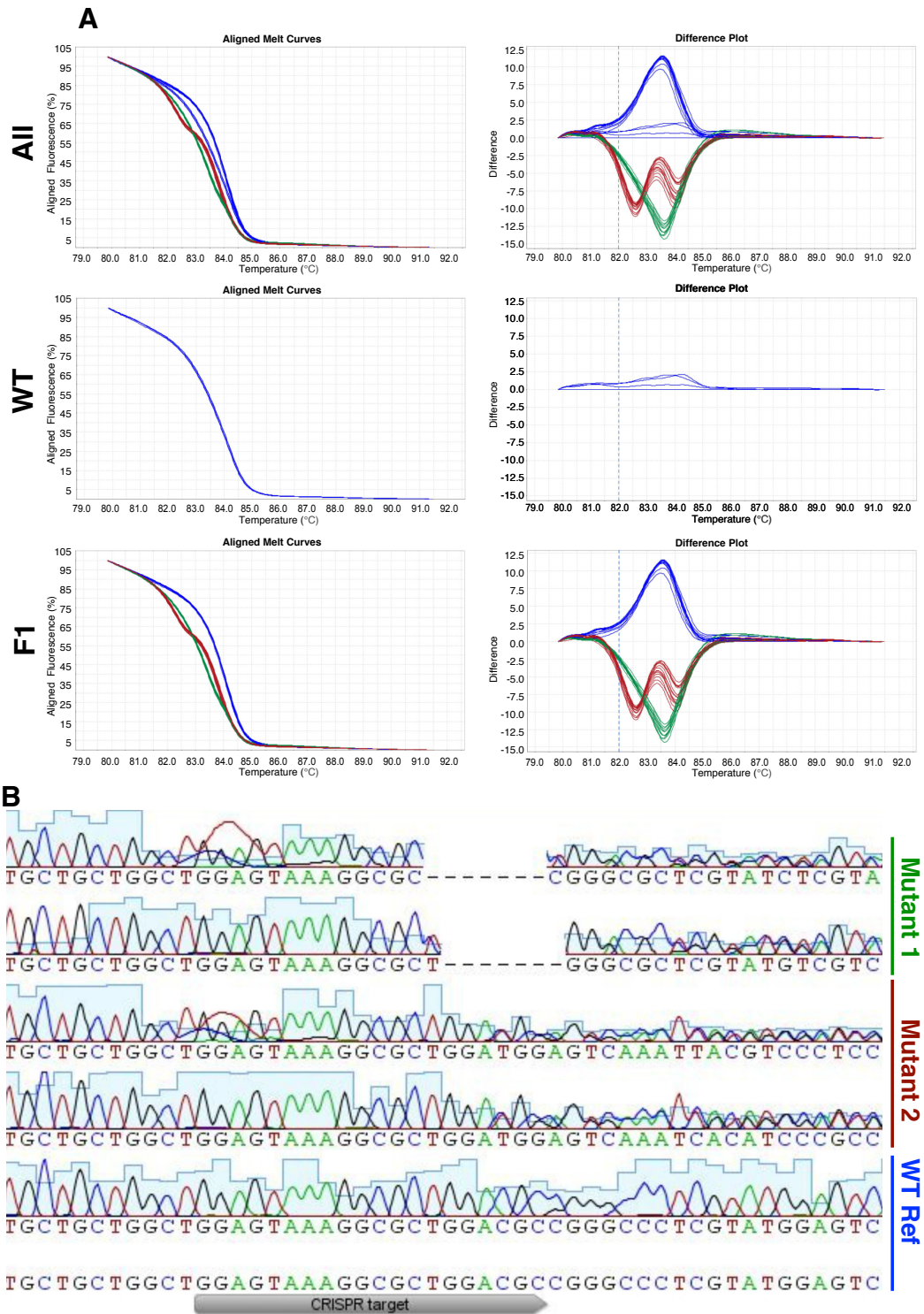
Figure 2.4 HRMA and sequencing of F_1 generation

(A) Aligned melt curves and difference plots of DNA from 20 heterozygous mutant fish (single mutant F_0 x WT outcross) and 3 WT control fish. Graphs depict all fish, WT fish or F_1 fish only. 3 groups were found in F_1 fish, where blue traces represent WT. **(B)** Analysis of 4 sequences. Compared to the WT reference sequences shown in blue (6/20), the two groups represent Mutant 1 (green traces, 7/20) or Mutant 2 (maroon traces, 6/20) genotypes.
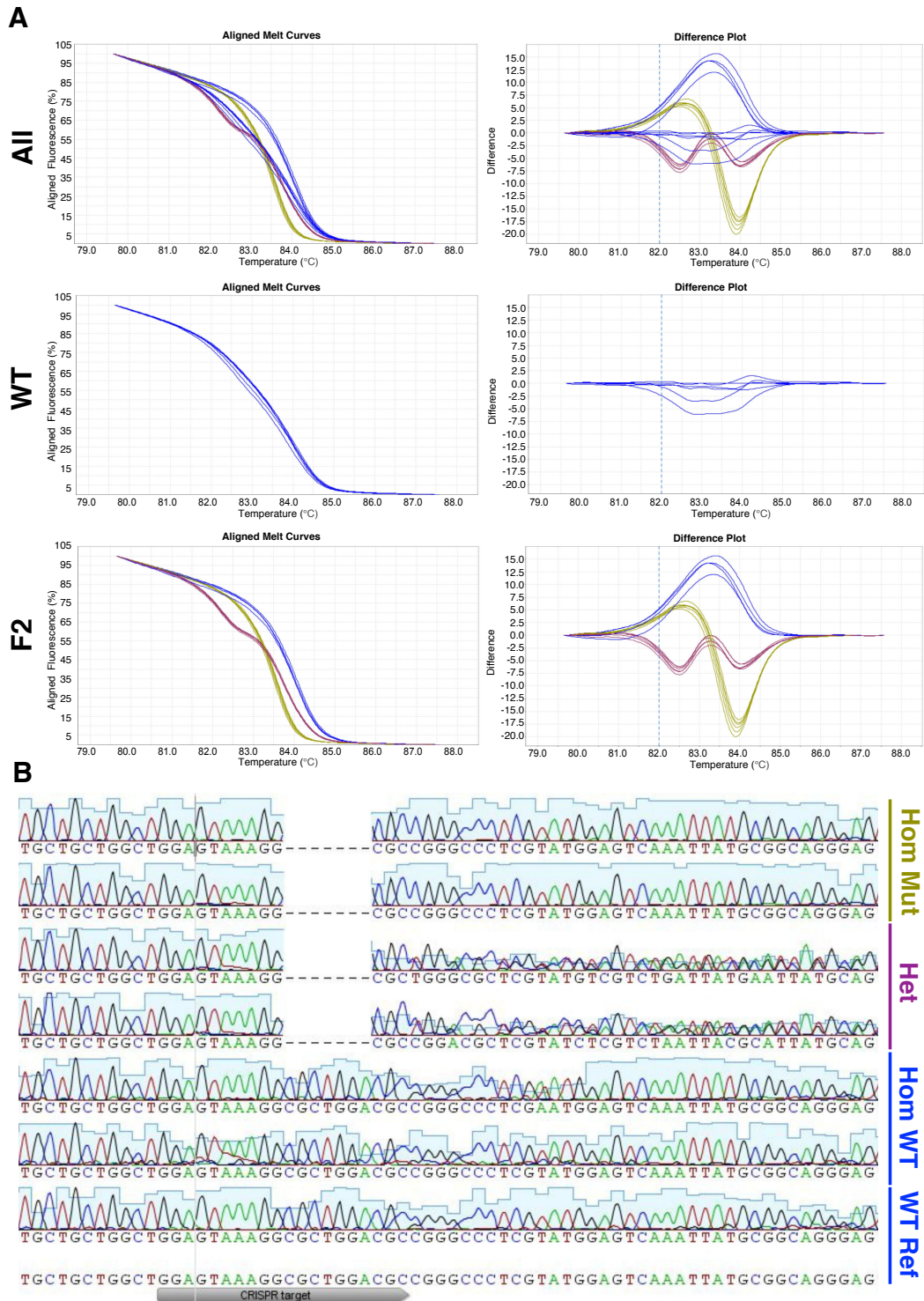
Figure 2.5 HRMA and sequencing of F_2 generation

(A) Aligned melt curves and difference plots of DNA from 8 embryos (Mutant 1 incross) and 3 WT controls. Graphs depict all fish, WT fish or F_2 fish only. From the HRMA, 3 groups were found in F_2 embryos. Blue traces represent WT. **(B)** Analysis of 6 sequences. Compared to the WT reference sequences shown in blue (2/8), the other two groups represent heterozygous mutants (purple traces, 2/8) or homozygous mutant traces (olive traces, 4/8) with a clear 7 bp deletion.

2.3.3.2   Restriction enzyme length polymorphism

Once mutant alleles were characterised, restriction enzyme cut sites within the mutated region allowed RLFP analysis as a quick and easy way to distinguish mutant and WT alleles. An SfoI cut site is present in the middle of the 481 bp amplicon of the *rln3a*^{sq4sj} mutant allele, giving rise to a blunt cut with two smaller fragments of 247 bp and 227 bp (Figure 2.6A). This cut site is not present in the WT allele. Before SfoI digest, the 7 bp difference between the mutant and WT amplicons is not distinguishable by gel electrophoresis (Figure 2.6B). After digest, the WT allele remains uncut at 481 bp, while smaller bands are present at 247/227 bp if the *rln3a*^{sq4sj} allele is present.
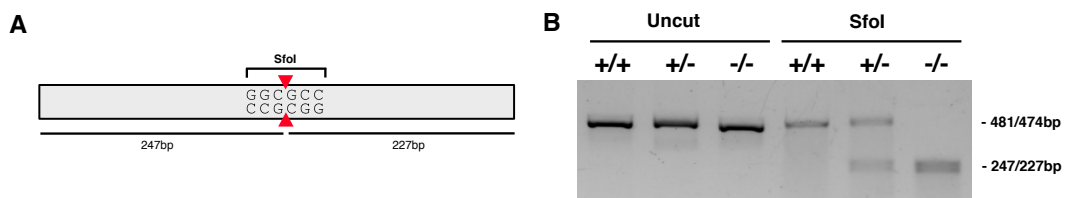
Figure 2.6 Detection of *rln3a*^{sq4sj} mutant allele using RFLP

(A) Schematic diagram depicting the location of the SfoI cut site within the 474 bp amplicon of the *rln3a*^{sq4sj} allele. This cut site is not present in the WT allele. **(B)** Gel electrophoresis of PCR amplicons for WT, heterozygous and homozygous DNA samples under the uncut and SfoI-digested conditions.

2.3.4   Summary of mutants created

The development of a quick workflow for creating and detecting CRISPR mutants allowed for the generation of multiple mutants for the *rln3a*, *rxfp3.2b* and *rxfp3.1* genes, and producing knockouts of both ligand and receptor in zebrafish. Table 2.6 summarizes the mutants created using this technique, and documents the percentage of mutations detected in both F_0 and F_1 generations, demonstrating the mutagenesis frequency for each target after injection, and the germline transmission rate for each mutant allele created.

Table 2.6 Summary of mutants created

sgRNA	%(#) Mosaic Adults (F0)	%(#) Mutant progeny (F1)	Mutant (F1) #	Mutation	%(#) Mutation type (F1)
rln3a	70% (14/20)	65% (13/20)	Variant 1	7bp del	54% (7/13)
			Variant 2	9bp in	46% (6/13)
rxfp3.2b	6.25% (1/16)	89% (17/19)	Variant 1	1bp del	53% (9/17)
			Variant 2	10bp del	47% (8/17)
rxfp3.1	80% (4/5)	100% (8/8)	Variant 1	3bp del	37.5% (3/8)
			Variant 2	5bp del	25% (2/8)
			Variant 3	N.D.	12.5% (1/8)
			Variant 4	N.D.	12.5% (1/8)
			Variant 5	N.D.	12.5% (1/8)

Abbreviations: del – deletions, in – insertions, N.D. – not determined

2.3.5   RNA Analysis

2.3.5.1   ISH and RT-PCR

ISH was conducted to determine the localisation of *rln3a* transcripts within the brain of *rln3a*$^{sq4sj-/-}$ mutants and WT siblings (Figure 2.7A, B). Fish were fixed at 4 dpf, as the PAG and NI are clearly labelled at this age (Donizetti et al. 2008), and this was observed in WT sibling fish (Figure 2.7A). The *rln3a*$^{sq4sj-/-}$ mutants, however, only displayed faint labelling (Figure 2.7B).

RT-PCR was used to detect full-length *rln3a* transcripts from cDNA of whole adult fish brains. Samples from WT fish presented strong bands, but only faint bands were present in samples obtained from *rln3a*$^{sq4sj-/-}$ mutants (Figure 2.7C). Both RT-PCR and ISH verify that RNA levels were reduced in the *rln3a*$^{sq4sj-/-}$ mutant, probably due to nonsense-mediated RNA decay mechanisms (Chang et al. 2007). This implies the lack of a functional peptide in the *rln3a*$^{sq4sj-/-}$ mutant, but not in WT siblings.

2.3.5.2   Quantitative expression of *rln3a*

qRT-PCR was used to quantify *rln3a* expression from *rln3a*$^{sq4sj-/-}$ mutants and WT siblings, using RNA extracted from whole adult fish brains (n=10). Primers demonstrated sufficient efficiency at 99.8% and 99.7% for *rln3a* and *actb1* respectively, validating the use of the 2$^{-\Delta\Delta Ct}$ method (Livak & Schmittgen 2001) for analysis (Figure 2.7E, G). The melt curve displayed a single peak for both amplicons, indicating specificity (Figure 2.7F, H). This was verified when the PCR products were visualised on agarose gel (Figure 2.7D), displaying single bands. The negative control without reverse transcriptase revealed no bands, indicating

no genomic contamination in the amplification.

The expression levels of *rln3a* were clearly depleted in the *rln3a*$^{sq4sj-/-}$ mutants (ΔCt *M* = -9.31, 95% CI [-9.69, -8.93]) with an approximately 16-fold decrease compared to WT siblings (ΔCt *M* = -5.32, 95% CI [-5.65, -4.99]) (Figure 2.7I), quantifying the lack of *rln3a* due to the mutagenesis.
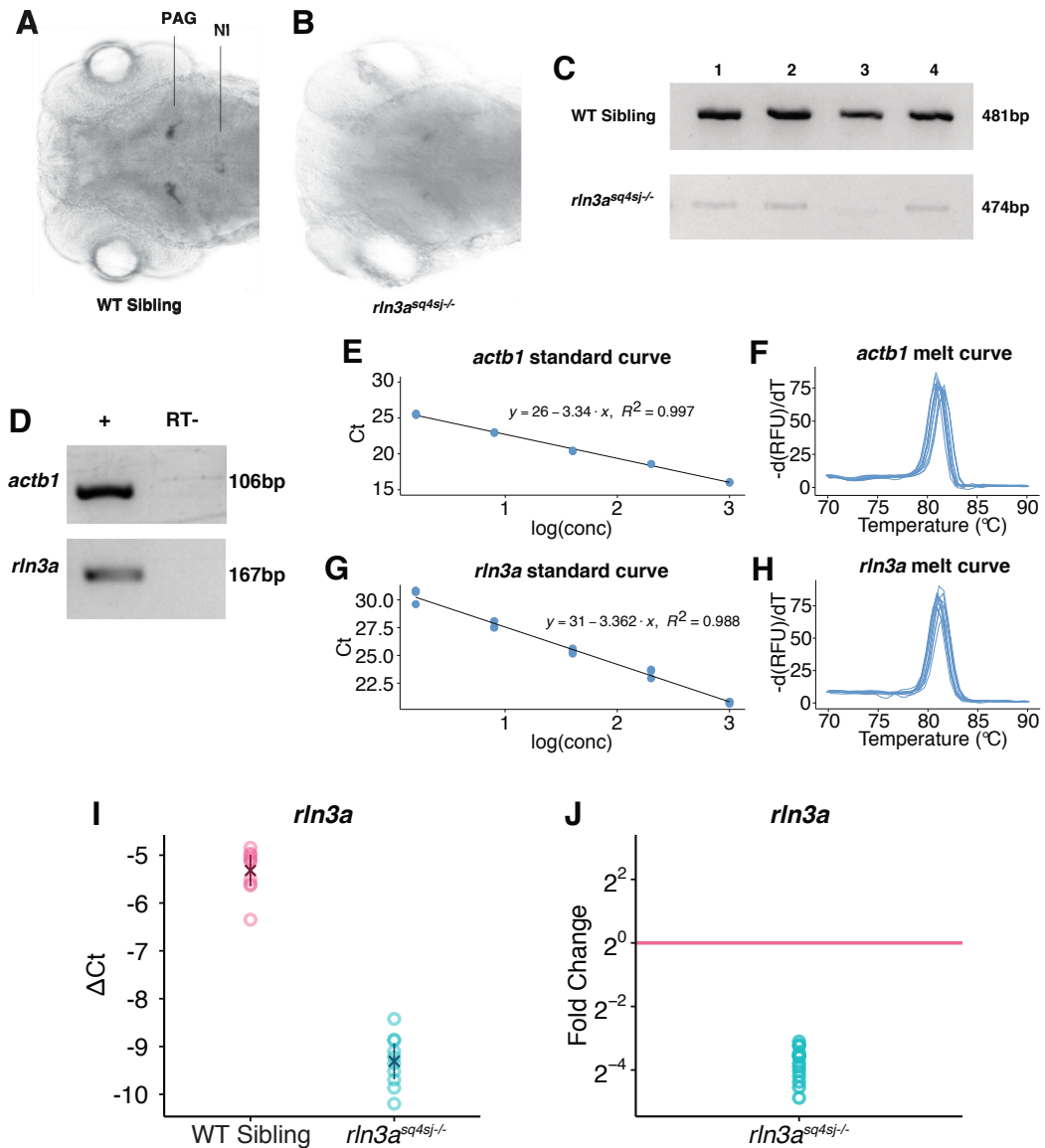
Figure 2.7 RNA analysis of *rln3a*^{sq4sj-/-} mutant

(A-B) ISH in 4 dpf larvae, where the PAG and NI are clearly stained in WT sibling fish but not in the mutant. **(C)** RT-PCR of full-length *rln3a* cDNA produces a strong band in WT sibling fish, while a faint band is observed from the mutant, implying *rln3a* depletion due to the mutation (4 representative fish). **(D)** qRT-PCR products display a single band on agarose gel, with no amplification in the RT– control. **(E-H)** Optimisation of primers. Standard curves indicate close to 100% efficiency in both primers used **(E, G)**. Melt curves display a single peak, indicating specificity of primers to the amplification product **(F, H)**. **(I)** Expression levels of *rln3a* in mutant and WT sibling fish ($n = 10$ per group), represented by normalised difference in threshold cycles ($\Delta Ct = Ct_{ref} - Ct_{gene}$). Individual fish samples are plotted as unfilled circles, crosses represent mean and error bars represent 95% confidence interval of the mean. **(J)** Fold change of expression, where averaged WT levels of *rln3a* are represented as 1 (pink line).

2.4 Discussion

2.4.1 CRISPR-based protocol for zebrafish mutagenesis

In the studies described in this chapter, *rln3a* mutants were created in a zebrafish line, which are useful in providing an alternative vertebrate non-rodent model to study the functions of RLN3. Zebrafish models are advantageous in neuroscience (Guo 2004), as they reproduce quickly and prolifically for high throughput screens for behavioural analysis, can be genetically manipulated to produce several useful transgenic lines for mapping networks, and the transparent larvae can also be imaged for brain activity *in vivo* (Friedrich et al. 2010, Kalueff et al. 2014). The advantage of using a CRISPR-based protocol for zebrafish mutagenesis is that it is quick and easy to implement, allowing multiple genes to be targeted and tested for mutations simultaneously.

Presented here is an optimised protocol for zebrafish mutagenesis using the CRISPR/Cas9 system. Initial methods for creating CRISPR mutations included lengthy cloning steps for sgRNA production (Chang et al. 2013, Hruscha et al. 2013, Hwang et al. 2013a), whereas this protocol uses a PCR-based method (Bassett et al. 2013) which dramatically reduces the time required from days to hours. This was coupled with a high-throughput screening method, HRMA, to increase the number of putative mutants that can be detected (Talbot & Amacher 2014). Mutants can be made in a week, from design of the CRISPR targets to the screening of injected embryos for mutations. However, it should be noted that not all the gene locations targeted were effectively mutated. For example, despite attempting to mutate the paralogue *rln3b* using 11 different sgRNAs, no mutation could be detected. This indicates that some genomic locations are more accessible for CRISPR cutting than others.

One way in which this protocol could be improved is to increase the mutagenesis frequency of the sgRNAs used, to enhance efficiencies in cutting, which range from 6.25% to 80% of injected embryos possessing mutations (Table 2.6). This is in line with various studies that also indicate target sequence-dependent mutagenesis efficiencies (Auer et al. 2014b, Burger et al. 2016, Gagnon et al. 2014, Hwang et al. 2013b, Jao et al. 2013, Varshney et al. 2015). Recent reports report that the efficiency of cutting can be increased by using a ribonucleoprotein complex for injection instead of the Cas9 mRNA, to ensure the activity of the Cas9-sgRNA complex before microinjection (Burger et al. 2016, Gagnon et al. 2014), which could be implemented to improve the mutagenesis frequency.

2.4.2 Genetic characterisation of zebrafish mutants

Although CRISPR mutants could be made and identified quickly, screening for mutants that could be used for behavioural analysis was a larger challenge. It is evident that the F_0 generation of CRISPR injected mutants possessed a high-level of mosaicism (Table 2.6), which could produce too much variability for behavioural experiments. Mosaicism occurs when CRISPRs cut the genome at different stages, and could be prevented by using active ribonucleoprotein CRISPR complexes that are saturating, such that cuts occur at the single-cell stage before division to produce limited mutant alleles (Burger et al. 2016). Furthermore, indels produced in multiples of three are unlikely to confer any change to the codon-reading frame, which might not disrupt protein function. As such, only alleles that lead to a production of a stop codon were used to propagate future generations, where minimally the F_2 generation would result in homozygous mutants for behaviour testing. Obtaining clean lines with this criteria required stringent screening protocols to ensure that differences in behaviour

could be attributed to a specific mutation type.

In this protocol, Sanger sequencing was used as the definitive method to determine mutagenesis, as sequences are clearly determined and the quality of reads can be defined. However, it is costly to run if many samples require processing. Hence, HRMA was employed due to its high sensitivity and high-throughput application, as well as the availability of a compatible qRT-PCR machine. HRMA managed to reliably detect mutations in the F_0, F_1 and F_2 generations of CRISPR mutants (Figure 2.3, Figure 2.4, and Figure 2.5 respectively) compared to Sanger sequencing. However, due to its high sensitivity, it required a high level of accuracy, especially in starting DNA concentration. This made it susceptible to errors due to pipetting inaccuracies or poor DNA quality, sometimes necessitating the use of Sanger sequencing to validate results. Frequent calibration of the machine was also required to maintain the quality of the results. Furthermore, there is limited choice for primer design to ensure accurate sequence detection. Some genomic loci may not be able to fit the criteria of having a single melt peak, immediately disqualifying the use of HRMA. A small amplicon of 150 bp–250 bp may not cover multiple target sites, such that only a small mutation region can be analysed at once. As such, it was difficult to obtain consistent results with multiple gene sets, and Sanger sequencing of PCR results proved to be more reliable.

Once mutation sequences were determined, RFLP proved to be a simple method to determine if offspring from a heterozygous incross were homozygous or heterozygous for WT or mutant alleles. Indels produced by CRISPR cuts are typically small (< 10 bp) and hard to resolve on agarose gel unless amplicons can

be differentially cut. Restriction enzyme digest is a technique that does not require much precision, and results were less ambiguous compared to HRMA. Restriction enzymes can also digest in as little as 15 minutes, which is faster than Sanger sequencing. However, this method is only applicable if there is a restriction site available to distinguish the WT from mutant allele, and would be more difficult when indels are smaller.

The mutation screening methods presented here are unable to detect the full amounts of mosaicism present in F0 injected embryos, for which deep sequencing is required, but which is costly to run (Burger et al. 2016, Gagnon et al. 2014). Cloning PCR products would be a more cost effective strategy, but is tedious and might be insufficient to detect low frequency alleles. An alternative would be to use fluorescent PCR coupled with capillary electrophoresis for high-throughput analyses at single bp resolution, which is more informative than HRMA, being able to determine allele length of various alleles in mosaics (Ramlee et al. 2015, Varshney et al. 2015), if such capabilities are available.

To ensure pure mutant lines for behavioural analyses despite our limited mutation detection capabilities, at least two outcrosses were performed to dilute residual mosaic or off target effects. Initially, multiple ligand and receptor genes were targeted with the intention of testing for effects in the various related genes, or produce double knockout mutants. However, the mosaicism produced by CRISPR/Cas9 caused difficulties in mutation screening, which made it increasingly difficult to maintain multiple mutation lines concurrently. To ensure that experiments were done with well-characterised mutants, only the $rln3a^{sq4sj-/-}$ mutant line was used for further behavioural analyses.

Being a relatively new technique, there has been some concern about off-target effects in CRISPR mutations, as guide RNAs are short at approximately 20 bp. However, detectable off-target effects have been shown to be low (Hruscha et al. 2013, Varshney et al. 2015) and found to be preventable depending on how target RNAs were chosen (Cho et al. 2014). In making the zebrafish mutants for the RLN3 system, sgRNA targets were chosen to have no predicted off-target effects as analysed by the web-based tools CHOPCHOP and ZiFit, and no similar sequences when searched in BLAST. In subsequent years after the mutant generation, an off target that contained two mismatches, at the bp 6 and 8 of the sgRNA, and was located on chromosome 13. This locus was screened and no mutation was detected.

With no known off-target effects, and with at least two generations of outcrossing, the CRISPR-generated $rln3a^{sq4sj-/-}$ mutants were tested for behavioural changes.

3. BEHAVIOURAL PHENOTYPING OF RLN3A MUTANTS

3.1   Introduction

Altered behaviour has been observed in *Rln3* mutant mice (Table 1.1), including behaviours such as feeding and the motivational aspects of feeding, anxiety, arousal, and locomotion, although described phenotypes were inconsistent between studies due to differences in background strain and other unknown factors. In the studies described in this chapter, the effects of mutations in the *rln3a* locus on stress and anxiety behaviours and body weight were tested in zebrafish.

One of the main features of RLN3 neurons is their activation in response to stress, which increases in RLN3 levels in rats (Banerjee et al. 2010, Tanaka et al. 2005, Watanabe et al. 2011a). As this response is dependent on CRF1 receptors, which are also implicated in anxiety behaviours in rats and humans (Hauger et al. 2009, Risbrough & Stein 2006), the loss of RLN3 may lead to altered anxiety levels.

Zebrafish have robust stress responses, and there are established methods for studying stress and anxiety in zebrafish (Cachat et al. 2010, Egan et al. 2009, Maximino et al. 2010). A number of manipulations have been demonstrated to be stressful for fish, including restraint, temperature, social isolation, predator exposure, crowding, chasing with a net and low tank water levels (Piato et al. 2011). Pharmacological agents can also alter zebrafish stress and anxiety behaviours, with fluoxetine and ethanol acting as anxiolytic agents; and caffeine and the alarm pheromone as anxiogenic agents (Cachat et al. 2010). The 'novel

tank diving' assay is a common method of testing anxiety in zebrafish, which quantifies exploratory behaviour in a novel space, and is likened to the large open field test for rodents. As the name suggests, zebrafish have an initial diving response to a novel tank for 70%–80% of the first minute (Gerlai et al. 2000, Levin et al. 2007), after which they begin to explore the tank. The tank is divided into the top and bottom halves, where fish would exhibit a chance level of being in either half after the first minute. Behaviours that reflect increased anxiety include increased latency to enter the top half of the tank, percentage time spent at the bottom, distance travelled at the bottom, number of erratic movements and number and frequency of freezing bouts (Cachat et al. 2010).

A behaviour that can be used to test dark-evoked responses is the visual motor response, where larval zebrafish display robust and distinctive patterns of increased and decreased locomotor activity according to alternating periods of light and darkness (Emran et al. 2008). At the transition from light to dark, the decrease in illumination triggers immediate extended swimming before activity levels decrease, while increased light causes a startle followed by transient freezing, before activity levels increase. Larval zebrafish are known to exhibit dark avoidance in a light-dark box, where dark stimuli appear to be aversive (Cheng et al. 2016, Colwill & Creton 2011). Hence, the visual motor response could be interpreted as stress-induced behavioural activation and has been used to test experience-dependent modulation of fear responses when exposed to repeated cycles of light OFF and light ON (Agetsuma et al. 2010). In this study, larvae with lesioned dorsal lateral habenula (dHbL) continued to have extended locomotion 14–24 min after the dark stimulus and did not reduce activity after multiple cycles as quickly as intact fish. In line with dorsal habenula's proposed

function of coping with stressors (Hsu et al. 2014, Lee et al. 2010), modified behaviour in lesioned fish was interpreted as an inability to regulate fear responses associated with the aversive light OFF stimulus despite multiple exposures to it. The PAG and NI are proposed downstream targets of the dHbL in zebrafish via the interpeduncular nucleus (Okamoto et al. 2012), implying that Rln3 may be involved in this behaviour through this pathway.

In our laboratory, calcium imaging of the zebrafish PAG revealed responses to light and dark stimuli (Figure 3.1A-E, unpublished data). Light ON did not have a consistent effect on PAG neurons, whilst light OFF consistently activated the lateral PAG, as indicated by a tonic rise in fluorescence of the genetically encoded calcium indicator GCaMP6f. There was no change to the activity of the NI in response to the light or dark stimuli. The dark-evoked activity occurred in the region of the PAG containing *rln3a*-expressing cells, as indicated by ISH (Figure 3.1). This raises the possibility that Rln3a signalling in the PAG may have a role in behavioural responses to dark stimuli.
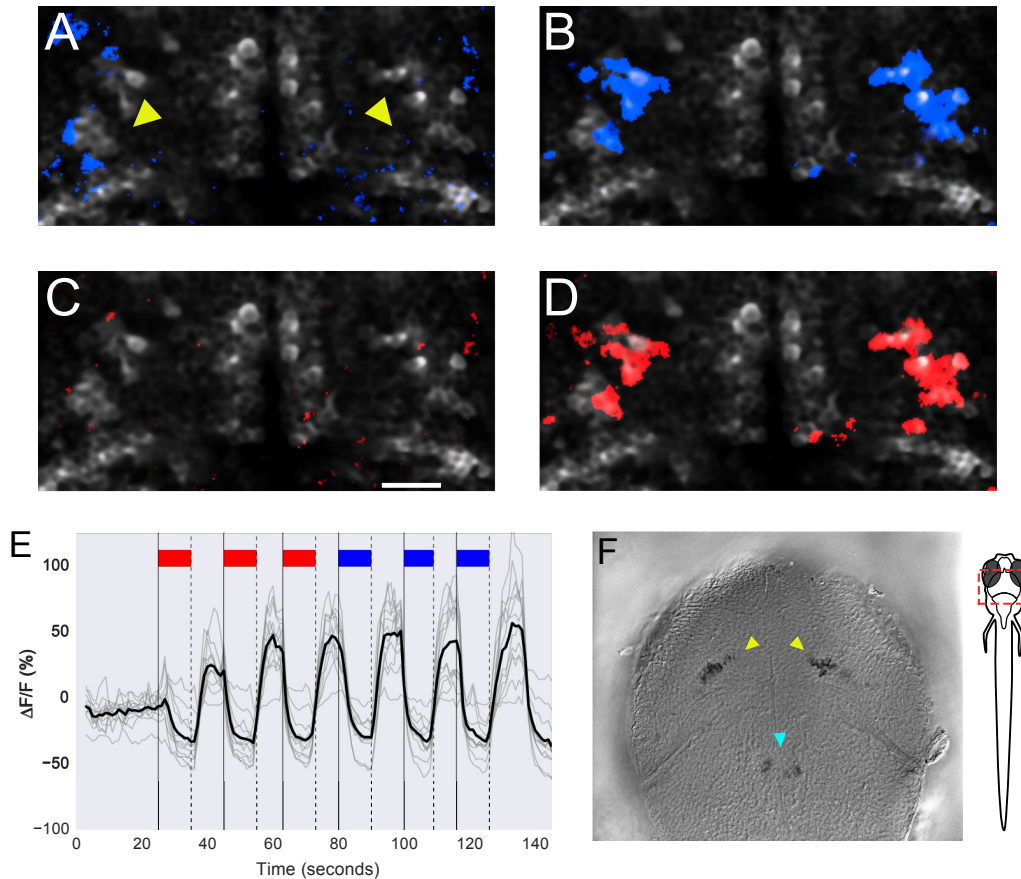
Figure 3.1 Two-photon calcium imaging of evoked activity in PAG.

(A-D) Yellow arrows indicate the lateral PAG in a single 7 dpf fish expressing elavl3:GCaMP6f. Blue pixels superimposed correspond to onset **(A)** and offset **(B)** of blue light and red pixels correspond to onset **(C)** and offset **(D)** of red light. The PAG responds only to offset of light. **(E)** Temporal traces obtained from the PAG to multiple pulses of light are shown in grey. Each grey trace comes from a single fish (n = 12). Black trace shows the average. Fluorescence increases in the PAG can only be seen when the light is switched off. Onset of light is indicated by a vertical black line and offset is indicated by dashed black line. Coloured wedges indicate the wavelength of light presented. ΔF/F is obtained by subtracting and dividing the raw fluorescence trace by its average. Scale bar = 25 µm. **(F)** *rln3a* is expressed in the PAG and in the NI in zebrafish. ISH, showing the location of *rln3a*-expressing cells in the PAG (yellow arrows) and NI (cyan arrow) in a 4 dpf fish. Figure kindly provided by Ruey-Kuang Cheng, Suresh Jesuthasan and Seetha Krishnan.

Although most of the literature on RLN3 has attributed functions of this peptide to expression in the NI, the PAG is involved in functions that have been ascribed to RLN3. The PAG has historically been identified as mediating defensive behaviours (Bandler & Depaulis 1991, De Oca et al. 1998, Fanselow 1991, Tovote et al. 2016) and has other roles in pain processing, vocalisation and autonomic regulation (Behbehani 1995). The columnar organisation within the PAG segregates defence circuits into opposing categories, where the ventrolateral unit is associated with quiescence and the lateral subunit controls defensive behaviours (Bandler & Shipley 1994). Notably, a study by Blasiak et al. (2013) demonstrated that the RLN3-producing neurons in the ventral and lateral portions of the PAG in rats innervates the intergeniculate leaflet, suggesting a role in circadian functions, sleep/arousal and visuomotor systems (Horowitz et al. 2004, Morin & Blanchard 2005). Furthermore, RLN3 null mutant mice exhibited reduced activity according to the circadian cycle (Smith et al. 2012), implying that this arousal function of RLN3 might be mediated by the PAG.

Hence, in addition to testing $rln3a^{sq4sj-/-}$ mutants for RLN3-associated behaviours such as feeding and anxiety, the visual motor response assay was used to determine if Rln3a is involved in a response to darkness.

3.2 Methods

3.2.1 Fish

Danio rerio AB strain was used as the WT strain for all behaviour assays conducted in these studies. Embryos were grown in an incubator at 28 °C for 3–5 days before being transferred to a facility with a 14 h light, 10 h dark cycle. Adult fish were fed three times daily with a mixture of fish flakes and brine shrimp.

3.2.2 Assessment of zebrafish feeding

Zebrafish embryos are grown in groups of 50 per petri dish in 35 mL of E3 (egg water, 5 mM NaCl, 0.17 mM KCl, 0.33 mM $CaCl_2$, 0.33 mM $MgSO_4$) in a dark incubator at 28 °C unfed, as they posses yolk stores. At 3 dpf, hatched larvae are relocated to the hatchery and grown in batches of 50 in 500 mL of E3, where they are subjected to a 14 h day, 10 h night cycle and fed with spirulina (dried algae). At about 10 dpf, fish were transferred into 3 L tanks in groups of 20 fish per tank, as fish density greatly affects body size. Measurements were taken at the juvenile stage, once per week at 5–7 weeks post fertilisation, as fish size starts to become most variable at this age. Fish were anesthetised in 1 x MS222 (0.4 g/L tricaine methanesulfonate, Sigma-Aldrich) before being measured for body weight and length, and then returned to their home tanks for further measurements to be taken in the following week.

3.2.3 Novel tank diving assay

Adult zebrafish (3.5 months old) were tested for anxiety using the novel tank diving assay. Fish were video tracked over a 5 min duration in a tank measuring 20 cm x 12 cm x 5 cm (L x W x H) containing 1 L of water. For a baseline

measurement of anxiety, fish were netted from their home tanks into a container for transport to the tank setup, before transferring into the test tanks as quickly as possible to minimise handling stress. An independent group of fish from the same home tank was subjected to mild restraint stress in a 100 mL beaker filled with 10 mL of water for 10 min, before testing in the novel tank. Fish were tested between 1 p.m.–5 p.m. to reduce the variation due to circadian effects. Percentage of time spent at the bottom half of the tank is used as a measure of anxiety, as the fish would spend less time exploring the top half if they are more anxious (Cachat et al. 2010). Additionally, locomotion in the novel tank was also measured.

3.2.4   Visual motor assay

Zebrafish embryos were grown as in section 3.2.2, where embryo/larval density was important for obtaining consistent behaviour. 7–14 dpf larvae were placed into 24- or 48-well plate filled with 2 or 1 mL of E3 respectively, using water from their home tank. After a 1 h habituation period in the light, six cycles of 30 minutes light OFF, 30 minutes light ON was administered during the circadian day, beginning at 4 p.m. and ending at the beginning of the circadian night at 10 p.m.

The behavioural setup was placed in an enclosed box with two light sources that controlled illumination from the bottom of the plate, using a light pad (Artograph) to control light stimuli, as well as four infra-red LED light bars for the video tracking. A translucent acrylic sheet was used to both diffuse the light source for even lighting to the camera, and to reduce heat to the plate, where the temperature did not exceed 28.5 °C. A camera was placed overhead to track zebrafish locomotion at 5 frames per second, using a custom written program.

Data was exported as images and x-y coordinates every 20 min, and analysed by a custom-written macro on Microsoft Excel, where the threshold for inactivity was considered to be 1 s/min. Activity per minute was converted into distance travelled, which was used for plotting locomotion (mm/min) over time.

3.2.5   qRT-PCR

qRT-PR was conducted as described in 2.2.3.3. Additional gene specific primers are for *rln3b* and *rxfp3.2b* are listed in Table 3.1. As the *rxfp3.2b* gene had no introns, DNAse treatment from the RNAqueous®-Micro Kit (ThermoFisher) was carried out on all samples.

Table 3.1 List of primers for qRT-PCR

Gene	Primer (5' → 3')	Amplicon size
rln3b	**F** CTGCGGGAGAGAGTTCATCC	172 bp
	R ACGGGGTCTGTATGATAGTCCA	
rxfp3.2b	**F** TTGTCCTAACCCTGCCGTTC	188 bp
	R GCGACTGTGCATCTTCAACG	

3.2.6   Statistics

Statistical analyses were performed using R (https://www.r-project.org). Shapiro-Wilk test was used to determine if samples were not different from the normal distribution under the null hypothesis. If the null hypothesis was accepted, samples were considered as normally distributed, and the mean (*M*) and 95% confidence intervals (95% CI) were reported. Welch's t-test for unequal variances was used to compare between two groups, with effect size calculated as Cohen's

d. If the null-hypothesis of the Shapiro-Wilk test was rejected, samples were considered as non-normally distributed, and the median (*Mdn*) and the interquartile range (IQR) were reported. The Mann-Whitney test was used as a nonparametric test, and effect size was reported as *r* ($Z / \sqrt{N}$, where *Z* is the z-statistic and *N* is the total sample size). If one of the groups being compared was not normally distributed, nonparametric tests were used as a conservative approach. All tests were conducted at a significance level of 0.05. *p*-values were indicated as *$p < .05$, **$p < .01$, ***$p < .001$.

Graphical representations of the data employed boxplots to represent group distributions, where centrelines indicate medians, and box limits indicate 25th and 75th percentiles with Tukey-style whiskers extending 1.5 times the IQR. Outliers are defined as data points that lie outside the whiskers of the boxplot (Tukey 1977). The mean of each group is represented by a cross symbol, and all error bars are shown as 95% CIs around the mean, as recommended by Krzywinski & Altman (2013). Sample points are plotted as unfilled circles, while filled circles represent outliers.

3.3 Results

3.3.1 Effects of mutation in *rln3a* on stress and anxiety

rln3a[sq4sj-/-] mutants and WT siblings were placed in a novel tank for five minutes, both under baseline conditions (unstressed) and after being stressed by being placed in an isolated beaker with shallow water for ten minutes.

In the novel tank diving assay, anxious fish would preferentially dwell in the bottom half of the tank (Egan et al. 2009). The total time spent in the bottom half of the tank during the non-stress condition were similar in *rln3a*[sq4sj-/-] mutants (M = 44.1%, 95% CI [35.2, 53.0]) and WT siblings (M = 50.2%, 95% CI [42.2, 58.2]) over the entire duration of the assay; this was also the case under stress conditions (WT sibling, M = 53.9%, 95% CI [50.0, 57.8]; *rln3a*[sq4sj-/-] mutants, M = 52.0%, 95% CI [40.9, 63.2]) (Figure 3.2A). However, in the stress condition, the distribution for the mutants was much wider than that of the WTs, with some still spending less than 25% in the bottom half and two fish remaining at the bottom for the entire duration. This implied that the mutants were more sensitive to the stress condition, where two fish displayed high levels of anxiety as compared to WT. A 2x2 analysis of variance (ANOVA) with genotype (WT sibling, *rln3a*[sq4sj-/-]) and condition (stress, non-stress) revealed no main effects in genotype [$F(1, 76)$ = 0.98, p = .33, η^2 = .012], condition [$F(1,76)$ = 2.09, p = .15, η^2 = .026] or interaction between genotype and condition [$F(1,76)$ = 0.28, p = .60, η^2 = .003] for the time spent at the bottom of the tank.

Locomotion in the novel tank was also quantified, where the total distance travelled by the *rln3a*[sq4sj-/-] mutants (M = 9.71 m, 95% CI [8.86, 10.6]) and WT siblings (M = 10.4 m, 95% CI [9.79, 11.0]) were similar in the non-stress

condition, but *rln3a*$^{sq4sj-/-}$ mutants (M = 8.04 m, 95% CI [7.20, 8.90]) had reduced locomotion compared to WT siblings (M = 9.44 m, 95% CI [8.85, 10.0]) under the stress condition (Figure 3.2B). Using a 2x2 ANOVA, both genotype [F(1,76) = 8.92, p = .004**, η^2 = .089] and condition [F(1,76) = 14.1, p < .001***, η^2 = .14] displayed main effects, while there was no main effect for the interaction [F(1,76) = 0.98, p = .33, η^2 = .010]. Tukey's post hoc test was used to conduct pairwise comparisons between groups, with Cohen's *d* used as a measure of effect size, as reported in Figure 3.2B. These comparisons revealed reduced locomotion in mutants compared to WT siblings in the stress condition, and also a decrease in distance travelled during the stress condition compared to the non-strss condition in the *rln3a*$^{sq4sj-/-}$ mutants, which was not observed in the WT sibling group. This could indicate an increased pausing and freezing episodes in *rln3a*$^{sq4sj-/-}$ mutants under stress conditions, showing increased sensitivity to stress compared to WT siblings.

The percentage of time spent at the bottom of the tank was analysed by minute during non-stress (Figure 3.2C) and stress (Figure 3.2D) conditions, as zebrafish tend to display novelty-induced anxiety-like behaviour in the first minute. In the non-stress condition, there was a main effect of time [F(4, 152) = 3.09, p = .024*, η^2 = .024] and the interaction of time and genotype [F(4, 152) = 4.06, p = .006**, η^2 = .032] but not genotype [F(1, 38) = 1.05, p = .31, η^2 = .019] (two-way repeated measures ANOVA). Violations to Mauchly's test for sphericity were subjected to Huynd-Feldt corrections. Welch's t-test was used to compare percentage time spent at the bottom between the two genotypes in each minute during the non-stress condition, where *rln3a*$^{sq4sj-/-}$ mutants spent less time in the bottom half of the tank compared to WT siblings only in the first minute (Table 3.2).

In the stress condition, two-way repeated measures ANOVA with Huynd-Feldt corrections only revealed a main effect of time [$F_{(4, 152)}$ = 4.70, p = .002**, η^2 = .045], but not genotype [$F_{(1, 38)}$ = 0.20, p = .66, η^2 = .003] or the interaction [$F_{(4, 152)}$ = 1.06, p = .38, η^2 = .010]. No difference was found in time spent in the bottom half of the tank between WT siblings and $rln3a^{sq4sj-/-}$ mutants using Welch's t-test (Table 3.2). This implies that $rln3a^{sq4sj-/-}$ mutants had mildly reduced baseline anxiety levels compared to WT siblings in the first minute of exposure to a novel environment, but no differences in anxiety levels were found under stress conditions.
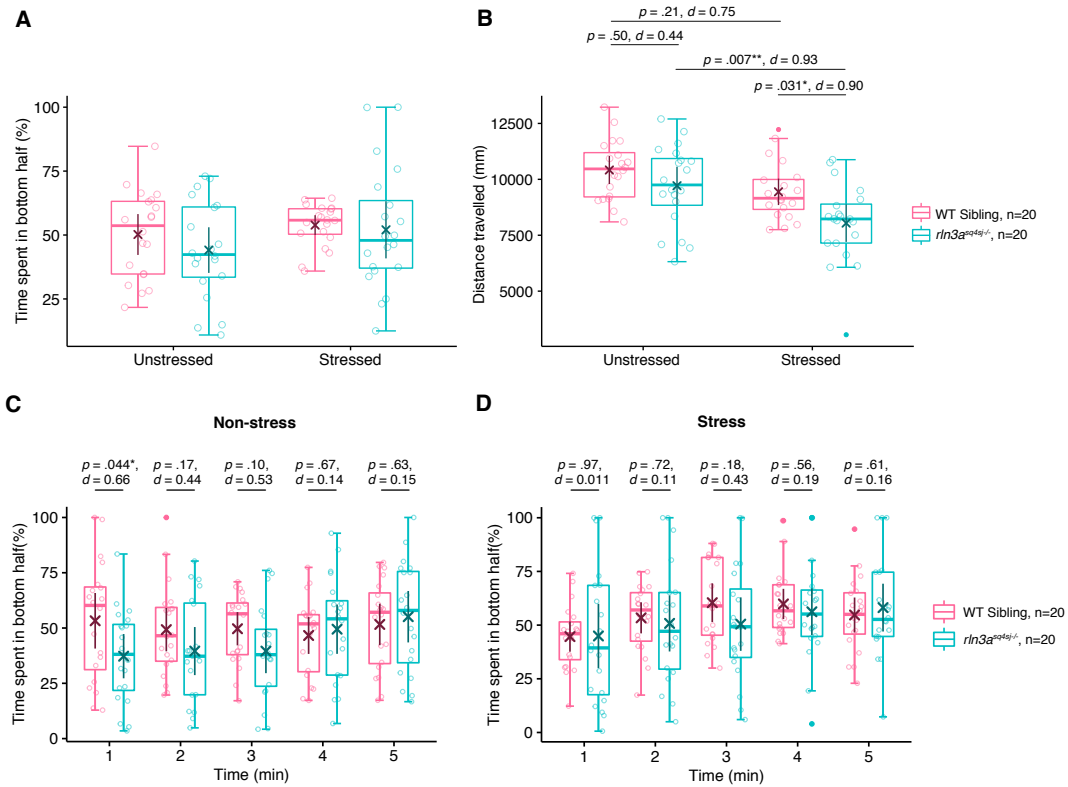
Figure 3.2 Stress and anxiety behaviours in *rln3a*^{sq4sj-/-} mutants

rln3a^{sq4sj-/-} mutant and WT sibling fish were assayed for anxiety behaviours using the novel tank assay under both non-stress and stress conditions. **(A)** Both groups spent a similar percentage of time in the bottom half of the tank throughout the entire test. **(B)** *rln3a*^{sq4sj-/-} mutants had reduced locomotion after stress, whereas WT siblings did not. After stress, distance travelled for *rln3a*^{sq4sj-/-} mutants was also reduced compared to WT siblings. Percentage of time spent in the bottom half was analysed by minute, in the non-stress **(C)** and stress **(D)** conditions. WT siblings displayed increased bottom dwelling time only in the first minute of the non-stress condition. Crosses represent mean and error bars represent 95% confidence intervals, individual fish measurements were plotted as unfilled circles and outliers as filled circles. **(B)** p values reported from Tukey's post hoc test following 2x2 ANOVA. **(C)** and **(D)** p values reported from Welch's t-test, effect size reported as Cohen's d.

Table 3.2 Statistical analysis of time spent in the bottom half (%) during the novel tank diving assay

Non-stress

Minute	WT sibling	$rln3a^{sq4sj-/-}$ mutant	p value	d
1	53.3 ± 12.6	37.3 ± 10.0	$t(36.2) = 2.09$, $p = .044$*	0.66
2	49.3 ± 9.8	39.6 ± 10.9	$t(37.6) = 1.39$, $p = .17$	0.44
3	49.7 ± 7.5	39.6 ± 10.0	$t(35.3) = 1.69$, $p = .10$	0.53
4	46.6 ± 8.3	49.5 ± 11.2	$t(35.2) = 0.43$, $p = .67$	0.14
5	51.6 ± 9.4	55.1 ± 11.6	$t(36.4) = 0.50$, $p = .63$	0.15

Stress

Minute	WT sibling	$rln3a^{sq4sj-/-}$ mutant	p value	d
1	44.7 ± 7.0	44.9 ± 15.0	$t(27.0) = 0.036$, $p = .97$	0.011
2	53.4 ± 7.2	50.8 ± 13.1	$t(29.6) = 0.36$, $p = .72$	0.11
3	60.4 ± 9.0	50.5 ± 12.4	$t(34.6) = 1.36$, $p = .18$	0.43
4	59.9 ± 1.0	56.2 ± 10.8	$t(32.6) = 0.59$, $p = .56$	0.19
5	54.7 ± 8.1	58.1 ± 11.1	$t(34.8) = 0.52$, $p = .61$	0.16

Values are means ± 95% CI. *$p < 0.05$. $n = 20$ in each group.

3.3.2 Effects of mutation in *rln3a* on the visual motor response

The visual motor response of *rln3a*$^{sq4sj-/-}$ mutants and WT siblings was compared to test if mutants exhibit an enhanced fear response, like dHbL-lesioned fish, where increased locomotion was observed in lesioned fish in minute 14–24 of the dark period compared to intact fish (Agetsuma et al. 2010). The analysis method of Agetsuma et al. (2010) was used to enable a direct comparison with this study. Some amendments to the analyses include testing for normality before applying hypothesis testing, as described in section 3.2.6, reporting effect sizes, plotting 95% CI as error bars, and including box plots and individual data points in the graphical representation for better visualisation of the responses.

Traces of locomotor activity during six repeated cycles of dark and light stimuli were similar in *rln3a*$^{sq4sj-/-}$ mutants and WT siblings (Figure 3.3A). A two-way repeated measures ANOVA of the entire dark cycle indicated no difference between the visual motor response in both groups, where the *p* value for the interaction between genotype and time for each cycle are as follows: Cycle 1, $F(29, 1276) = 0.89$, p = .49, $\eta^2 = .008$; Cycle 2, $F(29, 1276) = 0.80$, p = .57, $\eta^2 = .007$; Cycle 3, $F(29, 1276) = 0.80$, p = .54, $\eta^2 = .007$; Cycle 4, $F(29, 1276) = 0.33$, p = .88, $\eta^2 = .004$; Cycle 5, $F(29, 1276) = 0.46$, p = .73, $\eta^2 = .006$; Cycle 6, $F(29, 1276) = 0.41$, p = .77, $\eta^2 = .007$.

When comparing locomotor activity in the first 10 minutes of the dark period, *rln3a*$^{sq4sj-/-}$ mutants were less active in the first cycle (Figure 3.3B). No differences were observed in minute 14–24 of the dark period (Figure 3.3C), or in the entire light period (Figure 3.3D. For more details, see Table 3.3). Hence, the behaviour of *rln3a*$^{sq4sj-/-}$ mutants did not phenocopy fish with dHbL lesions.
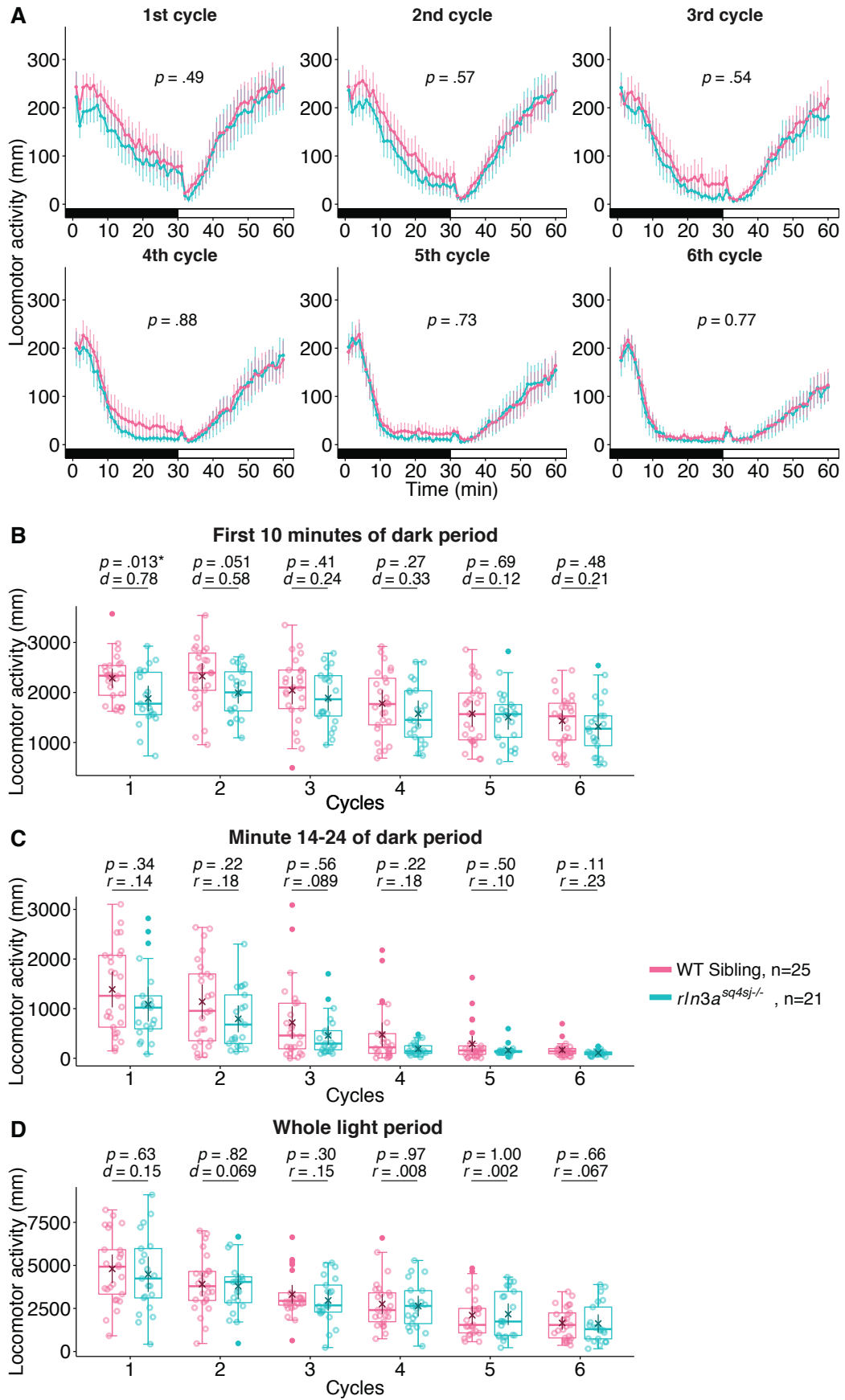
Figure 3.3 Visual motor response of *rln3a*$^{sq4sj-/-}$ mutants

 (A) Charts illustrating locomotor activity over 6 cycles of dark (black bars) and light (white bars), with each cycle lasting 1 h. Error bars show 95% CI. *p* value from the interaction term (Genotype x Time) of two-way repeated measures ANOVA against the entire dark period. Total locomotor activity was assessed every cycle in the first 10 minute **(B)** and from minute 14-24 **(C)** of the dark period, as well as the whole light period. **(D)** Locomotor activity of *rln3a*$^{sq4sj-/-}$ mutants was only decreased in the first cycle of **(B)**. **(B-D)** Crosses represent mean and error bars represent 95% CI, individual larval measurements were plotted as unfilled circles. For data satisfying normality criteria by the Shapiro-Wilk test, *p* values were reported from Welch's t-test, effect size as Cohen's *d*. Otherwise, *p* value were reported from Mann-Whitney test, *r* reported as non-parametric effect size.

Table 3.3 Statistical analysis of locomotor activity in the visual motor response of *rln3a*^{sq4sj-/-} mutants

First 10 minutes

Cycle	Total locomotor activity (mm)		p value	Effect size
	WT sibling	*rln3a*$^{sq4sj-/-}$ mutant		
1	M = 2285, 95% CI [2088, 2481]	M = 1881, 95% CI [1625, 2137]	$t(39.4)$ = 2.60, p = .013*	d = 0.78
2	M = 2326, 95% CI [2065, 2586]	M = 1996, 95% CI [1777, 2215]	$t(43.6)$ = 2.01, p = .051	d = 0.58
3	M = 2043, 95% CI [1763, 2323]	M = 1891, 95% CI [1637, 2145]	$t(44.0)$ = 0.83, p = .41	d = 0.24
4	M = 1779, 95% CI [1509, 2050]	M = 1574, 95% CI [1308, 1840]	$t(43.8)$ = 1.12, p = .27	d = 0.33
5	M = 1575, 95% CI [1315, 1835]	M = 1505, 95% CI [1256, 1754]	$t(43.9)$ = 0.41, p = .69	d = 0.12
6	M = 1434, 95% CI [1221, 1647]	M = 1319, 95% CI [1061, 1578]	$t(40.9)$ = 0.71, p = .48	d = 0.21

Minute 14–24

Cycle	Total locomotor activity (mm)		p value	Effect size
	WT sibling	*rln3a*$^{sq4sj-/-}$ mutant		
1	Mdn = 1259, IQR [627, 2075]	Mdn = 1020, IQR [594, 1258]	W = 307, p = .34	r = .14
2	Mdn = 956, IQR [353, 1670]	Mdn = 679, IQR [297, 1277]	W = 319, p = .22	r = .18
3	Mdn = 459, IQR [192, 1190]	Mdn = 296, IQR [171, 556]	W = 290, p = .56	r = .089
4	Mdn = 221, IQR [100, 497]	Mdn = 141, IQR [98.8, 253]	W = 319, p = .22	r = .18
5	Mdn = 158, IQR [78.8, 250]	Mdn = 131, IQR [118, 155]	W = 294, p = .50	r = .10
6	Mdn = 141, IQR [91.7, 196]	Mdn = 103, IQR [71.5, 128]	W = 335, p = .11	r = .23

WT sibling n = 25, *rln3a*$^{sq4sj-/-}$ mutant n = 21. *p < 0.05.

Table 3.3 Statistical analysis of locomotor activity in the visual motor response of *rln3a*$^{sq4sj-/-}$ mutants (continued)

Whole light period

Cycle	Total locomotor activity (mm)		p value	Effect size
	WT sibling	*rln3a*$^{sq4sj-/-}$ mutant		
1	M = 4798, 95% CI [3963, 5634]	M = 4484, 95% CI [3453, 5515]	$t(40.6)$ = 0.49, p = .63	d = 0.15
2	M = 3907, 95% CI [3224, 4591]	M = 3793, 95% CI [3043, 4543]	$t(42.7)$ = 0.23, p = .82	d = 0.069
3	*Mdn* = 2941, IQR [2693, 3408]	*Mdn* = 2679, IQR [2289, 3857]	W = 310, p = .30	r = .15
4	*Mdn* = 2404, IQR [1726, 3407]	*Mdn* = 2644, IQR [1618, 3534]	W = 265, p = .97	r = .008
5	*Mdn* = 1543, IQR [1080, 2501]	*Mdn* = 1739, IQR [935, 3485]	W = 262, p = 1.00	r = .002
6	*Mdn* = 1541, IQR [786, 2240]	*Mdn* = 1296, IQR [734, 2579]	W = 283, p = .66	r = .067

WT sibling n = 25, *rln3a*$^{sq4sj-/-}$ mutant n = 21. *p < 0.05.

3.3.3 Effects of mutation in *rln3a* on body weight and length

As stress affects food intake (Timofeeva et al. 2016), and RLN3 signalling is associated with changes in feeding behaviour (Calvez et al. 2016a,b; Ganella et al. 2012, Hida et al. 2006, Lenglos et al. 2014a, McGowan et al. 2005, 2006), juvenile *rln3a*$^{sq4sj-/-}$ mutants and WT siblings were measured for body length and weight at 5–7 weeks post fertilisation. Across all time periods, body length and remained similar in both groups. At week 5: WT sibling, *Mdn* = 15.0 mm, IQR [13.0, 17.0]; *rln3a*$^{sq4sj-/-}$ mutant, *Mdn* = 14.0 mm, IQR [12.0, 15.0]; *W* = 287, *p* = .092, *r* = .26, Mann-Whitney test. At week 6: WT sibling, *Mdn* = 18.0 mm, IQR [15.8, 19.0]; *rln3a*$^{sq4sj-/-}$ mutant, *Mdn* = 16.5 mm, IQR [15.0, 19.3]; *W* = 201, *p* = .54, *r* = .10, Mann-Whitney test. At week 7: WT sibling, *M* = 21.6 mm, 95% CI [20.0, 23.2]; *rln3a*$^{sq4sj-/-}$ mutant, *M* = 19.9 mm, 95% CI [18.5, 21.4]; *t*(33.9) = 1.66, *p* = .11, *d* = 0.55, Welch's t-test (Figure 3.4A).

Body weights of *rln3a*$^{sq4sj-/-}$ mutants and WT siblings were also similar, with the exception of week 5, where *rln3a*$^{sq4sj-/-}$ mutants (*M* = 23.9 mg, 95% CI [18.0, 29.8]) weighed less than WT siblings (*M* = 34.8 mg, 95% CI [27.9, 41.7]), *t*(39.0) = 2.5, *p* = .017*, *d* = 0.77, Welch's t-test. At week 6: WT sibling, *M* = 57.7 mg, 95% CI [45.9, 69.5]; *rln3a*$^{sq4sj-/-}$ mutant, *M* = 51.6 mg, 95% CI [38.5, 64.7]; *t*(35.2) = 0.73, *p* = .47, *d* = 0.24, Welch's t-test. At week 7: WT sibling, *M* = 112 mg, 95% CI [89.6, 135]; *rln3a*$^{sq4sj-/-}$ mutant, *M* = 94.3 mg, 95% CI [71.6, 117]; *t*(33.9) = 1.18, *p* = .24, *d* = 0.39, Welch's t-test (Figure 3.4B).
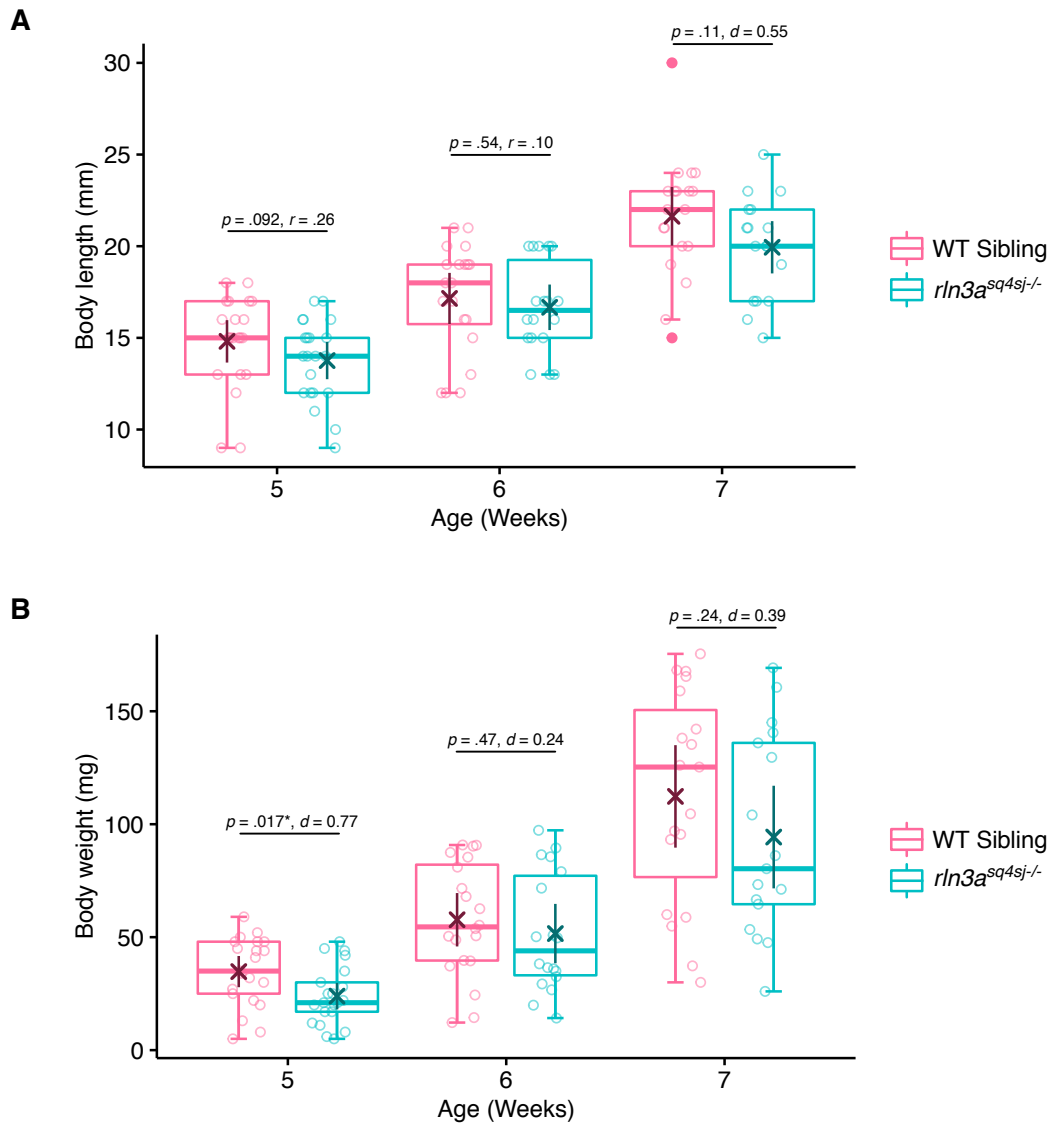
77

Figure 3.4 Body weight and length in *rln3a^{sq4sj-/-}* mutants

Body length **(A)** and body weight **(B)** of *rln3a^{sq4sj-/-}* mutants was similar to that of WT sibling at 5, 6, and 7 weeks post fertilisation, with the exception of body weight at week 5. Sample sizes varied per week due to fish deaths. Week 5: WT sibling n=21, *rln3a^{sq4sj-/-}* mutant n=21. Week 6: WT sibling n=20, *rln3a^{sq4sj-/-}* mutant n=18. Week 7: WT sibling n=19, *rln3a^{sq4sj-/-}* mutant n=17. Means were plotted as crosses and error bar represent 95% confidence intervals. Individual fish were plotted as unfilled circles, with outliers plotted as filled circles. For data satisfying normality criteria by the Shapiro-Wilk test, *p* values were reported from Welch's t-test, effect size as Cohen's *d*. Otherwise, *p* value were reported from Mann-Whitney test, *r* reported as non-parametric effect size.

3.3.4 Quantitative expression of *rln3a*-related genes

One explanation for a lack of a distinct behavioural phenotype in the *rln3a*$^{sq4sj-/-}$ mutants as compared to WT sibling controls is that there are compensatory effects from other genes. In light of the multiple duplicated genes in the zebrafish genome, possible candidates to compensate for a lack of *rln3a* would be its paralogue, *rln3b*, and its receptor, *rxfp3.2b*. Hence, qRT-PCR was used to check if the expression of these genes were altered in the mutants.

Whole adult fish brains (n=10) from *rln3a*$^{sq4sj-/-}$ mutants and WT siblings were analysed for *rln3b* and *rxfp3.2b* expression using qRT-PCR. After verifying that primers were sufficiently efficient at 98.9% and 99.7% for *rln3b* and *rxfp3.2b* respectively, the $2^{-\Delta\Delta Ct}$ method (Livak & Schmittgen 2001) was used for analysis (Figure 3.5B, D). The melt curve displayed a single peak for all amplicons (Figure 3.5C, E), while PCR products presented single bands when visualised on agarose gel (Figure 3.5A), indicating specificity. No genomic contamination was detected in the negative control without reverse transcriptase.

The expression levels of *rln3b* were upregulated approximately four-fold in the *rln3a*$^{sq4sj-/-}$ mutants (ΔCt M = -9.88, 95% CI [-10.3, -9.47]) compared to WT siblings (ΔCt M = -8.28, 95% CI [-8.81, -7.75]) (Figure 3.5F, G). *rln3b* could not be detected in two *rln3a*$^{sq4sj-/-}$ mutant fish, and these samples were omitted from the analysis. Additionally, *rxfp3.2b* expression in the *rln3a*$^{sq4sj-/-}$ mutant (ΔCt M = -9.43, 95% CI [-10.5, -8.36]) was similar to WT siblings (ΔCt M = -8.98, 95% CI [-9.75, -8.21]) (Figure 3.5H, I). This indicates a possible partial compensation of *rln3b* gene as a result of the mutagenesis.
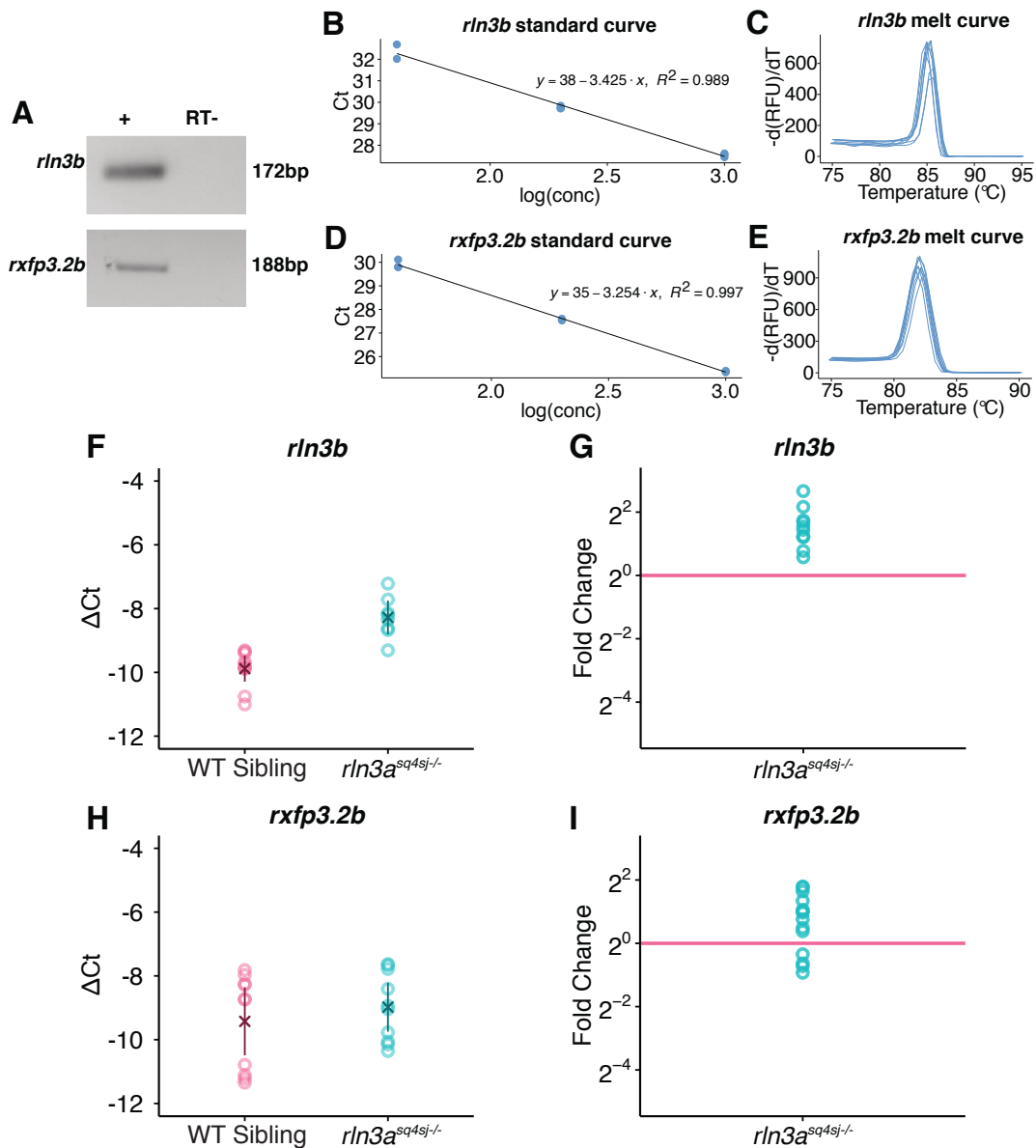
Figure 3.5 qRT-PCR analyses of *rln3a* related genes

(A) qRT-PCR products present a single band on agarose gel, with no amplification in the RT– control. **(B-E)** Optimisation of primers. Standard curves indicate close to 100% efficiency for all primers used **(B, D)**. Melt curves display a single peak, indicating specificity of primers to the amplification product **(C, E)**. The expression levels of *rln3b* and *rxfp3.2b* were compared in WT sibling and *rln3a^sq4sj-/-* fish ($n = 10$ per group). **(F, H)** Normalised difference in threshold cycles ($\Delta Ct = Ct_{ref} - Ct_{gene}$). Individual fish samples were plotted as unfilled circles, crosses represent mean and error bars represent 95% confidence interval of the mean. As two samples from mutant fish failed to produce amplification products with *rln3b* primers, they were removed from the analysis in **F** and **G**. **(G, I)** Fold change of expression, where averaged WT levels of *rln3a* are represented as 1 (pink line).

3.4 Discussion

3.4.1 Comparison of zebrafish *rln3a*^{*sq4sj-/-*} mutant with rodent studies

RLN3 signalling has been implicated as a regulator of stress and anxiety related behaviours in multiple studies involving drug-induced activation or inhibition of RXFP3 in rats (Ryan et al. 2013a, Zhang et al. 2015). However, mouse *Rln3* loss-of-function mutants do not display strong phenotypes, where mutants have been reported to be mildly hypersensitive to stress (Smith et al. 2009), slightly less anxious than controls (Watanabe et al. 2011b). In a separate study, mouse mutants behaved similarly to WT littermates under baseline conditions or after being chronically stressed (Smith et al. 2012). In *Rxfp3* null mutant mice, only a mild and inconsistent decrease in anxiety was observed in multiple tests (Hosken et al. 2015). Similarly, zebrafish *rln3a*^{*sq4sj-/-*} mutants only displayed a mild decrease in anxiety or hypersensitivity to stress. Under baseline (low) levels of anxiety, *rln3a*^{*sq4sj-/-*} mutants appeared less susceptible to novelty-induced stress compared to WT siblings, as they displayed a reduced percentage of time spent at the bottom of the tank in the initial minute of the novel tank diving assay. At the same time, a mild stressor elicited a decrease in locomotion in *rln3a*^{*sq4sj-/-*} mutants but not in WT siblings, which can be interpreted as increased sensitivity to stress in mutants. However, there was quite a high level of individual variation in both groups of fish to show a convincing effect. The effects may be too small to be detected by the current sample size, or the stressor may be too mild.

Initial studies of the effects of central administration of RLN3 on rodent behaviour suggested roles in feeding, with increased feeding upon i.c.v. injection of RLN3 (McGowan et al. 2005, 2006). However, in studies using *Rln3* mutant mice, only one report identified a possible effect with similar decreased body weight in

mutants fed a high fat diet (Sutton et al. 2009), while others found no differences in body weight between mutant and WT mice (Smith et al. 2009, 2012; Watanabe et al. 2011b). These contradictory reports were attributed to the fact that mixed background mutants were used, which would inherit an undetermined selection of genes from either genetic background that could affect the behaviour of these groups (Smith et al. 2012). Consistent with the latter reports, body weight and length measurements for zebrafish $rln3a^{sq4sj-/-}$ mutants were largely similar to WT siblings.

Overall, a comparison between RLN3/Rln3a-related behaviours tested using null mutations in mouse and zebrafish is summarised in Figure 3.6.

Figure 3.6 Comparison of the effects of RLN3/Rln3a null mutation on mouse and zebrafish behaviours

Summary of behavioural effects of a loss of RLN3 in mouse from various studies, compared to the loss of Rln3a in zebrafish from the studies conducted in this thesis. In particular, stress and anxiety behaviours and body weight was compared.

3.4.2 Involvement of Rln3a in the visual motor response

The visual motor response was used previously to test enhanced fear responses in zebrafish with dHbL lesions, which reduces the capability of zebrafish larvae to cope with stress (Agetsuma et al. 2010). As the dHbL projects to the PAG and NI, Rln3 may be acting downstream of the habenula (Okamoto et al. 2012), in line with its production in response to stress. Calcium imaging indicates that the PAG is activated by dark stimuli but not the NI, suggesting a possible involvement of the Rln3 population in the PAG in modulating fear responses to dark stimuli. However, $rln3a^{sq4sj-/-}$ mutants showed similar levels of activity to WT siblings, and only had decreased in activity in the initial presentation of dark stimuli, which could be interpreted as reduced responsiveness to stressful stimuli. Although these data indicate that the loss of Rln3a does not have similar effects to dHbL lesions, this is not surprising as the habenula regulates multiple other neuropeptides (Stephenson-Jones et al. 2012), and potentially the loss of one peptide might not modify behaviour significantly.

3.4.3 Compensatory effects in genetic mutant models

Compensatory effects are common in mutants, and as such there are no visible phenotypes. This is contrasted against knockdown approaches, such as morpholinos, that produce phenotypes when the same gene is targeted (Kok et al. 2015, Rossi et al. 2015). Despite the speculation that compensatory effects may be occurring, it is difficult to determine what might be compensating for the lack of Rln3. However, there are two possible levels of redundancies, one relates to the fact that different neuropeptide systems have similar functions, such as feeding and arousal. Another is teleost-specific whole genome duplication of genes. Compensation by Rln3a-related peptides in the mutant was tested by

measuring expression levels of *rln3b* and *rxfp3.2b*. Although the levels of the *rln3a* receptor, *rxfp3.2b*, remained the same, the paralogue *rln3b* was upregulated four-fold in mutants compared to wild types. This is a modest increase compared to the 16-fold decrease in *rln3a* expression, indicating that compensation by other genes is also likely. Nevertheless, this is the first report of the behavioural phenotyping of a Rln3a-deficient zebrafish line.

4. BEHAVIOURAL EFFECTS OF A C-PEPTIDE POLYMORPHISM

4.1 Introduction

Unexpectedly, a SNP was found in the 158th position of the sequenced coding DNA sequence, where the WT C nucleotide was replaced by a T nucleotide (polymorphism abbreviated as c.158C>T) in the C-peptide (Figure 4.1). The studies described in this chapter explore the possibility that this SNP contributed to altered behaviour.
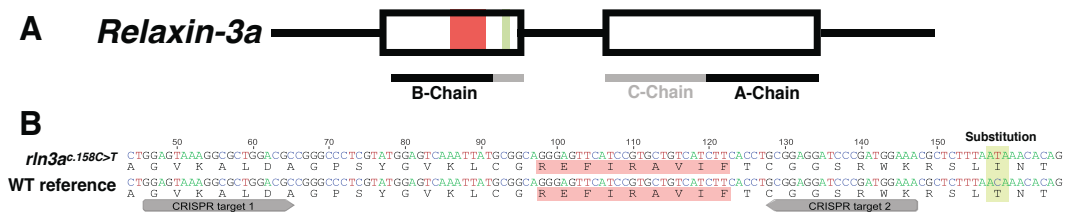
Figure 4.1 SNP within the *rln3a* locus

(A) Schematic representation of the Rln3a gene. Red box represents the receptor-binding motif; green box represents the genetic location of the SNP. **(B)** A SNP was found at position 158 of the cDNA with a single base pair change from C to T (c.158C>T). Predicted translation of the *rln3a*[c.158C>T] SNP variant reveals a non-synonymous substitution of the amino acid threonine to isoleucine in the Rln3a C-peptide.

The C-peptide, also called the connecting peptide, is cleaved from the propeptide of RLN3, with the remaining A- and B-chains forming mature RLN3 peptide. The A- and B-chains are highly conserved between mouse and human RLN3, with only two amino acid differences, compared to RLN which has 42% and 45% similarity in the A- and B-chains respectively (Bathgate et al. 2002). Within the RLN3 C-peptide, there is a surprisingly high conservation between mouse and human at 73%, compared with less than 20% in other RLNs (Bathgate et al. 2002). This highlights the possibility of more conserved functionality of the RLN3

C-peptide compared to other family members in mammals (Bathgate et al. 2002). Inter-species variation in RLN3 C-peptide sequences makes alignment difficult (Wilkinson et al. 2005), as in the comparison of zebrafish Rln3 with mammalian forms in Figure 2.1, where the discrepancies in peptide sequence are large even when comparing zebrafish Rln3a and Rln3b. However, although the C-peptide in the related peptide, insulin, is not conserved, it is thought to have commonalities at a structural level that can assist in chaperone-like functions, self assembly, and protein interactions (Landreh & Jornvall 2015, Landreh et al. 2014).

Although originally considered to be biologically inert, the C-peptide of insulin has been found to have bioactivity, although not directly related to insulin function of blood glucose regulation (Wahren et al. 2000, 2007). Instead, it has been linked with vascular, renal and neural dysfunctions in type I diabetics, where its administration is proposed for the treatment of such complications due to the lack of the C-peptide in patients (Ido et al. 1997, Wahren et al. 2007). However, in recent years, clinical evidence for the use of the insulin C-peptide has been controversial, where its efficacy is not clearly evident (Wahren & Larsson 2015). Within the RLN family, synthesis of two fragments of rat RLN C-peptide for assessment on the rat heart revealed no noticeable RLN-like activity (Dawson et al. 2001).

Localisation of the RLN3 C-peptide in the rat brain has been carried out with the immunohistochemical detection of a conserved portion of the C-peptide in mammals (Brailoiu et al. 2009, Ma et al. 2007). The expression pattern of the RLN3 C-peptide using this method was largely similar to that of the A-chain of the mature peptide (Tanaka et al. 2005), being expressed in the NI, ventrolateral

PAG, and parts of the dorsal raphe and substantia nigra. Only some differences were detected in RLN3-like fibres, with low levels present in the olfactory bulbs and the cortex (Ma et al. 2007), and a lack of detection in the medial accessory nucleus of the inferior olive, which was densely labelled in anterograde tracing studies of the NI (Goto et al. 2001). Also, immunohistochemical staining was specific to the C-peptide of RLN3, as the antibody used did not recognise the mature peptide and could detect the same loci after pre-absorption with RLN3 (Brailoiu et al. 2009).

There is some evidence that the RLN3 C-peptide is neuroactive, modulating calcium levels and membrane potential in cultured rat hypothalamic neurons (Brailoiu et al. 2009). Using calcium dyes, distinct patterns of calcium activity were detected when cultured neurons were activated by RLN3 and its C-peptide, where the latter had sustained activity after an initial phasic response, while RLN3 only elicited an initial fast transitory response. These effects were modulated by differing sources of calcium, and could imply different roles for the two peptides (Brailoiu et al. 2009). Also, both RLN3 and its C-peptide are able to depolarise and hyperpolarise target neurons, as detected by voltage dyes (Brailoiu et al. 2009). Furthermore, competitive binding studies suggest that RLN3 and its C-peptide activate different channels for their functions (Brailoiu et al. 2009). However, there is currently no functional role for the RLN3 C-peptide identified *in vivo*.

To investigate the effects of a *rln3a* C-peptide SNP on zebrafish behaviour, fish homozygous for the *rln3a*$^{c.158T}$ allele were tested against fish homozygous for the *rln3a*$^{c.158C}$ allele. This experiment was performed using two genetic backgrounds

within the AB WT strain, as background effects may interact with the polymorphism to generate a phenotype (Chandler et al. 2013). One concern was that the CRISPR mutagenesis could produce off target effects; hence one of the groups tested was WT siblings of the $rln3a^{sq4sj-/-}$ mutants, which were obtained from incrossed heterozygous mutants ($rln3a^{sq4sj+/-}$), while the other was WT fish from the facility.

4.2 Results

4.2.1 Sequencing of *rln3a* cDNA

An SNP was detected in nucleotide 158 of the coding sequence of *rln3a*, consisting of the C and T nucleotide variants (Figure 4.1). All WT siblings of CRISPR-injected mutants possessed the *rln3a*^{c.158T} allele (Figure 4.2A). Non-sibling WT fish were sequenced to check if the WT polymorphism existed in the population. Out of four non-sibling WT fish sequenced, one was homozygous for the SNP (*rln3a*^{c.158T}) and another was in the heterozygous form (shown as heterozygous form, *rln3a*^{c.158C/T}, in Figure 4.2B). The *rln3a*^{sq4sj-/-} mutant fish possessed the WT variant of the SNP (c.158C=) (Figure 4.2C). *In silico* translation of the *rln3a*^{c.158T} *allele* revealed a non-synonymous substitution from amino acid threonine to isoleucine, indicating that peptide function may be altered due to this SNP.
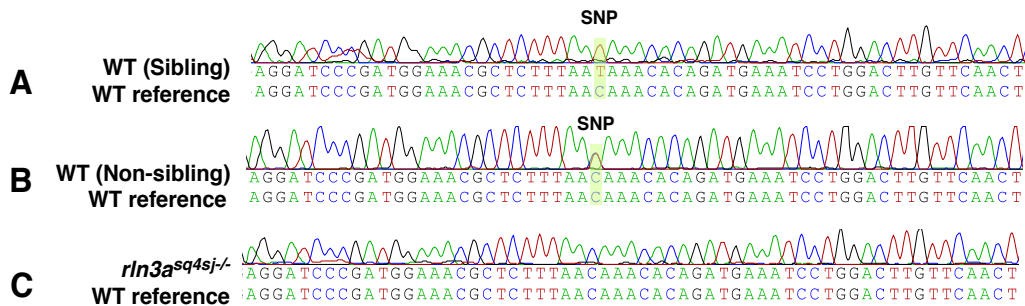
Figure 4.2 Sequencing of *rln3a* cDNA from WTs and *rln3a*^{sq4sj-/-} mutant

(A) WT sibling of CRISPR-injected fish is homozygous for the SNP (*rln3a*^{c.158T}). **(B)** Sequence from full-length cDNA of non-sibling WT fish, shown here as the heterozygous form of the SNP (*rln3a*^{c.158C/T}). **(C)** The mutant *rln3a*^{sq4sj-/-} has a 7bp deletion in the cDNA, with the WT SNP variant (c.158C=).

4.2.2   Effects of C-peptide polymorphism on visual motor response

The visual motor response was used to test if the SNP in the *rln3a* gene coding for the C-peptide would affect behaviour. In WT fish that were siblings of the *rln3a*$^{sq4sj-/-}$ mutants, those with the *rln3a*$^{c.158T}$ allele were more active across the entire dark period (Cycle 3 and Cycle 4) compared to fish with the *rln3a*$^{c.158C}$ allele (Figure 4.3). A two-way repeated measures ANOVA was conducted for data from the entire dark cycle, where the *p* values (with Greenhouse-Geisser correction) for the interaction between genotype and time for each cycle are as follows: Cycle 1, $F(29, 1247) = 0.89$, $p = .49$, $\eta^2 = .008$; Cycle 2, $F(29, 1247) = 1.71$, $p = .12$, $\eta^2 = .014$; Cycle 3, $F(29, 1247) = 1.40$, $p = .23$, $\eta^2 = .011$; Cycle 4, $F(29, 1247) = 3.61$, $p = .003^{**}$, $\eta^2 = .034$; Cycle 5, $F(29, 1247) = 2.56$, $p = .040^*$, $\eta^2 = .034$; Cycle 6, $F(29, 1247) = 1.27$, $p = .16$, $\eta^2 = .021$. When the visual motor response was analysed in separate time bins, the differences were seen mostly in the first 10 minutes of the dark period (Cycles 1, 2, 4, and 5), and the first cycle of the later part of the dark period (minute 14–24), but not during the light period (Table 4.1).

In fish that were not siblings of the *rln3a* mutants, *rln3a*$^{c.158T}$ fish had similar locomotor activity compared to *rln3a*$^{c.158C}$ fish in the visual motor response (Figure 4.4). A two-way repeated measures ANOVA was conducted on data from the entire dark cycle, where the *p* value (with Greenhouse-Geisser correction) for the interaction between genotype and time for each cycle are as follows: Cycle 1, $F(29, 1189) = 0.47$, $p = .88$, $\eta^2 = .004$; Cycle 2, $F(29, 1189) = 1.04$, $p = .40$, $\eta^2 = .009$; Cycle 3, $F(29, 1189) = 0.85$, $p = .56$, $\eta^2 = .008$; Cycle 4, $F(29, 1189) = 0.52$, $p = .79$, $\eta^2 = .005$; Cycle 5, $F(29, 1189) = 1.07$, $p = .38$, $\eta^2 = .011$; Cycle 6, $F(29, 1189) = 1.63$, $p = .14$, $\eta^2 = .016$. When the visual motor

response was analysed in time bins, there was no difference in the activity of both groups of fish in the first 10 minutes of the dark cycle, unlike the WT siblings (Table 4.2). This implies that the c.158T polymorphism in the C-peptide causes WT fish to be more active, although how this modifies the visual motor response depends on the genetic background.
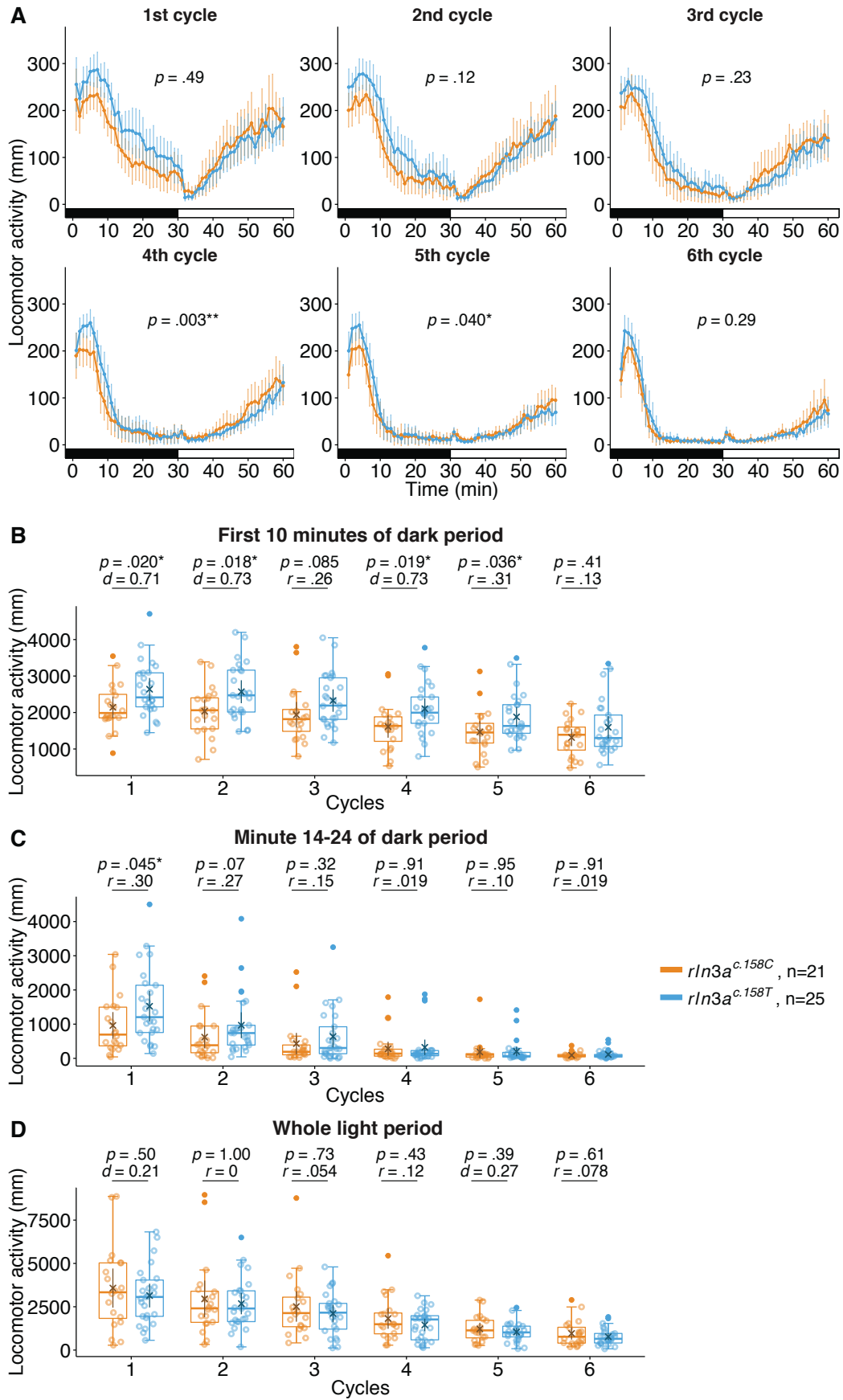
Figure 4.3 Visual motor response of *rln3a^c.158T^* and *rln3a^c.158C^* in WT siblings

(A) Charts illustrating locomotor activity over 6 cycles of dark (black bars) and light (white bars), with each cycle lasting 1 h. Error bars show 95% CI. *p* value from the interaction term (Genotype x Time) of two-way repeated measures ANOVA against the entire dark period. Total locomotor activity was assessed every cycle in the first 10 minute **(B)** and from minute 14-24 **(C)** of the dark period, as well as the whole light period. **(D)** *rln3a^c.158T^* was hyperactive in selected cycles, within dark periods **(B, C)**. **(B-D)** Crosses represent mean and error bars represent 95% CI, individual larval measurements were plotted as unfilled circles. For data satisfying normality criteria by the Shapiro-Wilk test, *p* values were reported from Welch's t-test, effect size as Cohen's *d*. Otherwise, *p* values were reported from Mann-Whitney test, *r* reported as non-parametric effect size.

Table 4.1 Statistical analysis of locomotor activity in the visual motor response of WT siblings

First 10 minutes

Cycle	Total locomotor activity (mm)		p value	Effect size
	$rln3a^{c.158C}$	$rln3a^{c.158T}$		
1	M = 2143, 95% CI [1846, 2440]	M = 2639, 95% CI [2333, 2946]	$t(42.8)$ = 2.42, p = .020*	d = 0.71
2	M = 2036, 95% CI [1716, 2356]	M = 2570, 95% CI [2255, 2885]	$t(42.4)$ = 2.48, p = .018*	d = 0.73
3	Mdn = 1818, IQR [1484, 2083]	Mdn = 2191, IQR [1813, 2951]	W = 174, p = .085	r = .26
4	M = 1613, 95% CI [1309, 1918]	M = 2104, 95% CI [1816, 2391]	$t(41.9)$ = 2.44, p = .019*	d = 0.73
5	Mdn = 1452, IQR [1164, 1704]	Mdn = 1631, IQR [1431, 2216]	W = 158, p = .036*	r = .31
6	Mdn = 1390, IQR [970, 1601]	Mdn = 1300, IQR [1071, 1931]	W = 213, p = .41	r = .13

Minute 14–24

Cycle	Total locomotor activity (mm)		p value	Effect size
	$rln3a^{c.158C}$	$rln3a^{c.158T}$		
1	Mdn = 695, IQR [365, 1497]	Mdn = 1205, IQR [756, 2138]	W = 162, p = .045*	r = .30
2	Mdn = 383, IQR [164, 946]	Mdn = 739, IQR [389, 967]	W = 171, p = .073	r = .27
3	Mdn = 192, IQR [104, 390]	Mdn = 303, IQR [136, 924]	W = 205.5, p = .32	r = .15
4	Mdn = 139, IQR [64, 268]	Mdn = 133, IQR [76.4, 228]	W = 255.5, p = .91	r = .019
5	Mdn = 108, IQR [37.5, 137]	Mdn = 64.3, IQR [41.5, 175]	W = 253, p = .95	r = .10
6	Mdn = 71.0, IQR [43.9, 114]	Mdn = 76.1, IQR [37.7, 113]	W = 244.5, p = .91	r = .019

$rln3a^{c.158C}$ n = 20, $rln3a^{c.158T}$ n = 25. *p < 0.05.

Table 4.1 Statistical analysis of locomotor activity in the visual motor response of WT siblings (continued)

Whole light period

Cycle	Total locomotor activity (mm)		p value	Effect size
	rln3a$^{c.158C}$	*rln3a*$^{c.158T}$		
1	*M* = 3578, 95% CI [2449, 4707]	*M* = 3146, 95% CI [2461, 3831]	*t*(32.4) = 0.68, *p* = .50	*d* = 0.21
2	*Mdn* = 2407, IQR [1600, 3395]	*Mdn* = 2400, IQR [1642, 3418]	*W* = 250, *p* = 1.00	*r* = 0
3	*Mdn* = 2134, IQR [1348, 3054]	*Mdn* = 2159, IQR [1209, 2693]	*W* = 266, *p* = .73	*r* = .054
4	*Mdn* = 1492, IQR [938, 2139]	*Mdn* = 1766, IQR [590, 1982]	*W* = 285, *p* = .43	*r* = .12
5	*M* = 1223, 95% CI [868, 1578]	*M* = 1045, 95% CI [809, 1280]	*t*(34.5) = 0.87, *p* = .39	*d* = 0.27
6	*Mdn* = 768, IQR [401, 1316]	*Mdn* = 650, IQR [408, 959]	*W* = 273, *p* = .61	*r* = .078

rln3a$^{c.158C}$ *n* = 20, *rln3a*$^{c.158T}$ *n* = 25. *p < 0.05.
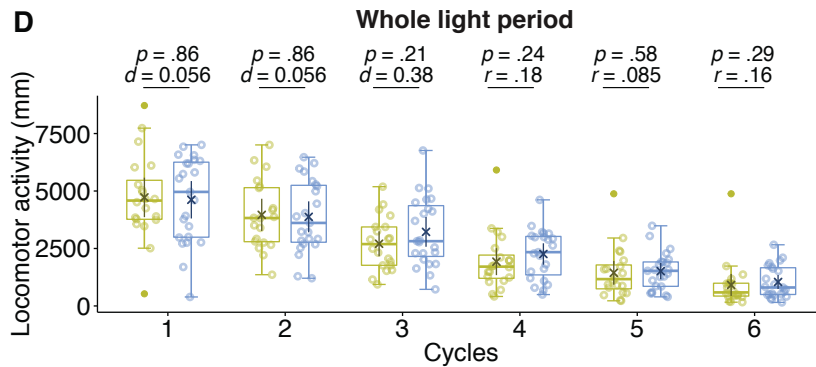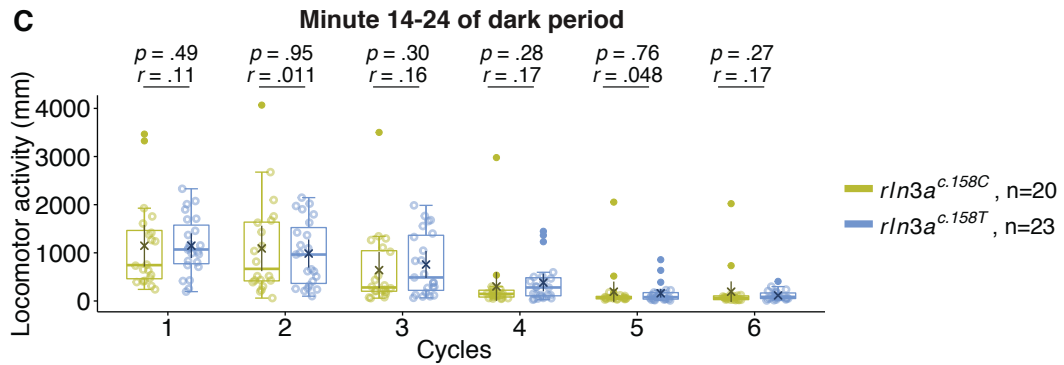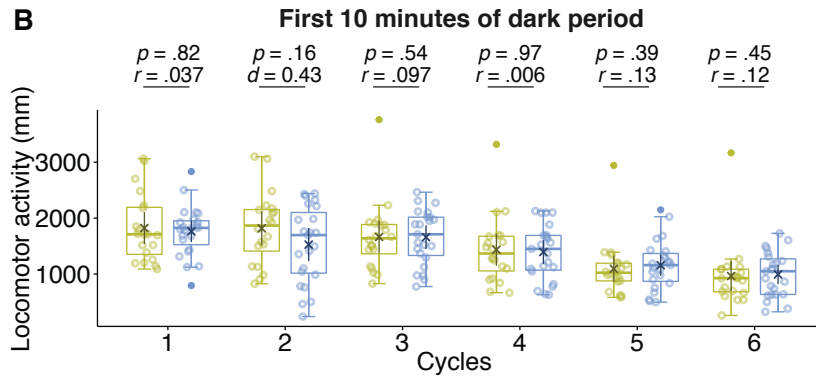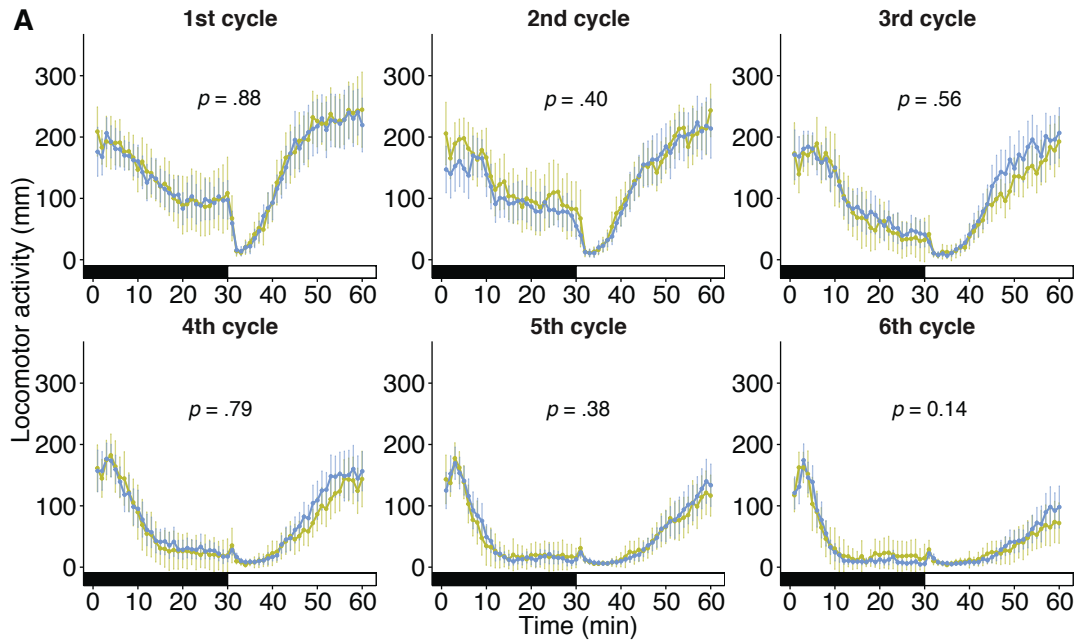
Figure 4.4 Visual motor response of *rln3a$^{c.158T}$* and *rln3a$^{c.158C}$* from non-sibling WT

(A) Charts illustrating locomotor activity over 6 cycles of dark (black bars) and light (white bars), with each cycle lasting 1 h. Error bars show 95% CI. *p* value from the interaction term (Genotype x Time) of two-way repeated measures ANOVA against the entire dark period. Total locomotor activity was assessed every cycle in the first 10 minute **(B)** and from minute 14–24 **(C)** of the dark period, as well as the whole light period **(D)**. *rln3a$^{c.158T}$* and *rln3a$^{c.158C}$* had similar levels of activity in all time periods tested **(B-D)**. **(B-D)** Crosses represent mean and error bars represent 95% CI, individual larval measurements were plotted as unfilled circles. For data satisfying normality criteria by the Shapiro-Wilk test, *p* values were reported from Welch's t-test, effect size as Cohen's *d*. Otherwise, *p* values were reported from Mann-Whitney test, *r* reported as non-parametric effect size.

Table 4.2 Statistical analysis of locomotor activity in the visual motor response of non-sibling WT

First 10 minutes

Cycle	Total locomotor activity (mm)		p value	Effect size
	$rln3a^{c.158C}$	$rln3a^{c.158T}$		
1	Mdn = 1711, IQR [1351, 2193]	Mdn = 1825, IQR [1525, 1953]	W = 220, p = .82	r = .037
2	M = 1817, 95% CI [1514, 2121]	M = 1526, 95% CI [1526, 1823]	t(40.7) = 1.43, p = .16	d = 0.43
3	Mdn = 1638, IQR [1361, 1886]	Mdn = 1711, IQR [1332, 2017]	W = 204, p = .54	r = .097
4	Mdn = 1367, IQR [1055, 1677]	Mdn = 1449, IQR [1070, 1691]	W = 231.5, p = .98	r = .006
5	Mdn = 1023, IQR [877, 1194]	Mdn = 1159, IQR [869, 1368]	W = 194, p = .39	r = .13
6	Mdn = 926, IQR [682, 1085]	Mdn = 1050, IQR [635, 1271]	W = 198, p = .45	r = .12

Minute 14–24

Cycle	Total locomotor activity (mm)		p value	Effect size
	$rln3a^{c.158C}$	$rln3a^{c.158T}$		
1	Mdn = 745, IQR [462, 1465]	Mdn = 1069, IQR [774, 1576]	W = 201, p = .49	r = .11
2	Mdn = 667, IQR [417, 1638]	Mdn = 965, IQR [365, 1525]	W = 227, p = .95	r = .011
3	Mdn = 281, IQR [202, 1044]	Mdn = 488, IQR [221, 1365]	W = 187, p = .30	r = .16
4	Mdn = 148, IQR [81.4, 224]	Mdn = 281, IQR [107, 483]	W = 185, p = .28	r = .17
5	Mdn = 67.1, IQR [44.4, 96.0]	Mdn = 79.3, IQR [38.7, 174]	W = 217, p = .76	r = .048
6	Mdn = 64.3, IQR [27.9, 106]	Mdn = 84.7, IQR [50.8, 166]	W = 184.5, p = .27	r = .17

$rln3a^{c.158C}$ n = 14, $rln3a^{c.158T}$ n = 14. *p < 0.05.

Table 4.2 Statistical analysis of locomotor activity in the visual motor response of non-sibling WT (continued)

Whole light period

Cycle	Total locomotor activity (mm)		p value	Effect size
	$rln3a^{c.158C}$	$rln3a^{c.158T}$		
1	M = 4722, 95% CI [3863, 5581]	M = 4619, 95% CI [3805, 5433]	$t(40.4)$ = 0.18, p = .86	d = 0.055
2	M = 3962, 95% CI [3261, 4663]	M = 3877, 95% CI [3204, 4550]	$t(40.6)$ = 0.18, p = .86	d = 0.056
3	M = 2706, 95% CI [2163, 3248]	M = 3222, 95% CI [2574, 3870]	$t(40.5)$ = 1.27, p = .21	d = 0.38
4	Mdn = 1717, IQR [1203, 2213]	Mdn = 2341, IQR [1351, 3024]	W = 181, p = .24	r = .18
5	Mdn = 1168, IQR [744, 1784]	Mdn = 1528, IQR [853, 1914]	W = 207, p = .59	r = .085
6	Mdn = 589, IQR [429, 989]	Mdn = 803, IQR [499, 1663]	W = 186, p = .29	r = .16

$rln3a^{c.158C}$ n = 14, $rln3a^{c.158T}$ n = 14. *p < 0.05.

4.3   Discussion

Initially, the C-peptide was dismissed as unimportant in Rln3 function due to its lack of conserved residues, compared to the A- and B-chains (Wilkinson et al. 2005). The zebrafish A- and B-chains have 79% and 86% sequence identity to human RLN3 respectively (Donizetti et al. 2009), compared to 21% in the zebrafish Rln3 C-peptide. In this study, fish possessing the $rln3a^{c.158T}$ allele exhibited increased activity in the visual motor response compared with fish possessing the $rln3a^{c.158C}$ allele. This effect is only seen in one of the two genetic backgrounds tested, indicating that it is likely that gene interactions are occurring and contributing to the effect.

In *Rln3* null mutant mice, the genetic background of the mice was thought to be the reason for contradicting phenotypes in feeding and stress responses, where mice with mixed genetic backgrounds displayed decreased body weight (Sutton et al. 2009) and slight hypersensitivity to stress (Smith et al. 2009), although these differences were not detected in backcrossed *Rln3a* null mutant mice (Smith et al. 2012). Hence, it is likely that genetic background would affect the phenotypes detected in the $rln3a^{sq4sj-/-}$ mutant line as well. Mutants were outcrossed twice before behavioural testing to dilute potential CRISPR off-target effects, which could introduce different polymorphisms. Although mutants were outcrossed to the same AB WT strain, genetic variability within inbred zebrafish strains are estimated to be as high as 7% (Guryev et al. 2006). One genetic difference between tested groups in this study is the presence of the c.158C>T polymorphism in WT siblings. $rln3a^{sq4sj-/-}$ mutants always inherited the c.158C= form, implying genetic linkage, which may obscure mutant effects (Gerlai 1996).

As the c.158C>T polymorphism causes a non-synonymous change in the amino acid threonine to isoleucine, it may represent a loss of function, changing from a polar amino acid with a reactive hydroxyl group to one that has a hydrophobic, non-reactive side chain (Betts & Russell 2003). Due to the proximity of the substituted residue to the cleavage site of the propeptide, it may affect its processing, although it does not reside in the furin convertase cleavage site (RWRR) which lies between the B- and C-chain (Liu et al. 2003b).

The RLN3 C-peptide was found to have distinct neuronal activity in cultured rat hippocampal neurons, and the C-peptide induced sustained calcium activity than the RLN peptide (Brailoiu et al. 2009). This role could be unrelated to RLN3 function, as the peptide has different receptor binding efficiencies to brain membranes than RLN3. However, despite a potential behavioural function in zebrafish, the highly non-conserved nature of C-peptide indicates that this might be a species-specific function.

5.   GENERAL DISCUSSION AND FUTURE DIRECTIONS

5.1   General discussion

To better understand the behavioural role of the neuropeptide RLN3, zebrafish *rln3a* mutants were created, which introduced the genetic study of a different organism into the RLN3 field. An optimised protocol using the CRISPR/Cas9 system was developed, producing zebrafish mutants within a week, and allowed the successful generation of nine mutant variants in three *rln3*-related genes (Table 2.6). The mutant with a 7 bp deletion in the *rln3a* gene (mutant allele denoted as *rln3a$^{sq4sj-/-}$*, Figure 2.1) was chosen for further behavioural analysis.

rln3a$^{sq4sj-/-}$ mutants were compared with WT siblings in behaviours known to be affected by RLN3 in rodents, such as stress and anxiety, and body weight. In the novel tank diving assay, zebrafish displayed mildly reduced anxiety levels, where it was only significantly different from WTs in the first minute. If exposed to stress prior to the assay, locomotion was significantly decreased in mutants but not in WTs, implying sensitivity to stress (Figure 3.2). Mutants displayed significantly reduced body weight in week 5 compared to WT, although body weights in the two groups remained similar subsequently (Figure 3.4). These findings are consistent with mouse null mutation studies, where only mild changes were observed (Figure 3.6).

Additionally, the visual motor response was introduced to study the effects of Rln3 function. This was to test if *rln3a* was acting downstream of the dHbL via the interpeduncular nucleus which projects to the PAG and NI, which presumably would have resulted in delayed recovery of dark-evoked hyperactivity (Agetsuma

et al. 2010). However, the visual motor response was similar in both groups of fish (Figure 3.3). One problem with using knockout mutations is that compensation can occur, allowing the animal to adapt to the loss of the gene. This could be a reason why only mild differences in behaviour were observed. The paralogue *rln3b* was upregulated by four-fold in mutants compared to WTs (Figure 3.5), indicating that it was possibly compensating by for the loss of *rln3a*.

A SNP was discovered (*rln3a$^{c.158C>T}$*) in the WT siblings of the mutants that were used for behavioural testing (Figure 4.1, Figure 4.2). When WT siblings were tested in the visual motor response, fish with the *rln3a$^{c.158T}$* allele were hyperactive in the early dark period (first 10 minutes) compared to fish with the *rln3a$^{c.158C}$* allele (Figure 4.3). However, using the non-sibling WT fish, there was no difference in behaviour between these two groups (Figure 4.4). This implies that the C-peptide may have a function in the behaviour, and behavioural effects are susceptible to different genetic backgrounds.

5.2   Future directions

One conclusion is that the loss-of-function via genetic mutation fails to provide evidence for a role of Rln3 in behaviours that have been proposed to involve the peptide. Although studying mutants are one way to elucidate biological functions, there are multiple problems in the method of testing that may result in the lack of a distinct phenotypic abnormality (Barbaric et al. 2007). A main consideration is that biological systems are robust, and are often able to adapt despite the removal of a single component. The Rln3/RXFP3 system in zebrafish has duplicated members due whole genome duplication in teleosts (Good et al. 2012, Yegorov et al. 2014), and there were attempts to mutate multiple components

simultaneously using efficient CRISPR methods to create double knockouts of ligand and receptors. However, CRISPR/Cas9 introduced multiple alleles with varying indels. This mosaicism caused difficulties in mutation detection and screening. It became increasingly difficult to maintain multiple mutation lines concurrently; therefore a single clean mutation was used for behavioural testing. Also, neuropeptide systems are somewhat redundant in nature, and a variety of neuropeptides act together to control complex behaviours such as feeding and arousal, and compensation is likely to occur.

Two alternative methods are proposed to overcome this issue. Firstly, a heat shock-induced overexpression line with the heat shock promoter 70 (*hsp70*) can induce acute gain-of-function, such that compensation will not take place (Halloran et al. 2000). This method has been used to overexpress various neuropeptides in zebrafish, allowing effective and detailed analysis of how these neuropeptides affect sleep (Woods et al. 2014).

In preliminary studies, a transgenic line Tg(*hsp70:rln3a-T2A-GFP*) was generated, and demonstrated to increase *rln3a* expression after incubating larvae at 37°C for 1 h (Figure 5.1). Cells expressing *rln3a* mRNA were observed in the entire zebrafish larvae using ISH, even in the trunk, verifying the construct used for overexpression. However, using qRT-PCR to quantify levels of expression showed that rln3a transcripts returned to baseline levels 75 min after the removing fish from 37°C. This was insufficient time to conduct behavioural experiments and more optimisation was required before these larvae can be used reliably.
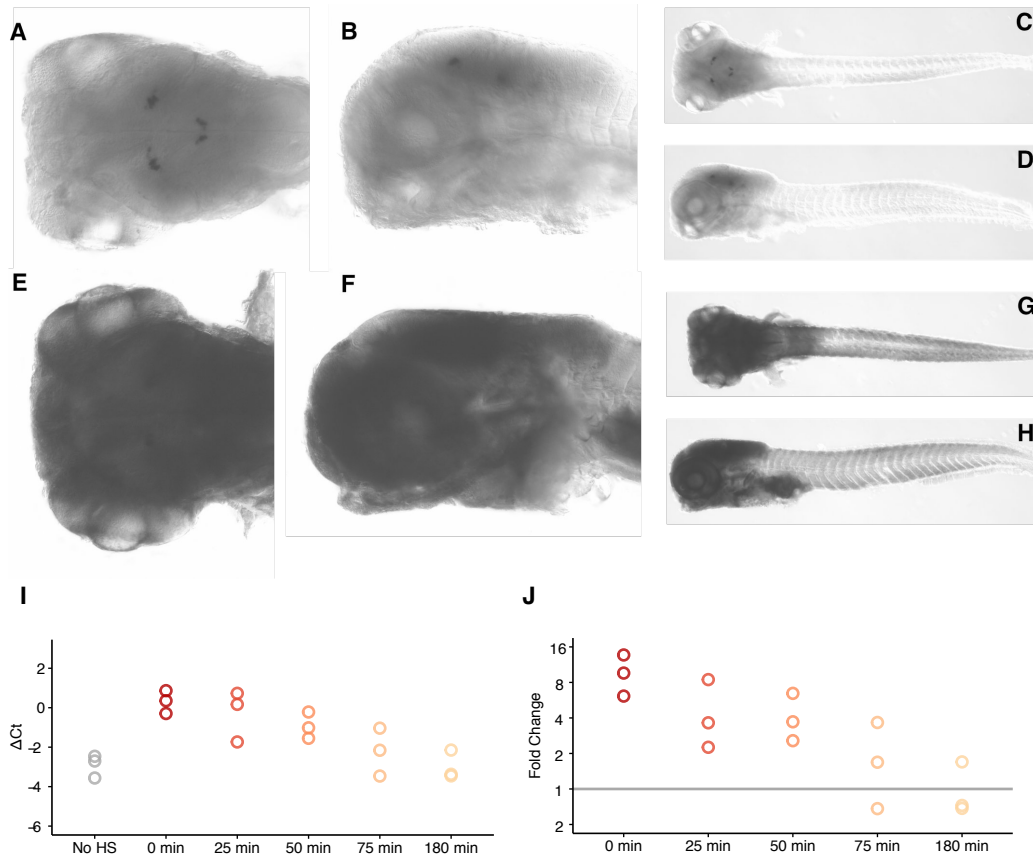
Figure 5.1 Heat shock overexpression of *rln3a*

(A-D) ISH of *rln3a* in Tg(*hsp70:rln3a-T2A-GFP*) larvae at 4 dpf before heat shock. **(A)** Head, dorsal view. **(B)** Head, lateral view. **(C)** Whole larvae, dorsal view. **(D)** Whole larvae, lateral view. **(E-H)** ISH of *rln3a* in Tg(*hsp70:rln3a-T2A-GFP*) larvae at 4 dpf after heat shock at 37°C for 1h. **(E)** Head, dorsal view. **(F)** Head, lateral view. **(G)** Whole larvae, dorsal view. **(H)** Whole larvae, lateral view. **(I-J)** Quantitative reverse-transcriptase PCR showing expression levels of *rln3a* without heat shock (no HS), and at time points after the heat shock expressed as normalised threshold cycle values **(I)** or fold change **(J)**. By about 75 minutes, *rln3a* expression returned to baseline levels. Individual fish are plotted as unfilled circles, where each biological sample is represented by an average of three technical repeats.

Secondly, driver lines can be created for Rln3a-producing neurons. This could be done by knocking in transgenes into the *rln3a* locus as an extension of CRISPR capabilities. Several knock-in methods have been presented to insert large transgenes into targeted gene loci (Auer et al. 2014a, Bedell & Ekker 2015, Hisano et al. 2015, Kimura et al. 2014, Li et al. 2015, Sakuma et al. 2015), but

these methods have proven to be technically difficult. Instead of attempting to insert full-length transgenes into the genome, small, single stranded DNAs could be inserted more easily (Bedell & Ekker 2015, Bedell et al. 2012). Hence, an attP landing site for *PhiC31* transposase (Lu et al. 2011, Mosimann et al. 2013) was used for insertion into the *rln3a* locus (Figure 5.2), providing a specific site for recombination of a separate construct containing the desired transgene. Although 50% of the F_0 injected fish contained the inserted fragment as detected by PCR, the germline transmission rate was too low, and attempts at producing an F_1 generation were unsuccessful.
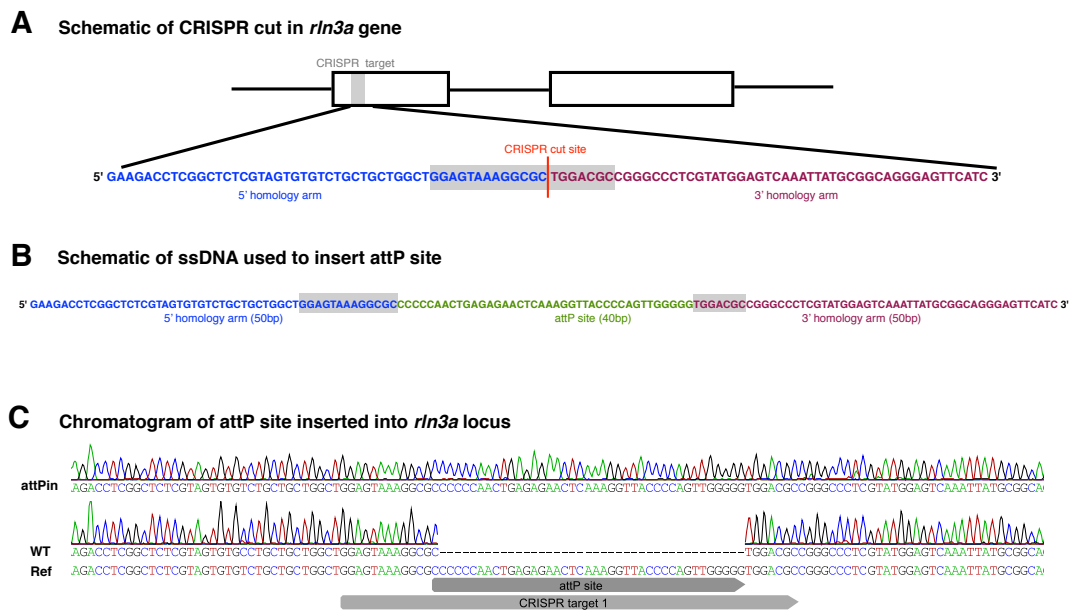
Figure 5.2 Insertion of attP landing site into the *rln3a* locus using ssDNA

(A) Schematic diagram of *rln3a* gene. CRISPR target located in exon 1 shaded in grey. Homology arms were taken 50 bp upstream and downstream of the CRISPR cut site. **(B)** Schematic diagram of the ssDNA design used, consisting of the attP site flanked by arms homologous to the *rln3a* cut site. **(C)** Sequencing chromatogram showing insertion of the attP site into injected fish. DNA from mosaic injected fish fins was cloned into the vector pGEM-T Easy (Promega) to obtain clean sequences. The chromatogram labelled 'attPin' represents allele with attP site inserted into the *rln3a* CRISPR target site. The WT chromatogram is also shown, while 'Ref' represents the annotated reference sequence of the *rln3a* CRISPR site with the inserted attP site.

Inserting the transcription activator Gal4 can into the *rln3a* locus could allow specific manipulations in Rln3-expressing neurons when combined with transgenes, such as optogenetic tools, or toxins such as tetradotoxin (Asakawa et al. 2007) or nitroreductase (Curado et al. 2008), coupled to the upstream activator sequence (Halpern et al. 2008, Scheer & Campos-Ortega 1999). This would provide more specific tools to improve the understanding of the role of Rln3a in the zebrafish brain and how it controls behaviour.

Moreover, it would be interesting to investigate the involvement of the PAG in the visual motor response. One study would be to determine if the cells containing Rln3a are the ones that activated to dark stimuli. Having a driver line that expresses a fluorescent reporter in Rln3a-containing cells will allow easy identification of these cells within the PAG. This would greatly improve the localisation of these cells, as the only available method currently is ISH, which has limited resolution.

Another direction would be to conduct more studies to investigate the behavioural effects of the SNP in the C-peptide, which has demonstrated some effect in the visual motor response. This can be done by overexpressing the peptide and testing for behaviour. Furthermore, other RLN3-associated behaviours can be tested. However, it would be important to know which cells respond to the peptide, which requires knowledge of the receptor and downstream pathways.

6. BIBLIOGRAPHY

Agetsuma M, Aizawa H, Aoki T, Nakayama R, Takahoko M, Goto M, Sassa T, Amo R, Shiraki T, Kawakami K, Hosoya T, Higashijima S, Okamoto H. 2010. The habenula is crucial for experience-dependent modification of fear responses in zebrafish. *Nat. Neurosci.* 13(11):1354–56

Asakawa K, Suster ML, Mizusawa K, Nagayoshi S, Kotani T, Urasaki A, Kishimoto Y, Hibi M, Kawakami K. 2007. Genetic dissection of neural circuits by Tol2 transposon-mediated Gal4 gene and enhancer trapping in zebrafish. *Proc Nat Acad Sci USA.* 105(4):1255–60

Auer TO, Duroure K, Concordet J-P, Del Bene F. 2014a. CRISPR/Cas9-mediated conversion of eGFP- into Gal4-transgenic lines in zebrafish. *Nat. Protoc.* 9(12):2823–40

Auer TO, Duroure K, De Cian A, Concordet J-P, Del Bene F. 2014b. Highly efficient CRISPR/Cas9-mediated knock-in in zebrafish by homology-independent DNA repair. *Genome Res.* 24(1):142–53

Bandler R, Depaulis A. 1991. Midbrain periaqueductal gray control of defensive behavior in the cat and the rat. In *The Midbrain Periaqueductal Gray Matter*, eds. A Depaulis, R Bandler, pp. 175–98. New York: Plenum Press

Bandler R, Shipley MT. 1994. Columnar organization in the midbrain periaqueductal gray: modules for emotional expression? *Trends Neurosci.* 17(9):379–89

Banerjee A, Shen P-J, Ma S, Bathgate RAD, Gundlach AL. 2010. Swim stress excitation of nucleus incertus and rapid induction of relaxin-3 expression via CRF1 activation. *Neuropharmacology.* 58(1):145–55

Barbaric I, Miller G, Dear TN. 2007. Appearances can be deceiving: Phenotypes of knockout mice. *Briefings Funct. Genomics Proteomics.* 6(2):91–103

Bassett AR, Tibbit C, Ponting CP, Liu J-L. 2013. Highly efficient targeted mutagenesis of Drosophila with the CRISPR/Cas9 system. *Cell Rep.* 4(1):220–28

Bathgate RAD, Hsueh AJW, Sherwood OD. 2006. Physiology and molecular biology of the relaxin peptide family. In *Knobil and Neill's Physiology of Reproduction*, ed. DN Jimmy, pp. 679–768. Elsevier Inc. Third Edit ed.

Bathgate RAD, Oh MHY, Ling WJJ, Kaas Q, Hossain MA, Gooley PR, Rosengren KJ. 2013. Elucidation of relaxin-3 binding interactions in the extracellular loops of RXFP3. *Front. Endocrinol.* 4(13):1–9

Bathgate RAD, Samuel CS, Burazin TCD, Layfield S, Claasz AA, Reytomas IGT, Dawson NF, Zhao C, Bond C, Summers RJ, Parry LJ, Wade JD, Tregear GW. 2002. Human relaxin gene 3 (H3) and the equivalent mouse relaxin (M3) gene: Novel members of the relaxin peptide family. *J. Biol. Chem.* 277(2):1148–57

Bedell VM, Ekker SC. 2015. Using engineered endonuclease to create knockout and knockin zebrafish models. In *Chromosomal Mutagenesis*, Vol. 1239, ed. SM Pruett-Miller, pp. 291–305. New York: Springer

Bedell VM, Wang Y, Campbell JM, Poshusta TL, Starker CG, Krug RG, Tan W, Penheiter SG, Ma AC, Leung AYH, Fahrenkrug SC, Carlson DF, Voytas DF, Clark KJ, Essner JJ, Ekker SC. 2012. In vivo genome editing using a high-efficiency TALEN system. *Nature*. 491(7422):114–18

Behbehani MM. 1995. Functional characteristics of the midbrain periaqueductal gray. *Prog. Neurobiol.* 46:575–605

Betts MJ, Russell RB. 2003. Amino acid properties and consequences of subsitutions. In *Bioinformatics for Geneticists*, eds. MR Barnes, IC Gray. Wiley

Blackburn PR, Campbell JM, Clark KJ, Ekker SC. 2013. The CRISPR system - keeping zebrafish gene targeting fresh. *Zebrafish*. 10(1):116–18

Blasiak A, Blasiak T, Lewandowski MH, Hossain MA, Wade JD, Gundlach AL. 2013. Relaxin-3 innervation of the intergeniculate leaflet of the rat thalamus - neuronal tract-tracing and in vitro electrophysiological studies. *Eur. J. Neurosci.* 37(8):1284–94

Blasiak A, Siwiec M, Grabowiecka A, Blasiak T, Czerw A, Blasiak E, Kania A, Rajfur Z, Lewandowski MH, Gundlach AL. 2015. Excitatory orexinergic innervation of rat nucleus incertus - Implications for ascending arousal, motivation and feeding control. *Neuropharmacology*. 99:432–47

Brailoiu E, Dun SL, Gao X, Brailoiu GC, Li JG, Luo JJ, Yang J, Chang JK, Liu-Chen LY, Dun NJ. 2009. C-peptide of preproinsulin-like peptide 7: Localization in the rat brain and activity in vitro. *Neuroscience*. 159(2):492–

500

Burazin TCD, Bathgate RAD, Macris M, Layfield S, Gundlach AL, Tregear GW. 2002. Restricted, but abundant, expression of the novel rat gene-3 (R3) relaxin in the dorsal tegmental region of brain. *J. Neurochem.* 82(6):1553–57

Burbach JPH. 2011. What are neuropeptides? In *Neuropeptides: Methods and Protocols*, ed. A Merighi, pp. 1–36. Humana Press

Burger A, Lindsay H, Felker A, Hess C, Anders C, Chiavacci E, Zaugg J, Weber LM, Catena R, Jinek M, Robinson MD, Mosimann C. 2016. Maximizing mutagenesis with solubilized CRISPR-Cas9 ribonucleoprotein complexes. *Development.* 143(11):2025–37

Cachat J, Stewart A, Grossman L, Gaikwad S, Kadri F, Chung KM, Wu N, Wong K, Roy S, Suciu C, Goodspeed J, Elegante M, Bartels B, Elkhayat S, Tien D, Tan J, Denmark A, Gilder T, Kyzar E, Dileo J, Frank K, Chang K, Utterback E, Hart P, Kalueff A V. 2010. Measuring behavioral and endocrine responses to novelty stress in adult zebrafish. *Nat. Protoc.* 5(11):1786–99

Calvez J, De Ávila C, Matte LO, Guèvremont G, Gundlach AL, Timofeeva E. 2016a. Role of relaxin-3/RXFP3 system in stress-induced binge-like eating in female rats. *Neuropharmacology.* 102:207–15

Calvez J, de Avila C, Timofeeva E. 2016b. Sex-specific effects of relaxin-3 on food intake and body weight gain. *Br. J. Pharmacol.*

Calvez J, Lenglos C, de Ávila C, Guèvremont G, Timofeeva E. 2015. Differential effects of central administration of relaxin-3 on food intake and hypothalamic

neuropeptides in male and female rats. *Genes, Brain Behav.* 14(7):550–63

Chandler CH, Chari S, Dworkin I. 2013. Does your gene need a background check? How genetic background impacts the analysis of mutations, genes, and evolution. *Trends Genet.* 29(6):358–66

Chang N, Sun C, Gao L, Zhu D, Xu X, Zhu X, Xiong J-W, Xi JJ. 2013. Genome editing with RNA-guided Cas9 nuclease in zebrafish embryos. *Cell Res.* 23(4):465–72

Chang YFF, Imam JS, Wilkinson MF. 2007. The nonsense-mediated decay RNA surveillance pathway. *Annu. Rev. Biochem.* 76:51–74

Chen J, Kuei C, Sutton SW, Bonaventure P, Nepomuceno D, Eriste E, Sillard R, Lovenberg TW, Liu C. 2005. Pharmacological characterization of relaxin-3/INSL7 receptors GPCR135 and GPCR142 from different mammalian species. *J. Pharmacol. Exp. Ther.* 312(1):83–95

Cheng R-K, Krishnan S, Jesuthasan S. 2016. Activation and inhibition of tph2 serotonergic neurons operate in tandem to influence larval zebrafish preference for light over darkness. *Sci. Rep.* 6(October 2015):20788

Cho SW, Kim S, Kim Y, Kweon J, Kim HS, Bae S, Kim J. 2014. Analysis of off-target effects of CRISPR/Cas-derived RNA-guided endonucleases and nickases. *Genome Res.* 24:132–41

Colwill RM, Creton R. 2011. Imaging escape and avoidance behavior in zebrafish larvae. *Rev. Neurosci.* 22(1):63–73

Cong L, Ran FA, Cox D, Lin S, Barretto R, Habib N, Hsu PD, Wu X, Jiang W, Marraffini LA, Zhang F. 2013. Multiplex genome engineering using CRISRP/Cas9 systems. *Science*. 339(6121):819–23

Curado S, Stainier DYR, Anderson RM. 2008. Nitroreductase-mediated cell/tissue ablation in zebrafish: a spatially and temporally controlled ablation method with applications in developmental and regeneration studies. *Nat. Protoc.* 3(6):948–54

Dawson NF, Tan Y, Summers RJ, Otvos ML, Tregear JGW, Wade JD. 2001. Solid phase syntheses of rat prorelaxin C-peptides (1-73) and (76-101). In *Relaxin 2000*, pp. 249–50

De Oca BM, DeCola JP, Maren S, Fanselow MS. 1998. Distinct regions of the periaqueductal gray are involved in the acquisition and expression of defensive responses. *J. Neurosci.* 18(9):3426–32

Donizetti A, Fiengo M, Iazzetti G, del Gaudio R, Di Giaimo R, Pariante P, Minucci S, Aniello F. 2015. Expression analysis of five zebrafish rxfp3 homologues reveals evolutionary conservation of gene expression pattern. *J. Exp. Zool. Part B Mol. Dev. Evol.* 324(1):22–29

Donizetti A, Fiengo M, Minucci S, Aniello F. 2009. Duplicated zebrafish relaxin-3 gene shows a different expression pattern from that of the co-orthologue gene. *Dev. Growth Differ.* 51(8):715–22

Donizetti A, Grossi M, Pariante P, D'Aniello E, Izzo G, Minucci S, Aniello F. 2008. Two neuron clusters in the stem of postembryonic zebrafish brain

specifically express relaxin-3 gene: first evidence of nucleus incertus in fish. *Dev. Dyn.* 237:3864–69

Dwight Z, Palais R, Wittwer CT. 2011. uMELT: prediction of high-resolution melting curves and dynamic melting profiles of PCR products in a rich web application. *Bioinformatics.* 27(7):1019–20

Egan RJ, Bergner CL, Hart PC, Cachat JM, Canavello PR, Elegante MF, Elkhayat SI, Bartels BK, Tien AK, Tien DH, Mohnot S, Beeson E, Glasgow E, Amri H, Zukowska Z, Kalueff A V. 2009. Understanding behavioral and physiological phenotypes of stress and anxiety in zebrafish. *Behav. Brain Res.* 205(1):38–44

Emran F, Rihel J, Dowling JE. 2008. A behavioral assay to measure responsiveness of zebrafish to changes in light intensities. *J. Vis. Exp.* e923(20):1–6

Fang Y, Gupta V, Karra R, Holdway JE, Kikuchi K, Poss KD. 2013. Translational profiling of cardiomyocytes identifies an early Jak1/Stat3 injury response required for zebrafish heart regeneration. *Proc. Natl. Acad. Sci. U. S. A.* 110(33):13416–21

Fanselow MS. 1991. The midbrain periaqueductal gray as a coordinator of action in response to fear and anxiety. In *The Midbrain Periaqueductal Gray Matter*, eds. A Depaulis, R Bandler, pp. 151–73. New York: Plenum Press

Fiengo M, Del Gaudio R, Iazzetti G, Di Giaimo R, Minucci S, Aniello F, Donizetti A. 2013. Developmental expression pattern of two zebrafish rxfp3 paralogue

114

genes. *Dev. Growth Differ.* 3:766–75

Fiengo M, Donizetti A, del Gaudio R, Minucci S, Aniello F. 2012. Characterization, cDNA cloning and expression pattern of relaxin gene during embryogenesis of Danio rerio. *Dev. Growth Differ.* 54(5):579–87

Flicek P, Amode MR, Barrell D, Beal K, Billis K, Brent S, Carvalho-Silva D, Clapham P, Searle SMJ, et al. 2014. Ensembl 2014. *Nucleic Acids Res.* 42(D1):749–55

Friedrich RW, Jacobson GA, Zhu P. 2010. Circuit neuroscience in zebrafish. *Curr. Biol.* 20(8):R371-81

Gagnon JA, Valen E, Thyme SB, Huang P, Ahkmetova L, Pauli A, Montague TG, Zimmerman S, Richter C, Schier AF. 2014. Efficient mutagenesis by Cas9 protein-mediated oligonucleotide insertion and large-scale assessment of single-guide RNAs. *PLoS One*. 9(5):5–12

Gaj T, Gersbach CA, Barbas CF. 2013. ZFN, TALEN, and CRISPR/Cas-based methods for genome engineering. *Trends Biotechnol.* 31(7):397–405

Ganella DE, Ma S, Gundlach AL. 2013. Relaxin-3/RXFP3 signaling and neuroendocrine function - a perspective on extrinsic hypothalamic control. *Front. Endocrinol.* 4(128):1–11

Ganella DE, Ryan PJ, Bathgate RAD, Gundlach AL. 2012. Increased feeding and body weight gain in rats after acute and chronic activation of RXFP3 by relaxin-3 and receptor- selective peptides : functional and therapeutic implications. *Behav. Pharmacol.* 23:516–25

Gerlai R. 1996. Gene-targeting studies of mammalian behavior: Is it the mutation or the background genotype? *Trends Neurosci.* 19(5):177–81

Gerlai R, Lahav M, Guo S, Rosenthal A. 2000. Drinks like a fish: zebra fish (Danio rerio) as a behavior genetic model to study alcohol effects. *Pharmacol. Biochem. Behav.* 67:773–82

Getting P. 1989. Emerging principles governing the operation of neural networks. *Annu. Rev. Neurosci.* 185–204

Ghattas MH, Mehanna ET, Mesbah NM, Abo-Elmatty DM. 2013. Relaxin-3 is associated with metabolic syndrome and its component traits in women. *Clin. Biochem.* 46(1–2):45–48

Good-Avila S V, Yegorov S, Harron S, Bogerd J, Glen P, Ozon J, Wilson BC. 2009. Relaxin gene family in teleosts: phylogeny, syntenic mapping, selective constraint, and expression analysis. *BMC Evol. Biol.* 9:293

Good S, Yegorov S, Martijn J, Franck J, Bogerd J. 2012. New insights into ligand-receptor pairing and coevolution of relaxin family peptides and their receptors in teleosts. *Int. J. Evol. Biol.* 2012(310278):1–14

Goto M, Swanson LW, Canteras NS, Sa CEP. 2001. Connections of the Nucleus Incertus. *J. Comp. Neurol.* 438:86–122

Gray JA, McNaughton N. 2003. *The Neuropsychology of Anxiety: An Enquiry into the Functions of the Septo-Hippocampal System*. Oxford University Press. 2nd ed.

Grone BP, Marchese M, Hamling KR, Kumar MG, Krasniak CS, Sicca F, Santorelli FM, Patel M, Baraban SC. 2016. Epilepsy, behavioral abnormalities, and physiological comorbidities in syntaxin-binding protein 1 (STXBP1) mutant zebrafish. *PLoS One*. 11(3):1–25

Grosse J, Heffron H, Burling K, Akhter M, Habib AM, Rogers GJ, Richards P, Larder R, Rimmington D, Adriaenssens AA, Parton L, Powell J, Binda M, Colledge WH, Doran J, Toyoda Y, Wade JD, Aparicio S, Carlton MBL, Coll AP, Reimann F, O'Rahilly S, Gribble FM. 2014. Insulin-like peptide 5 is an orexigenic gastrointestinal hormone. *Proc Nat Acad Sci USA*. 111(30):11133–38

Gundlach AL, Smith CM, Ryan PJ, Blasiak A, Olucha-Bordonau FE, Ma S. 2013. Relaxins. In *Handbook of Biologically Active Peptides*, ed. A Kastin, pp. 907–16. Academic Press. 2nd ed.

Guo S. 2004. Linking genes to brain, behavior and neurological diseases: what can we learn from zebrafish? *Genes, Brain Behav*. 3(2):63–74

Guryev V, Koudijs MJ, Berezikov E, Johnson SL, Plasterk RH a, Eeden JM Van, Cuppen E, Eeden FJM Van. 2006. Genetic variation in the zebrafish. *Genome Res*. (16):491–97

Halloran MC, Sato-Maeda M, Warren JT, Su F, Lele Z, Krone PH, Kuwada JY, Shoji W. 2000. Laser-induced gene expression in specific cells of transgenic zebrafish. *Development*. 127:1953–60

Halls ML, van der Westhuizen ET, Bathgate RAD, Summers RJ. 2007. Relaxin

Family Peptide Receptors – former orphans reunite with their parent ligands to activate multiple signalling pathways. *Br. J. Pharmacol.* 150:677–91

Halpern ME, Rhee J, Goll MG, Akitake CM, Parsons M, Leach SD. 2008. Gal4/UAS transgenic tools and their applications to zebrafish. *Zebrafish.* 5(2):97–110

Haugaard-Kedstrom LM, Shabanpoor F, Hossain MA, Clark RJ, Ryan PJ, Craik DJ, Gundlach AL, Wade JD, Bathgate RAD, Rosengren KJ. 2011. Design, synthesis, and characterization of a single-chain peptide antagonist for the relaxin-3 receptor RXFP3. *J. Am. Chem. Soc.* 133:4965–74

Hauger RL, Risbrough VB, Oakley RH, Olivares-Reyes JA, Dautzenberg FM. 2009. Role of CRF receptor signaling in stress vulnerability, anxiety, and depression. *Ann. N. Y. Acad. Sci.* 1179:120–43

Herbert J. 1993. Peptides in the limbic system: Neurochemical codes for co-ordinated adaptive responses to behavioural and physiological demand. *Prog. Neurobiol.* 41(6):723–91

Hida T, Takahashi E, Shikata K, Hirohashi T, Sawai T, Seiki T, Tanaka H, Kawai T, Ito O, Arai T, Yokoi A, Hirakawa T, Ogura H, Nagasu T, Miyamoto N, Kuromitsu J. 2006. Chronic Intracerebroventricular Administration of Relaxin-3 Increases Body Weight in Rats. *J. Recept. Signal Transduct.* 26(3):147–58

Hisano Y, Sakuma T, Nakade S, Ohga R, Ota S, Okamoto H, Yamamoto T, Kawahara A. 2015. Precise in-frame integration of exogenous DNA

mediated by CRISPR/Cas9 system in zebrafish. *Sci. Rep.* 5:8841

Horowitz SS, Blanchard JH, Morin LP. 2004. Intergeniculate leaflet and ventral lateral geniculate nucleus afferent connections: An anatomical substrate for functional input from the vestibulo-visuomotor system. *J. Comp. Neurol.* 474(2):227–45

Hosken IT, Sutton SW, Smith CM, Gundlach AL. 2015. Relaxin-3 receptor (Rxfp3) gene knockout mice display reduced running wheel activity: Implications for role of relaxin-3/RXFP3 signalling in sustained arousal. *Behav. Brain Res.* 278:167–75

Hruscha A, Krawitz P, Rechenberg A, Heinrich V, Hecht J, Haass C, Schmid B. 2013. Efficient CRISPR/Cas9 genome editing with low off-target effects in zebrafish. *Development.* 140(May):4982–87

Hsu SYT. 2003. New insights into the evolution of the relaxin - LGR signaling system. *Trends Endocrinol. Metab.* 14(7):303–9

Hsu Y-W a, Wang SD, Wang S, Morton G, Zariwala H a, de la Iglesia HO, Turner EE. 2014. Role of the dorsal medial habenula in the regulation of voluntary activity, motor function, hedonic state, and primary reinforcement. *J. Neurosci.* 34(34):11366–84

Hwang WY, Fu Y, Reyon D, Maeder ML, Kaini P, Sander JD, Joung JK, Peterson RT, Yeh J-RJ. 2013a. Heritable and precise zebrafish genome editing using a CRISPR-Cas system. *PLoS One.* 8(7):

Hwang WY, Fu Y, Reyon D, Maeder ML, Tsai SQ, Sander JD, Peterson RT, Yeh

J-RJ, Joung JK. 2013b. Efficient genome editing in zebrafish using a CRISPR-Cas system. *Nat. Biotechnol.* 31(3):227–29

Ido Y, Vindigni A, Chang K, Stramm L, Chance R, Heath WF, DiMarchi RD, Di Cera E, Williamson JR. 1997. Prevention of vascular and neural dysfunction in diabetic rats by C-peptide. *Science*. 277(5325):563–66

Jao L-E, Wente SR, Chen W. 2013. Efficient multiplex biallelic zebrafish genome editing using a CRISPR nuclease system. *Proc. Natl. Acad. Sci. U. S. A.* 110(34):13904–9

Jinek M, Chylinski K, Fonfara I, Hauer M, Doudna JA, Charpentier E. 2012. A programmable dual-RNA-guided DNA endonuclease in adaptive bacterial immunity. *Science*. 337(6096):816–21

Kalueff A V., Stewart AM, Gerlai R. 2014. Zebrafish as an emerging model for studying complex brain disorders. *Trends Pharmacol. Sci.* 35(2):63–75

Kastman HE, Blasiak A, Walker L, Siwiec M, Krstew E V, Gundlach AL, Lawrence AJ. 2016. Nucleus incertus Orexin2 receptors mediate alcohol seeking in rats. *Neuropharmacology*. 110(2016):82–91

Kearse M, Moir R, Wilson A, Stones-Havas S, Cheung M, Sturrock S, Buxton S, Cooper A, Markowitz S, Duran C, Thierer T, Ashton B, Meintjes P, Drummond A. 2012. Geneious Basic: An integrated and extendable desktop software platform for the organization and analysis of sequence data. *Bioinformatics*. 28(12):1647–49

Kimura Y, Hisano Y, Kawahara A, Higashijima S. 2014. Efficient generation of

knock-in transgenic zebrafish carrying reporter/driver genes by CRISPR/Cas9-mediated genome engineering. *Sci. Rep.* 4(6545):1–7

Krzywinski M, Altman N. 2013. Points of significance: Error bars. *Nat. Methods*. 10(10):921–22

Kumar JR, Rajkumar R, Farooq U, Lee LC, Tan FCK, Dawe GS. 2015. Evidence of D2 receptor expression in the nucleus incertus of the rat. *Physiol. Behav.* 151:525–34

Kumar JR, Rajkumar R, Jayakody T, Marwari S, Hong JM, Ma S, Gundlach AL, Lai MKP, Dawe GS. 2016. Relaxin' the brain: A case for targeting the nucleus incertus network and relaxin-3/RXFP3 system in neuropsychiatric disorders. *Br. J. Pharmacol.* doi:10.1111/bph.13564

Kusakabe M, Ishikawa A, Kitano J. 2014. Relaxin-related gene expression differs between anadromous and stream-resident stickleback (Gasterosteus aculeatus) following seawater transfer. *Gen. Comp. Endocrinol.* 205:197–206

Landreh M, Johansson J, Wahren J, Jörnvall H. 2014. The structure, molecular interactions and bioactivities of proinsulin C-peptide correlate with a tripartite molecule. *Biomol. Concepts*. 5(2):109–18

Landreh M, Jornvall H. 2015. C-peptide evolution: Generation from few structural restrictions of bioactivities not necessarily functional. *FEBS Lett.* 589(4):415–18

Lawther AJ, Clissold ML, Ma S, Kent S, Lowry CA, Gundlach AL, Hale MW. 2015.

Anxiogenic drug administration and elevated plus-maze exposure in rats activate populations of relaxin-3 neurons in the nucleus incertus and serotonergic neurons in the dorsal raphe nucleus. *Neuroscience*. 303:270–84

Lee A, Mathuru AS, Teh C, Kibat C, Korzh V, Penney TB, Jesuthasan S. 2010. The habenula prevents helpless behavior in larval zebrafish. *Curr. Biol.* 20(24):2211–16

Lee JH, Koh SQ, Guadagna S, Francis PT, Esiri MM, Chen CP, Wong PT-H, Dawe GS, Lai MKP. 2016. Altered relaxin family receptors RXFP1 and RXFP3 in the neocortex of depressed Alzheimer's disease patients. *Psychopharmacology (Berl).* 233(4):591–98

Lenglos C, Calvez J, Timofeeva E. 2014a. The role of relaxin-3 and its receptor RXFP3 in defense of elevated body weight in diet-induced obesity. *Recept. Clin. Investig.* 1–15

Lenglos C, Mitra A, Guevremont G, Timofeeva E. 2014b. Regulation of expression of relaxin-3 and its receptor RXFP3 in the brain of diet-induced obese rats. *Neuropeptides*. 48(3):119–32

Levin ED, Bencan Z, Cerutti DT. 2007. Anxiolytic effects of nicotine in zebrafish. *Physiol. Behav.* 90:54–58

Li J, Zhang B, Ren Y, Gu S, Xiang Y, Huang C, Du J. 2015. Intron targeting-mediated and endogenous gene integrity-maintaining knockin in zebrafish using the CRISPR/Cas9 system. *Cell Res.* 634–37

Liu C, Chen J, Kuei C, Sutton SW, Nepomuceno D, Bonaventure P, Lovenberg TW. 2005. Relaxin-3/insulin-like peptide 5 chimeric peptide, a selective ligand for G protein-coupled receptor (GPCR)135 and GPCR142 over leucine-rich repeat-containing G protein-coupled receptor 7. *Mol. Pharmacol.* 67(1):231–40

Liu C, Chen J, Sutton SW, Roland B, Kuei C, Farmer N, Sillard R, Lovenberg TW. 2003a. Identification of Relaxin-3 / INSL7 as a Ligand for GPCR142. *J. Biol. Chem.* 278(50):50765–70

Liu C, Eriste E, Sutton SW, Chen J, Roland B, Kuei C, Farmer N, Jörnvall H, Sillard R, Lovenberg TW. 2003b. Identification of relaxin-3/INSL7 as an endogenous ligand for the orphan G-protein-coupled receptor GPCR135. *J. Biol. Chem.* 278(50):50754–64

Livak KJ, Schmittgen TD. 2001. Analysis of relative gene expression data using real-time quantitative PCR and the 2(-Delta Delta C(T)) Method. *Methods.* 25:402–8

Lu C, Walker WH, Sun J, Weisz OA, Gibbs RB, Witchel SF, Sperling MA, Menon RK. 2006. Insulin-Like Peptide 6 : Characterization of Secretory Status and Posttranslational Modifications. *Endocrinology.* 147(12):5611–23

Lu J, Maddison L a, Chen W. 2011. PhiC31 integrase induces efficient site-specific excision in zebrafish. *Transgenic Res.* 20:183–89

Ma S, Blasiak A, Olucha-Bordonau FE, Verberne AJM, Gundlach AL. 2013. Heterogeneous responses of nucleus incertus neurons to corticotrophin-

releasing factor and coherent activity with hippocampal theta rhythm in the rat. *J. Physiol.* 591(Pt 16):3981–4001

Ma S, Bonaventure P, Ferraro T, Shen P-J, Burazin TCD, Bathgate RAD, Liu C, Tregear GW, Sutton SW, Gundlach AL. 2007. Relaxin-3 in GABA projection neurons of nucleus incertus suggests widespread influence on forebrain circuits via G-protein-coupled receptor-135 in the rat. *Neuroscience.* 144(1):165–90

Ma S, Gundlach AL. 2007. Relaxin-family peptide and receptor systems in brain: Insights from recent anatomical and functional studies. *Adv. Exp. Med. Biol.* 612:119–37

Ma S, Olucha-Bordonau FE, Hossain MA, Lin F, Kuei C, Liu C, Wade JD, Sutton SW, Nuñez A, Gundlach AL. 2009a. Modulation of hippocampal theta oscillations and spatial memory by relaxin-3 neurons of the nucleus incertus. *Learn. Mem.* 16(11):730–42

Ma S, Sang Q, Lanciego JL, Gundlach AL. 2009b. Localization of relaxin-3 in brain of Macaca fascicularis: Identification of a nucleus incertus in primate. *J. Comp. Neurol.* 517(6):856–72

Ma S, Shen PJ, Burazin TCD, Tregear GW, Gundlach AL. 2006. Comparative localization of leucine-rich repeat-containing g-protein-coupled receptor-7 (RXFP1) mRNA and [33P]-relaxin binding sites in rat brain: Restricted somatic co-expression a clue to relaxin action? *Neuroscience.* 141(1):329–44

Ma S, Smith CM, Blasiak A, Gundlach AL. 2016. Distribution, physiology and pharmacology of relaxin-3/RXFP3 systems in brain. *Br. J. Pharmacol.* 1–15

Mali P, Yang L, Esvelt KM, Aach J, Guell M, Dicarlo JE, Norville JE, Church GM. 2013. RNA-guided human genome engineering via Cas9. *Science.* 339(6121):823–26

Marder E. 2012. Neuromodulation of neuronal circuits: back to the future. *Neuron.* 76(1):1–11

Marder E, Bucher D. 2007. Understanding Circuit Dynamics Using the Stomatogastric Nervous System of Lobsters and Crabs. *Annu. Rev. Physiol.* 69:291–316

Maximino C, de Brito TM, da Silva Batista AW, Herculano AM, Morato S, Gouveia A. 2010. Measuring anxiety in zebrafish: a critical review. *Behav. Brain Res.* 214(2):157–71

McGowan BMC, Minnion JS, Murphy KG, Roy D, Stanley SA, Dhillo WS, Gardiner J V., Ghatei MA, Bloom SR. 2014. Relaxin-3 stimulates the neuro-endocrine stress axis via corticotrophin-releasing hormone. *J. Endocrinol.* 221(2):337–46

McGowan BMC, Stanley SA, Ghatei MA, Bloom SR. 2009. Relaxin-3 and its role in neuroendocrine function. *Ann. N. Y. Acad. Sci.* 1160:250–55

McGowan BMC, Stanley SA, Smith KL, Minnion JS, Donovan J, Thompson EL, Patterson M, Connolly MM, Abbott CR, Small CJ, Gardiner J V., Ghatei MA, Bloom SR. 2006. Effects of acute and chronic relaxin-3 on food intake and

energy expenditure in rats. *Regul. Pept.* 136:72–77

McGowan BMC, Stanley SA, Smith KL, White NE, Connolly MM, Thompson EL, Gardiner J V., Murphy KG, Ghatei MA, Bloom SR. 2005. Central relaxin-3 administration causes hyperphagia in male wistar rats. *Endocrinology.* 146(8):3295–3300

McNaughton N, Corr PJ. 2004. A two-dimensional neuropsychology of defense: fear/anxiety and defensive distance. *Neurosci. Biobehav. Rev.* 28(3):285–305

Mehta TK, Ravi V, Yamasaki S, Lee AP, Lian MM, Tay B-H, Tohari S, Yanai S, Tay A, Brenner S, Venkatesh B. 2013. Evidence for at least six Hox clusters in the Japanese lamprey (Lethenteron japonicum). *Proc. Natl. Acad. Sci. U. S. A.* 110(40):16044–49

Millar L, Streiner N, Webster L, Yamamoto S, Okabe R, Kawamata T, Shimoda J, Büllesbach E, Schwabe C, Bryant-greenwood G. 2005. Early placental insulin-like protein (INSL4 or EPIL) in placental and fetal membrane growth. *Biol. Reprod.* 73(4):695–702

Minagawa I, Fukuda M, Ishige H, Kohriki H, Shibata M, Park EY, Kawarasaki T, Kohsaka T. 2012. Relaxin-like factor (RLF)/ insulin-like peptide 3 (INSL3) is secreted from testicular Leydig cells as a monomeric protein comprising three domains B – C – A with full biological activity in boars. *Biochem. J.* 441:265–73

Miyamoto Y, Watanabe Y, Tanaka M. 2008. Developmental expression and

serotonergic regulation of relaxin 3/INSL7 in the nucleus incertus of rat brain. *Regul. Pept.* 145(1–3):54–59

Montague TG, Cruz JM, Gagnon JA, Church GM, Valen E. 2014. CHOPCHOP: a CRISPR/Cas9 and TALEN web tool for genome editing. *Nucleic Acids Res.* 42(Web Server issue):W401-407

Morin LP, Blanchard JH. 2005. Descending projections of the hamster intergeniculate leaflet: Relationship to the sleep/arousal and visuomotor systems. *J. Comp. Neurol.* 487(2):204–16

Mosimann C, Puller A-C, Lawson KL, Tschopp P, Amsterdam A, Zon LI. 2013. Site-directed zebrafish transgenesis into single landing sites with the phiC31 integrase system. *Dev. Dyn.* 242(8):949–63

Munro J, Skrobot O, Sanyoura M, Kay V, Susce MT, Glaser PEA, de Leon J, Blakemore AIF, Arranz MJ. 2012. Relaxin polymorphisms associated with metabolic disturbance in patients treated with antipsychotics. *J. Psychopharmacol.* 26(3):374–79

Nadim F, Bucher D. 2014. Neuromodulation of neurons and synapses. *Curr. Opin. Neurobiol.* 29:48–56

Nakazawa CM, Shikata K, Uesugi M, Katayama H, Aoshima K, Tahara K, Takahashi E, Hida T, Shibata H, Ogura H, Seiki T, Oda Y, Kuromitsu J, Miyamoto N. 2013. Prediction of relaxin-3-induced downstream pathway resulting in anxiolytic-like behaviors in rats based on a microarray and peptidome analysis. *J. Recept. Signal Transduct. Res.* 33(4):224–33

Nusbaum MP, Blitz DM, Marder E. 2017. Functional consequences of neuropeptide and small-molecule co-transmission. *Nat. Rev. Neurosci.* 18(7):389–403

Okamoto H, Agetsuma M, Aizawa H. 2012. Genetic dissection of the zebrafish habenula, a possible switching board for selection of behavioral strategy to cope with fear and anxiety. *Dev. Neurobiol.* 72(3):386–94

Olucha-Bordonau FE, Otero-garcı M, Ma S, Gundlach AL. 2012. Distribution and Targets of the Relaxin-3 Innervation of the Septal Area in the Rat. *J. Comp. Neurol.* 520:1903–39

Olucha-Bordonau FE, Teruel V, Barcia-González J, Ruiz-Torner A, Valverde-Navarro AA, Martínez-Soriano F. 2003. Cytoarchitecture and efferent projections of the nucleus incertus of the rat. *J. Comp. Neurol.* 464(1):62–97

Piato ÂL, Capiotti KM, Tamborski AR, Oses JP, Barcellos LJG, Bogo MR, Lara DR, Vianna MR, Bonan CD. 2011. Unpredictable chronic stress model in zebrafish (Danio rerio): behavioral and physiological responses. *Prog. Neuropsychopharmacol. Biol. Psychiatry*. 35(2):561–67

Purves D, Augustine GJ, Fitzpatrick D, Hall WC, Lamantia A-S, Mcnamara JO, Willians SM. 2004. *Neuroscience*. 3rd ed.

Ramlee MK, Yan T, Cheung AMS, Chuah CTH, Li S. 2015. High-throughput genotyping of CRISPR/Cas9-mediated mutants using fluorescent PCR-capillary gel electrophoresis. *Sci. Rep.* 5(15587):1–13

Reichmann F, Holzer P. 2016. Neuropeptide Y: A stressful review.

Neuropeptides. 55:99–109

Risbrough VB, Stein MB. 2006. Role of corticotropin releasing factor in anxiety disorders: A translational research perspective. *Horm. Behav.* 50(4):550–61

Rotzinger S, Lovejoy DA, Tan LA. 2010. Behavioral effects of neuropeptides in rodent models of depression and anxiety. *Peptides*. 31(4):736–56

Ryan PJ, Büchler E, Shabanpoor F, Hossain MA, Wade JD, Lawrence AJ, Gundlach AL. 2013a. Central relaxin-3 receptor (RXFP3) activation decreases anxiety- and depressive-like behaviours in the rat. *Behav. Brain Res.* 244:142–51

Ryan PJ, Kastman HE, Krstew E V, Rosengren KJ, Hossain MA, Churilov L, Wade JD, Gundlach AL, Lawrence AJ. 2013b. Relaxin-3/RXFP3 system regulates alcohol-seeking. *Proc. Natl. Acad. Sci. U. S. A.* 110(51):20789–94

Ryan PJ, Krstew E V., Sarwar M, Gundlach AL, Lawrence AJ. 2014. Relaxin-3 mRNA levels in nucleus incertus correlate with alcohol and sucrose intake in rats. *Drug Alcohol Depend.* 140:8–16

Ryan PJ, Ma S, Olucha-Bordonau FE, Gundlach AL. 2011. Nucleus incertus--an emerging modulatory role in arousal, stress and memory. *Neurosci. Biobehav. Rev.* 35(6):1326–41

Sagata D, Minagawa I, Kohriki H, Pitia AM, Uera N, Katakura Y, Sukigara H, Terada K, Shibata M, Park EY, Hasegawa Y, Sasada H, Kohsaka T. 2015. The insulin-like factor 3 (INSL3) -receptor (RXFP2) network functions as a germ cell survival/anti-apoptotic factor in boar testes. *Endocrinology*.

156(4):1523–39

Sakuma T, Nakade S, Sakane Y, Suzuki K-IT, Yamamoto T. 2015. MMEJ-assisted gene knock-in using TALENs and CRISPR-Cas9 with the PITCh systems. *Nat. Protoc.* 11(1):118–33

Sander JD, Joung JK. 2014. CRISPR-Cas systems for editing, regulating and targeting genomes. *Nat. Biotechnol.* 32(4):347–55

Sander JD, Zaback P, Joung JK, Voytas DF, Dobbs D. 2007. Zinc Finger Targeter (ZiFiT): an engineered zinc finger/target site design tool. *Nucleic Acids Res.* 35(Web Server issue):W599-605

Sanogo YO, Hankison S, Band M, Obregon A, Bell AM. 2011. Brain Transcriptomic Response of Threespine Sticklebacks to Cues of a predator. *Brain. Behav. Evol.* 77:270–85

Santos FN, Pereira CW, Sánchez-Pérez AM, Otero M, Ma S, Gundlach AL, Olucha-Bordonau FE. 2016. Comparative distribution of relaxin-3 inputs and calcium-binding protein-positive neurons in rat amygdala. *Front. Neuroanat.* (1–15):1–23

Scheer N, Campos-Ortega JA. 1999. Use of the Gal4-UAS technique for targeted gene expression in the zebrafish. *Mech. Dev.* 80:153–58

Shabanpoor F, Akhter Hossain M, Ryan PJ, Belgi A, Layfield S, Kocan M, Zhang S, Samuel CS, Gundlach AL, Bathgate RAD, Separovic F, Wade JD. 2012. Minimization of human relaxin-3 leading to high-affinity analogues with increased selectivity for relaxin-family peptide 3 receptor (RXFP3) over

RXFP1. *J. Med. Chem.* 55(4):1671–81

Sherwood OD. 2004. Relaxin's physiological roles and other diverse actions. *Endocr. Rev.* 25(2):205–34

Shirahase T, Aoki M, Watanabe R, Watanabe Y, Tanaka M. 2016. Increased alcohol consumption in relaxin-3 deficient male mice. *Neurosci. Lett.* 612:155–60

Silvertown JD, Neschadim A, Liu HN, Shannon P, Walia JS, Kao JCH, Robertson J, Summerlee AJS, Medin JA. 2010. Relaxin-3 and receptors in the human and rhesus brain and reproductive tissues. *Regul. Pept.* 159(1–3):44–53

Smith CM, Chua BE, Zhang C, Walker AW, Haidar M, Hawkes D, Shabanpoor F, Hossain MA, Wade JD, Rosengren KJ, Gundlach AL. 2014a. Central injection of relaxin-3 receptor (RXFP3) antagonist peptides reduces motivated food seeking and consumption in C57BL/6J mice. *Behav. Brain Res.* 268:117–26

Smith CM, Hosken I, Sutton SW, Lawrence AJ, Gundlach AL. 2012. Relaxin-3 null mutation mice display a circadian hypoactivity phenotype. *Genes. Brain. Behav.* 11(1):94–104

Smith CM, Lawrence AJ, Sutton SW, Gundlach AL. 2009. Behavioral phenotyping of mixed background (129S5:B6) relaxin-3 knockout mice. *Ann. N. Y. Acad. Sci.* 1160:236–41

Smith CM, Ryan PJ, Hosken IT, Ma S, Gundlach AL. 2011. Relaxin-3 systems in the brain--the first 10 years. *J. Chem. Neuroanat.* 42(4):262–75

Smith CM, Shen PJ, Banerjee A, Bonaventure P, Ma S, Bathgate RAD, Sutton SW, Gundlach AL. 2010. Distribution of relaxin-3 and RXFP3 within arousal, stress, affective, and cognitive circuits of mouse brain. *J. Comp. Neurol.* 518(19):4016–45

Smith CM, Walker LL, Chua BE, McKinley MJ, Gundlach AL, Denton DA, Lawrence AJ. 2015. Involvement of central relaxin-3 signalling in sodium (salt) appetite. *Exp. Physiol.* 100(9):1064–72

Smith CM, Walker AW, Hosken IT, Chua BE, Zhang C, Haidar M, Gundlach AL. 2014b. Relaxin-3/RXFP3 networks: an emerging target for the treatment of depression and other neuropsychiatric diseases? *Front. Pharmacol.* 5(46):1–17

Steimer T. 2002. The biology of fear- and anxiety-related behaviors. *Dialogues Clin. Neurosci.* 4(3):231–49

Stephenson-Jones M, Orestis F, Robertson B, Grillner S. 2012. Evolutionary conservation of the habenular nuclei and their circuitry controlling the dopamine and 5-hydroxytryptophan (5-HT) systems. *Proc. Natl. Acad. Sci.* 109(3):E164-173

Sudo S, Kumagai J, Nishi S, Layfield S, Ferraro T, Bathgate RAD, Hsueh AJW. 2003. H3 relaxin is a specific ligand for LGR7 and activates the receptor by interacting with both the ectodomain and the exoloop 2. *J. Biol. Chem.* 278(10):7855–62

Sutton SW, Bonaventure P, Kuei C, Nepomuceno D, Wu J, Zhu J, Lovenberg

TW, Liu C. 2005. G-protein-coupled receptor (GPCR)-142 does not contribute to relaxin-3 binding in the mouse brain: Further support that relaxin-3 is the physiological ligand for GPCR135. *Neuroendocrinology.* 82(3–4):139–50

Sutton SW, Bonaventure P, Kuei C, Roland B, Chen J, Nepomuceno D, Lovenberg TW, Liu C. 2004. Distribution of G-protein-coupled receptor (GPCR) 135 binding sites and receptor mRNA in the rat brain suggests a role for relaxin-3 in neuroendocrine and sensory processing. *Neuroendocrinology.* 92121(80):298–307

Sutton SW, Shelton J, Smith CM, Williams J, Yun S, Motley T, Kuei C, Bonaventure P, Gundlach AL, Liu C, Lovenberg T. 2009. Metabolic and neuroendocrine responses to RXFP3 modulation in the central nervous system. *Ann. N. Y. Acad. Sci.* 1160:242–49

Taghert PH, Nitabach MN. 2012. Peptide neuromodulation in invertebrate model systems. *Neuron.* 76(1):82–97

Talbot JC, Amacher SL. 2014. A streamlined CRISPR pipeline to reliably generate zebrafish frameshifting alleles. *Zebrafish.* 11(6):583–85

Tanaka M, Iijima N, Miyamoto Y, Fukusumi S, Ito Y, Ozawa H, Ibata Y. 2005. Neurons expressing relaxin 3/INSL 7 in the nucleus incertus respond to stress. *Eur. J. Neurosci.* 21(6):1659–70

Thisse C, Thisse B. 2008. High-resolution in situ hybridization to whole-mount zebrafish embryos. *Nat. Protoc.* 3(1):59–69

Timofeeva E, Calvez J, Avila C De. 2016. Stress differentially regulates brain expression of corticotropin- releasing factor in binge-like eating prone and resistant female rats ve Gu e. *Appetite*. 107:585–95

Tovote P, Esposito MS, Botta P, Chaudun F, Fadok JP, Markovic M, Wolff SBE, Ramakrishnan C, Fenno L, Deisseroth K, Herry C, Arber S, Luthi A. 2016. Midbrain circuits for defensive behaviour. *Nature*. 534:206–12

Tovote P, Fadok JP, Lüthi A. 2015. Neuronal circuits for fear and anxiety. *Nat. Rev. Neurosci*. 16(6):317–31

Tukey JW. 1977. *Exploratory Data Analysis*. Addison-Wesley

Untergasser A, Cutcutache I, Koressaar T, Ye J, Faircloth BC, Remm M, Rozen SG. 2012. Primer3 - new capabilities and interfaces. *Nucleic Acids Res*. 40(15):1–12

Vaaga CE, Borisovska M, Westbrook GL. 2014. Dual-transmitter neurons: Functional implications of co-release and co-transmission. *Curr. Opin. Neurobiol*. 29:25–32

van den Pol AN. 2012. Neuropeptide Transmission in Brain Circuits. *Neuron*. 76(1):98–115

van der Westhuizen ET, Werry TD, Sexton PM, Summers RJ. 2007. The Relaxin Family Peptide Receptor 3 Activates Extracellular Signal-Regulated Kinase 1 / 2 through a Protein Kinase C-Dependent Mechanism. *Mol. Pharmacol*. 71(6):1618–29

Varshney GK, Pei W, LaFave MC, Idol J, Xu L, Gallardo V, Carrington B, Bishop K, Jones M, Li M, Harper U, Huang SC, Prakash A, Chen W, Sood R, Ledin J, Burgess SM. 2015. High-throughput gene targeting and phenotyping in zebrafish using CRISPR/Cas9. *Genome Res.* 25:1030–42

Wahren J, Ekberg K, Johansson J, Henriksson M, Pramanik A, Johansson BL, Rigler R, Jörnvall H. 2000. Role of C-peptide in human physiology. *Am. J. Physiol. Endocrinol. Metab.* 278(1):E759–68

Wahren J, Ekberg K, Jörnvall H. 2007. C-peptide is a bioactive peptide. *Diabetologia.* 50(3):503–9

Wahren J, Larsson C. 2015. C-peptide: New findings and therapeutic possibilities. *Diabetes Res. Clin. Pract.* 107(3):309–19

Walker AW, Smith CM, Chua BE, Krstew E V, Zhang C, Gundlach AL, Lawrence AJ. 2015a. Relaxin-3 receptor (RXFP3) signalling mediates stress-related alcohol preference in mice. *PLoS One.* 10(4):e0122504

Walker AW, Smith CM, Gundlach AL, Lawrence AJ. 2015b. Relaxin-3 receptor (Rxfp3) gene deletion reduces operant sucrose- but not alcohol-responding in mice. *Genes, Brain Behav.* 14(8):625–34

Watanabe Y, Miyamoto Y, Matsuda T, Tanaka M. 2011a. Relaxin-3/INSL7 regulates the stress-response system in the rat hypothalamus. *J. Mol. Neurosci.* 43(2):169–74

Watanabe Y, Tsujimura A, Takao K, Nishi K, Ito Y, Yasuhara Y, Nakatomi Y, Yokoyama C, Fukui K, Miyakawa T, Tanaka M. 2011b. Relaxin-3-deficient

mice showed slight alteration in anxiety-related behavior. *Front. Behav. Neurosci.* 5(50):1–11

Wilkinson TN, Bathgate RAD. 2007. The evolution of the relaxin peptide family and their receptors

Wilkinson TN, Speed TP, Tregear GW, Bathgate RAD. 2005. Evolution of the relaxin-like peptide family from neuropeptide to reproduction. *BMC Evol. Biol.* 5(14):530–33

Wilson BC, Burnett D, Rappaport R, Parry LJ, Fletcher EK. 2009. Relaxin-3 and RXFP3 expression, and steroidogenic actions in the ovary of teleost fish. *Comp. Biochem. Physiol.* Part A 153:69–74

Woods IG, Schoppik D, Shi VJ, Zimmerman S, Coleman HA, Greenwood J, Soucy ER, Schier AF. 2014. Neuropeptidergic signaling partitions arousal behaviors in zebrafish. *J. Neurosci.* 34(9):3142–60

Yates A, Akanni W, Amode MR, Barrell D, Billis K, Carvalho-Silva D, Cummins C, Clapham P, Fitzgerald S, Gil L, Girón CG, Gordon L, Hourlier T, Hunt SE, Janacek SH, Johnson N, Juettemann T, Keenan S, Lavidas I, Martin FJ, Maurel T, McLaren W, Murphy DN, Nag R, Nuhn M, Parker A, Patricio M, Pignatelli M, Rahtz M, Riat HS, Sheppard D, Taylor K, Thormann A, Vullo A, Wilder SP, Zadissa A, Birney E, Harrow J, Muffato M, Perry E, Ruffier M, Spudich G, Trevanion SJ, Cunningham F, Aken BL, Zerbino DR, Flicek P. 2016. Ensembl 2016. *Nucleic Acids Res.* 44(Database issue):D710–16

Yegorov S, Bogerd J, Good S V. 2014. The relaxin family peptide receptors and

their ligands: New developments and paradigms in the evolution from jawless fish to mammals. *Gen. Comp. Endocrinol.* 209:93–105

Yelin-Bekerman L, Elbaz I, Diber A, Dahary D, Gibbs-Bar L, Alon S, Lerer-Goldshtein T, Appelbaum L. 2015. Hypocretin neuron-specific transcriptome profiling identifies the sleep modulator Kcnh4a. *Elife*. 4:1–25

Zhang C, Chua BE, Yang A, Shabanpoor F, Hossain MA, Wade JD, Rosengren KJ, Smith CM, Gundlach AL. 2015. Central relaxin-3 receptor (RXFP3) activation reduces elevated, but not basal, anxiety-like behaviour in C57BL/6J mice. *Behav. Brain Res.* 292:125–32

Publications

1. Lupton C, Sengupta M, Cheng R, Chia J. 2017. Loss of the habenula neuromodulator kisspeptin1 affects learning in larval zebrafish. *eNeuro.* 4(3):1–9.

Poster presentations

1. Chia, J. and Jesuthasan, S. Habenula-dependent neural circuits regulating anxiety. Genetics, Genomics and Phenomics in fish, Cold Spring Harbour Asia conferences, Suzhou, China, 2014.

2. Chia, J. and Jesuthasan, S. Relaxin-3 as a mediator of dorsal habenula function. 9th IBRO World Congress of Neuroscience, International Brain Research Organization, Rio de Janeiro, Brazil, 2015.

3. Chia, J., Cheng, R-.K., and Jesuthasan, S. Relaxin-3 as a mediator of dorsal habenula function. 7th International Conference on Relaxin and Related Peptides, Kuching, Malaysia, 2015.

4. Chia, J., Cheng, R-.K., Krishnan, S., and Jesuthasan, S. The relaxin-3a mutant identifies the PAG as a component of the visual motor response in larval zebrafish. 10th FENS Forum of Neuroscience, Federation of European Neuroscience, Copenhagen, Denmark, 2016.

5. Chia, J., Cheng, R-.K., Krishnan, S., and Jesuthasan, S. The relaxin-3a mutant identifies the PAG as a component of the visual motor response in larval zebrafish. 8th models of physiology and disease symposium, Department of Physiology, National University of Singapore, Singapore, 2016.